

RECEIVED: August 26, 2023 Accepted: December 11, 2023 Published: January 4, 2024

Twisted Fibrations in M/F-theory

Lara B. Anderson^a James Gray^a Paul-Konstantin Oehlmann^b

^aPhysics Department, Robeson Hall, Virginia Tech, Blacksburg, VA 24061, U.S.A.

^bDepartment of Physics & Department of Mathematics, Northeastern University, 360 Huntington Avenue, Boston, MA 02115, U.S.A.

E-mail: lara.anderson@vt.edu, jamesgray@vt.edu,

p.oehlmann@northeatern.edu

ABSTRACT: In this work we investigate 5-dimensional theories obtained from M-theory on genus one fibered threefolds which exhibit twisted algebras in their fibers. We provide a base-independent algebraic description of the threefolds and compute light 5D BPS states charged under finite sub-algebras of the twisted algebras. We further construct the Jacobian fibrations that are associated to 6-dimensional F-theory lifts, where the twisted algebra is absent. These 6/5-dimensional theories are compared via twisted circle reductions of F-theory to M-theory. In the 5-dimensional theories we discuss several geometric transitions that connect twisted with untwisted fibrations. We present detailed discussions of $\mathfrak{e}_6^{(2)}$, $\mathfrak{so}_8^{(3)}$ and $\mathfrak{su}_3^{(2)}$ twisted fibers and provide several explicit example threefolds via toric constructions. Finally, limits are considered in which gravity is decoupled, including Little String Theories for which we match 2-group symmetries across twisted T-dual theories.

Keywords: Gauge Symmetry, M-Theory, Discrete Symmetries, F-Theory

ArXiv ePrint: 2308.07364

Contents

1	Introduction	1		
2	Circle reductions of F-theory to M-theory			
	2.1 A brief review of twisted circle reductions	5		
	2.2 F/M-theory circle reductions and Calabi-Yau geometry	6		
3	Twisted dimensional reductions in F-theory?	g		
	3.1 A twisted circle reduction of a $U(1) \times U(1)$ theory	12		
	3.1.1 The Calabi-Yau geometry	12		
	3.1.2 Field theory: twisted dimensional reduction	13		
	3.2 A non-Abelian twisted circle reduction: the $E_7 \times \mathrm{U}(1)/\mathbb{Z}_2$ theory	16		
4	Phases and lifts of $\mathfrak{e}_6^{(2)}$ in 5D	18		
	4.1 The geometry of $\mathfrak{e}_6^{(2)}$	19		
	4.2 Geometric state counting	22		
	4.3 Transitions to $\mathfrak{e}_6^{(2)}$	28		
5	More twisted affine fibrations	37		
	5.1 The geometry of $\mathfrak{su}_3^{(2)}$	37		
	5.1.1 Counting states in the $\mathfrak{su}_3^{(2)}$ genus-one model	39		
	5.1.2 Transitions to $\mathfrak{su}_3^{(2)}$	43		
	5.2 The geometry of $\mathfrak{so}_8^{(3)}$	47		
	5.2.1 State counting in $\mathfrak{so}_8^{(3)}$ genus-one fibration	50		
	5.2.2 Transitions to $\mathfrak{so}_8^{(3)}$	5 4		
6	Decoupling gravity and non-compact limits	58		
	6.1 Supergravity phase and T-duality	59		
	6.2 Little string limit and twisted T-duality	60		
7	Twisted VS. untwisted genus-one fibers	6 4		
7	7.1 Enhanced symmetries and non-poly defs	65		
	7.2 $\mathfrak{e}_{6}^{(2)}$ vs $\mathfrak{f}_{4}^{(1)}$ genus-one fibers	66		
	7.3 $\mathfrak{so}_8^{(3)}$ vs $\mathfrak{g}_2^{(1)}$ genus-one fibers 7.4 $\mathfrak{su}_3^{(2)}$ vs $\mathfrak{su}_2^{(1)}$ genus-one fibers	71		
	7.4 $\mathfrak{su}_3^{(2)}$ vs $\mathfrak{su}_2^{(1)}$ genus-one fibers	7 5		
8	Summary and outlook	78		
\mathbf{A}	Toric data for threefold geometries	81		
	A.1 $\mathfrak{su}_3^{(2)}$ example geometries	81		
	A.2 $\mathfrak{e}_6^{(2)}$ example geometries	82		
	A.3 $\mathfrak{so}_8^{(3)}$ example geometries	83		
В	Line bundle data for genus-one fibrations	84		

1 Introduction

String compactifications lead to a rich array of effective supergravity (SUGRA) and quantum (and sometimes conformal) field theories in 6- and 5- dimensions which have been the focus of much recent work [1–11]. The close relationship between the 5/6-dimensional theories under a circle (S^1) reduction has yielded much information about the possible structure of both theories (see e.g. [12-14]) and inspired many recent classifications. In this work, we are interested in a new example of such 6D/5D relationships as they arise in compactications of M/F-theory on elliptically and genus one fibered Calabi-Yau threefolds. In particular, we are interested in circle reductions of 6-dimensional F-theory effective theories which include flux along the circle and the possibility of twisted circle reductions [7, 15–19] (leading to different ranks in the 5-dimensional gauge theories compared to their 6-dimensional uplifts). It is important to note at this point that the phrase "twisted reduction" has been used in multiple ways in the literature (sometimes indicating only circle reductions including flux/Wilson lines). In the context of this work we will only use the term "twisted reduction" to refer to reductions which change the rank of the gauge group. This will include an F-/M-theory realization of automorphisms that "fold" affine Dynkin diagrams [20–22] to produce twisted algebras and Calabi-Yau genus-one geometries with markedly different physics (including different rank gauge groups) to their Jacobian fibrations.

Let us begin by briefly reviewing a now well-established story [23–25] of F-theory circle reductions with Abelian gauge groups and M-theory on genus one fibered Calabi-Yau manifolds. We will outline a few key ideas here and leave a more detailed review for section 2. For the purposes of this discussion it should be noted that a "genus-one fibered" manifold is one whose generic fiber is a T^2 and which does not in general admit a section to that fibration, but rather a multi-section (which intersects the generic fiber n > 1 times). In contrast, a T^2 -fibered manifold which does admit a rational section is referred to as an "elliptically fibered" manifold. A 5-dimensional compactification of M-theory on a genus one fibered Calabi-Yau threefold X is closely related to a 6-dimensional compactification of F-theory on a particular elliptically fibered Calabi-Yau threefold known as the Jacobian of X and denoted X and denoted X is manifold which shares the same base and discriminant locus to the fibration (and the same J-function). In general, for torus-fibered CY threefolds X are topologically distinct and many different genus one fibered manifolds can share the same Jacobian.

The set of such geometries (together with information about the form of the birational mapping takes) form the group of CY Torsors [26, 27]. In many cases this reduces to the Weil-Châtalet group WC(X) [22, 26, 28–30]. The Weil-Châtalet group contains the Tate-Shafarevich (TS) group III(X) [28, 29] as a subgroup and the two coincide if the genus-one fibrations do not contain isolated multiple fibres. In such simple situations, the number of Kähler moduli among all TS elements have been observed to match [31–34]. Multiple fibres over smooth points¹ on the other hand appear to be closely linked to the

¹For a discussion of multiple fibres over isolated singularities in B_2 see [22, 30] and for smooth points see eq. B of [21].

twisted affine algebras that we construct in this work and hence in these cases the WC(X) group does not simply reduce to the TS group III(X).

Returning to the F-/M-theory physics of these manifolds, a compactification of F-theory requires the existence of a section in addition to a T^2 fiber [35, 36] and thus, we can consider defining F-theory on a given elliptically fibered CY threefold. However, this single compactification of F-theory can give rise to a number of distinct 5-dimensional compactifications of M-theory via circle reduction with Wilson lines (and possibly matter field vevs). As an example, if we consider a purely Abelian 6D effective theory arising from F-theory, then it is possible to choose a non-trivial U(1)-charged vev $\langle \phi_q \rangle \neq 0$ and discrete Wilson line (i.e. discrete circle flux) along the circle

$$\xi \sim \int_{S^1} A. \tag{1.1}$$

As was demonstrated in [31, 32, 37], different choices of ξ lead to compactifications of M-theory on (possibly) distinct genus-one manifolds which are elements of the group of CY torsors (note that the reduction with $\xi = 0$ leads to an M-theory compactification on the elliptically fibered manifold $J(X/B_2)$ itself). The set of these 5-dimensional theories are connected by geometric transitions in the underlying genus one fibered manifolds [31, 32, 37, 38]. This framework has been used to gain a deep understanding of discrete symmetries in F-/M-theory. In particular the associated Jacobian fibrations admit non-trivial torsion [32] and terminal singularities that do not admit a crepant resolution [39, 40]. When compactified on one more circle to 4D, one obtains type IIA strings on the same geometry but it is possible to twist along this additional cycle, which allows to resolve the singularity via a non-commutative resolution [41–43].

In the present paper, we will be interested in compactifications of F-theory in 6-dimensions which include not only an Abelian factor, but also a non-Abelian gauge algebra (e.g. $\mathfrak{g} \times \mathbb{Z}_n$ for the Jacobian theory or $\mathfrak{g} \times \mathfrak{u}(1)$ if we move to an enhanced loci in moduli space to simply describe the dimensional reduction). In this case, the circle reductions can involve flux from gauge fields in the Cartan subalgebra of \mathfrak{g} as well as the U(1) factors. Importantly, a feature that is possible in this context is the presence of boundary conditions which can mix these different fluxes together in non-trivial ways:

$$A^{B}(y) = \sigma^{B}(A^{C}(y+2\pi)) \tag{1.2}$$

where σ is associated to a discrete automorphism of the gauge group. In reductions of pure gauge theories the discrete symmetry action σ is known to be an outer automorphism of the gauge group. As we will discuss in this work, in the context of F-theory (as a theory of supergravity) this discrete symmetry is expected to be gauged and to be locally realized in the Calabi-Yau geometry. This involves a more complex interplay between the gauge theory and local discrete automorphisms of the Calabi-Yau geometry.

Non-trivial circle boundary conditions such as in (1.2) (and fluxes) have been implemented in a variety of other contexts under the name of "twisted" circle reductions (see e.g. [7, 15, 17, 44]) but have not been previously studied in the compact setting in F-theory. As we mention above, we will refer to reductions implementing non-trivial boundary

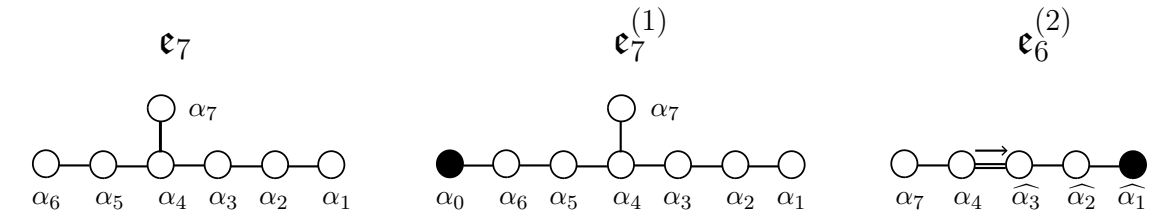


Figure 1. From left to right: upon affinization, the \mathfrak{e}_7 Dynkin diagram obtains an \mathbb{Z}_2 outer automorphism that interchanges the affine and fundamental root α_0 and α_1 . Quotienting by that automorphism, yields twisted affine $\mathfrak{e}_6^{(2)}$.

conditions such a (1.2) as "twisted reductions". We find that in the presence of these boundary conditions we generate a new set of 5-dimensional vacua associated to M-theory compactifications on genus-one fibered manifolds with "twisted" torus fibrations realizing twisted Lie algebras (e.g. $\mathfrak{e}_6^{(2)}$) in their fibers and non-Abelian gauge algebras of the form $\mathfrak{h}_i \times \mathfrak{u}(1)$ where $\mathfrak{h}_i \subseteq \mathfrak{g}$ is a sub-group of the 6D F-theory gauge algebra. Geometrically, these geometries are intriguing in that the genus one fibered manifold and its Jacobian can realize different non-Abelian gauge groups, despite the fact that they share a discriminant locus. This arises through a discrete "folding" of the affine Dynkin diagrams found in the elliptic/genus-one fibers.

In this work we will provide several examples of the geometric structure described above in which a genus-one fibered CY manifold and its Jacobian differ significantly in terms of their respective 5D/6D physics. As our central, illustrative example, we will study in detail the geometry and BPS spectra of a manifold whose fibers correspond to the twisted algebra $\mathfrak{e}_6^{(2)}$. The $\mathfrak{e}_6^{(2)}$ twisted algebra admits an \mathfrak{f}_4 finite sub-algebra, as observed from the Dynkin diagram in figure 1. Upon unfolding one notices that the Dynkin diagram is obtained from an $\mathfrak{e}_7^{(1)}$ cover, twisted by its outer automorphism. A key feature of this construction is that this folding symmetry only exists in the diagram upon affine extension but not the finite \mathfrak{e}_7 gauge algebra alone. Correspondingly, if this is to be realized inside a compact CY fibration, the folding is incompatible with the existence of a single section, as that would mark the affine node α_0 breaking the symmetry $\alpha_0 \leftrightarrow \alpha_1$. Instead, as we will review in detail below, the folded fibers appear in genus one geometries with a 2-section [7]. As described in section 4, such a 2-section comes with a special divisor $\overline{D}_2 = d_8^2 + 4d_5$ across which the two branch points are interchanged. This monodromy divisor plays a crucial role in realizing the folded fibers: to obtain the $\mathfrak{e}_6^{(2)}$ geometry, we require the \mathfrak{e}_7 divisor in the base to intersect \overline{D}_2 non-trivially. As we will outline in detail in section 4 below, the singular genus-one fibration admits a quartic fiber presentation in \mathbb{F}_2 , given as

$$Z^{2} = z^{3}d_{1}X^{4} + z^{3}d_{2}X^{3}Y + z^{2}d_{3}X^{2}Y^{2} + zd_{4}XY^{3}$$

+ $d_{5}Y^{4} + d_{6}z^{2}X^{2}Z + zd_{7}XYZ + d_{8}Y^{2}Z,$ (1.3)

with what we call a type III^* non-split fiber that can be resolved to $\mathfrak{e}_6^{(2)}$.

This fiber structure leads to several open questions regarding the 5D/6D effective physics which are explored in this work. The torus-fiber of the genus-one fibration indicates a 6D F-theory uplift. As the 6D F-theory geometry is simply the encoding of the monodromy

data of the IIB axio-dilaton, this information can be obtained by mapping the singular genus-one model into the Jacobian fibration [45] which takes at leading order the form

$$f = z^3 \overline{D}_2 + \mathcal{O}(z^4), \quad g = z^5 q + \mathcal{O}(z^6), \quad \Delta = z^9 \overline{D}_2^3 + \mathcal{O}(z^{10}).$$
 (1.4)

Due to the presence of the section in the Jacobian, the Kodaira/Tate classification applies and we do not obtain an \mathfrak{f}_4 (e.g. via a $IV^{*,ns}$ -singularity) but instead a type III^* which yields an \mathfrak{e}_7 gauge algebra. Thus, we find an enhancement of the non-Abelian gauge symmetry in the 6D theory compared to that in 5D. This observation regarding the F-theory lift of such genus-one models differs from those previously studied in the literature (see e.g. [46]). In particular we find a difference of the Kähler moduli of the (maximally resolvable) Jacobian and the genus-one fibrations as also observed in [20, 21, 47]. From the point of view of circle reductions of 6D gauge theories, this may come as a surprise, as "twisted" dimensional reductions leading to $\mathfrak{e}_6^{(2)}$ fibers are realized in theories decoupled from gravity by twisted reductions of \mathfrak{e}_6 (see e.g. [7, 19]). In the present context, we find that the Jacobian symmetry instead reflects the geometric cover of $\mathfrak{e}_6^{(2)}$, that is \mathfrak{e}_7 . This is further discussed in section 3. This structure appears in each of our examples and applies also to the $\mathfrak{su}_3^{(2)}$ and $\mathfrak{so}_8^{(3)}$ geometries that are explored in section 5.

Further interesting differences between the 5/6D theories arise when considering the spectrum of light states in the two theories. Upon resolving the genus-one model, we study the geometry over an arbitrary two-fold base and compute the number of light 5D BPS states associated to the twisted fibration which are determined by the number of $R = [z] \cdot \overline{D}_2$ ramification points and the genus g of the base curve. Computing those we find that our results are in full agreement with the multiplicities of 5D states that would arise from an \mathfrak{e}_6 twisted circle reduction (despite the fact that the apparent 6D gauge symmetry is \mathfrak{e}_7 as described above). We also discuss several conifold-type transitions of the threefold, and match it to 5D geometric transitions which change the fiber structure as $\mathfrak{e}_7^{(1)} \to \mathfrak{e}_6^{(2)}$. Field theoretically we realize this transition via motion along the Higgs/Coulomb branches of the theories. We test our constructions also in the context of little string theories, by matching higher group symmetries across T-dual pairs, as well as SCFTs.

The structure of this paper is as follows. In section 2 we give a brief introduction to circle compactifications in F-theory and M-theory on genus-one fibrations. In section 3 we discuss twisted circle reductions of \mathfrak{u}_1^2 and $\mathfrak{e}_7 \times \mathfrak{u}_1$ theories and a rich array of questions that arise in those contexts. From there we proceed to the discussion of 5D M-theory vacua and genus one fibrations with $\mathfrak{e}_6^{(2)}$ fibers in section 4, where we describe the full geometry, compute BPS multiplicities and geometric transitions to untwisted theories. In section 5 we then discuss further examples including $\mathfrak{su}_3^{(2)}$ and $\mathfrak{so}_8^{(3)}$ twisted fibers. In section 6 we employ the geometric constructions described above to discuss twisted T-dual little string theories and match their global symmetries. These considerations provide a non-trivial cross-check for our constructions. Finally, in section 7 we compare the moduli spaces of twisted and untwisted genus-one fibrations before we conclude in section 8. Appendix A and appendix B are devoted to additional geometric data for some of the explicit examples presented in this work.

2 Circle reductions of F-theory to M-theory

In the following sections we provide a brief review of the relationships between 6/5 dimensional theories and the geometry of Calabi-Yau elliptic and genus-one fibrations.

2.1 A brief review of twisted circle reductions

Following the analysis of [31, 48], one can consider a compactification of a 6-dimensional U(1) gauge theory on a circle of radius R. In particular, we consider the possibility of giving a field ϕ of charge q an expectation value, possibly depending upon the circle direction, whose coordinate we denote by y. Denoting the five-dimensional coordinates by x we can perform the usual Fourier expansion of the scalar field.

$$\phi(x,y) = \sum_{n \in \mathbb{Z}} \phi_n(x) e^{2\pi i n y \tau}, \qquad (2.1)$$

with the inverse circle radius $\tau = \frac{1}{R}$. In addition to a scalar field vev, one could consider turning on a Wilson line associated to the U(1) gauge field which can be denoted by $\xi = \int_{S^1} A$ as in (1.1). In such a background, the mass term obtained for the *n*'th Kaluza-Klein (KK) mode ϕ_n is proportional to the following

$$m_n = |q\xi + n\tau| \,. \tag{2.2}$$

In this setting that there are several distinct possibilities for the nature of the compactified theory. The mode of ϕ which is given an expectation value must be massless according to (2.2). For example, if we choose $\xi = -\tau k/q$ this is simply the mode n = k. One can then ask, if we give an expectation value to a KK mode ϕ_n then what symmetry is preserved? This is straightforward, but we write out the argument below here as we will soon need to repeat it for more complicated examples. The mode transforms under the symmetry as follows.

$$\phi_n \to e^{i(q\theta + n\psi)}\phi_n$$
 (2.3)

Here θ and ψ are the parameters associated to U(1)_{6D} and U(1)_{KK} respectively. Given (2.3) the expectation value is invariant if,

$$q\theta + n\psi = 2\pi\gamma, \tag{2.4}$$

where $\gamma \in \mathbb{Z}$. Clearly we will always have a U(1) symmetry simply by taking $\gamma = 0$ and $\theta = n/q\psi$. To complete the analysis we simply need to decide if any non-zero values of γ are not identified with the $\gamma = 0$ case.

The two gauge parameters are identified under

$$\theta \approx \theta + 2\pi\alpha$$
, $\psi \approx \psi + 2\pi\beta$. (2.5)

Therefore,

$$q\theta + n\psi \approx q\theta + n\psi + 2\pi(q\alpha + n\beta)$$
. (2.6)

Comparing (2.6) and (2.4), we see that values of γ for which $\gamma = (q\alpha + n\beta)$ can be identified with zero. The question therefore becomes what is the smallest positive integer combination

of q and n. This is, of course gcd(q, n) and thus values of γ can be identified under integer multiples of this greatest common divisor. Given this analysis, a dimensional reduction of this type results in a symmetry $U(1) \times \mathbb{Z}_{gcd(q,n)}$.

As an example, we see from this analysis that if q = 3 then one should obtain a U(1) symmetry unless n is an integer multiple of 3 as noted in [31]. It should be noted that this result has implications of the structure of the group of Calabi-Yau Torsors under the standard F-theory framework of how such geometries are related to sets of genus one fibered geometries which share a Jacobian [26, 31, 38, 46, 48] as we discuss next.

2.2 F/M-theory circle reductions and Calabi-Yau geometry

In this section we review the geometry and physics of genus-one fibrations in M-and F-theory on a compact threefold and its relation to discrete symmetries. Those properties can be deduced intrinsically from the threefolds [41, 49, 50] however we will rather discuss them in terms of a Higgs transition following [32].

In that we discuss with an elliptic threefold with a rank one MW group [2, 23, 25] (also see the reviews [51, 52] and reference therein). A well explored example is the Morrison-Park [2] model [24] given as the elliptic curve inside of $BL_1\mathbb{P}^2_{1,1,2}$,

$$p = e_1^3 s_1 X^4 + e_1^2 s_2 X^3 Y + e_1 s_3 X^2 Y^2 + s_4 X Y^3 + e_1^2 s_6 X^2 Z + e_1 s_7 X Y Z + s_8 Y^2 Z + e_1 s_9 Z^2 \,. \tag{2.7}$$

Here the X, Y, Z, e_1 can be thought of the analog of the Weierstrass coordinates, and the s_i are some non-vanishing sections of the base that are specified in appendix B. The fibral part of the Stanley-Reisner ideal (SRI) is given by

$$SRI: \{XZ, e_1Y\}, \tag{2.8}$$

where both X = 0 and $e_1 = 0$ are sections S_0 and S_1 respectively, that generate a MW group given by the Shioda map:

$$\sigma(s_1) = [e_1] - [X]. \tag{2.9}$$

The form dual to this divisor leads to a U(1) gauge potential by an expansion of the M-theory three-form that also survives in the F-theory limit. Notably, this fibration admits two kinds of reducible curves over codimension two points in the base, where the fiber becomes of I_2 form. The first is over the toric locus $s_4 = s_8 = 0$ where the fiber degenerates into $\mathbb{T}^2 \to C_1 + C_2$ and the other one over a non-toric ideal $I_{(2)}$ where the fiber becomes $\mathbb{T}^2 \to B_1 + B_2$. The fiber structures and especially their intersections with the two set of sections are given as

The volumes of those effective curves were computed using the fibral part of the Kähler form (see [48]) given as

$$J = t_0 S_0 + t_s (S_0 + S_1). (2.11)$$

This geometry admits two conifold transitions that either branch towards a genus-one fibration or its Jacobian respectively. In order to do so, either of the two \mathbb{P}^1 's must be blown-down which yields a singularity which we can then deform. The two phases are topologically distinct geometries:

- 1. $t_0 \to 0$ yields the genus-one fibration (after deformation). Note that the residual fibers $B_{1/2}$ stay at finite volume.
- 2. $t_s \to 0$ yields the Jacobian fibration (after deformation). The curve B_2 shrinks to zero size, which results in an I_2 singularity that can not be (crepantly) resolved.

In the genus-one fibration we deform the singular curves C_1 by adding the terms s_5Y^4 to obtain

$$p = s_1 X^4 + s_2 X^3 Y + s_3 X^2 Y^2 + s_4 X Y^3 + s_5 Y^4 + s_6 X^2 Z + s_7 X Y Z + s_8 Y^2 Z + s_9 Z^2,$$
(2.12)

which yields the genus-one fibration. Shrinking C_2 preserves the section and yields the Jacobian fibration. From a 6D perspective, the resulting F-theory lift yields a discrete \mathbb{Z}_2 symmetry. This is clear once from observing that we Higgs on a non-minimal U(1) charged state but also due to the fact the all elements in the TS group $\mathrm{III}(X)$ must yield the same 6D F-theory and thus a (discrete) gauge symmetry.

In the absence of a section we can at most define an N-section, which refers to a divisor S_0^N that intersects the generic torus N times

$$S_0^N \cdot [T^2] = N. (2.13)$$

Those N-points make sense only as a collection, as they are permuted along monodromies in the base along the *Monodromy divisor* \overline{D}_{N,S_0} . This divisor can be computed from the discriminant locus of S_0^N . For the quartic the relevant monodromy divisor is given as

$$\overline{D}_{2,X} = s_8^2 - 4s_9 s_5. (2.14)$$

While the different elements of $\mathrm{III}(X)$ uplift to the same 6D F-theory, their 5D M-theory physics differs. As described previously, since M-theory is related to F-theory by a circle compactification, the differences in 5D effective theory arise from a choice of a circle flux ξ in the 6D gauge algebra $G \times \mathrm{U}(1)$. In the context of the geometries above, these choices can be seen by following the Higgsing in 5D and noting that M2 branes can wrap the curves C_i which, on a generic point on the Coulomb branch (CB) obtain the masses

$$m_{w,n} = |w^I \xi_I + q \xi + n \tau|,$$
 (2.15)

whereas w^I denotes a weight of the 6D representation \mathbf{R}_q under $G \times \mathrm{U}(1)$. The ξ_I and ξ denote the 5D Coulomb branch parameters of the non-Abelian and Abelian gauge algebras respectively. Geometrically, those 5D Coulomb branch parameters correspond to fibral Kähler parameters and the weights w^I and q can be explicitly computed via the intersections of the fibral curve C with the fibral divisors D_I and the U(1) Shioda map respectively. For a singlet state under the non-Abelian gauge algebra, $\mathbf{1}_N$, the choice of circle flux $\xi = -\frac{n}{N}$ from the perspective of the 6D theory allows for massless states in the 5D theory that enable the geometric/Higgsing transitions described above. The choice of $\xi = 0$ corresponds to the Jacobian geometry.

From the point of view of the circle reduction, the unbroken $U(1)_E$ in 5D is a linear combination of both $U(1)_{6D}$ and $U(1)_{KK}$ symmetries given as

flux 5D symmetry
$$\xi = -\frac{n}{N} U(1)_E = n \cdot U(1)_{6D} - N \cdot U(1)_{KK}$$

$$\xi = 0 \qquad \mathbb{Z}_N \times U(1)_{KK}$$
(2.16)

(where we have taken gcd(q, n) = 1 here for simplicity). Also note that the Jacobian vacuum with $\xi = 0$ preserves the discrete gauge algebra factor in $5D^2$ The choice with a discrete holonomy will be relevant in the next section in conjunction with additional non-trivial 6d gauge symmetries to lead to twisted affine type of fibers.

Note that at the origin of the Coulomb branch in the Jacobian, with $\xi = 0$ there are KK zero-modes which yield massless 5D states. Note also that discrete charged singlets stay massless on a generic point of the Coulomb branch moduli space. These states correspond to terminal I_2 fibral singularities, that do not admit any crepant resolution [39, 40]. In the genus-one fibration on the other hand every massless 6D state with representation \mathbf{R}_q and \mathbb{Z}_N remnant charge $q \mod N$ admits shifted 5D mass

$$m_{w,n} = |w^I \xi_I + \left(n - q \frac{n_0}{N}\right) \tau|.$$
 (2.17)

The total contribution $q_E = (n - q \frac{n}{N})$ is identified with the charge³ under $U(1)_E$ which is the shifted $U(1)_{KK}$. The $U(1)_E$ charges can be computed geometrically via the intersections with the "discrete Shioda map"⁴ which is used to construct multi-section that is orthogonalized with respect to all shrinkable fibral curves (see [45] and eq. (5.23) in [50]). Note that states with weight $w \in \mathbf{R}$ and non-trivial $U(1)_E$ charges stay massive at the origin of the Coulomb branch $\xi_I = 0$.

Whenever \mathfrak{g} is an untwisted algebra the codimension one and two singularity structure in either elements of the TS group $\mathrm{III}(X)$ are the same, as observed in all known examples [20, 34, 45, 49], with the only exception that singularities are terminal in the Jacobian. Hence for computational purposes it is often times more convenient to use the genus-one fibration

²See [32, 41] for a discussion of the torsion cycles in the Jacobian that yield the discrete symmetry.

 $^{^3}$ The $q \mod N$ identification of the 6D discrete charges is resembled by the integer shift symmetry of the KK charges n in 5D.

⁴Note that the $U(1)_{KK}$ -tower is still integer spaced, while we will mostly use a $U(1)_E$ charge normalization for the N-section such that KK-charges have N-integer spacing.

to compute states and charges, as the geometry can be fully resolved.⁵ These states then become massless in the 6D F-theory uplift and therefore must satisfy the 6D (SUGRA) anomaly cancellation conditions.

When moving away from untwisted algebras to twisted ones however, the simple relationship between states no longer holds. In the following we discuss in detail that these geometries admit multiple fibers and hence, we expect that the Weil-Châtalet group WC(X) will not reduce to the Tate-Shafarevich group $\mathrm{III}(X)$ in these cases.

3 Twisted dimensional reductions in F-theory?

The geometries described in section 1 highlight an intriguing possibility, namely that circle reductions of F-theory to M-theory may dramatically change the nature of non-Abelian factors in the gauge group in a way that cannot be explained by standard circle fluxes alone. The natural question then arises: what is the physical mechanism that accomplishes this change?

At least a partial answer seems to lie within the study of twisted circle reductions of gauge theories which have appeared in a wide range of contexts (see e.g. [7, 15, 17, 19, 44, 53]). In brief, if we begin with a theory with gauge symmetry G, in n-dimensions and consider the dimension reduction of this theory on an S^1 to produce an (n-1)-dimensional theory, it is natural to consider the possibility of non-trivial boundary conditions on S^1 for the gauge theory. Denoting the coordinate along the S^1 as y, the fields of the theory could experience 'twisting' conditions around the circle. For example the gauge potentials could obey a schematic relationship of the form

$$A^{B}(y) = \sigma^{B}(A^{C}(y+2\pi)) \tag{3.1}$$

where σ is some discrete action mixing components of the gauge field. For pure gauge theories, the possible discrete actions σ are well understood [7]. In particular, σ must be compatible with gauge transformations of the theory but not trivializable under them, leaving the group of outer automorphisms of G as a natural choice.

Importantly for our present purposes, for simple Lie algebras the group of outer automorphisms are exactly the group of graph automorphisms of the associated Dynkin diagram. This means that there is a natural identification of nodes of the Dynkin diagrams that can "fold" the diagram in way a that feels similar in spirit to the relationship between fibers of the twisted genus one fibered manifold X and it's Jacobian, $J(X/B_2)$ sketched in section 1 and explored in detail in section 4. For example, a natural \mathbb{Z}_2 automorphism of \mathfrak{e}_6 can fold the group to its \mathfrak{f}_4 subgroup (see figure 2). Physically, then this symmetry in (3.1) would lead to a breaking of \mathfrak{e}_6 symmetry to \mathfrak{f}_4 under a circle reduction.

Within gauge theories, the mechanism above is well understood and frequently utilized. However in theories coupled to supergravity new subtleties arise. The most important of these is that it is believed that discrete symmetries such as those appearing in (3.1) must be gauged in the full supergravity theory. Thus, one must ask how the local discrete actions such as σ in (3.1) are realized explicitly in a given string/M-/F-theory context?

⁵As shown in [41, 42], terminal singularities can be resolved with non-Kähler non-commutative resolutions in the type IIA compactifications. Using those resolutions, discrete charged Gopakumar-Vafa invariants have been proposed [41], that allow to compute charges and states in the Jacobian directly.

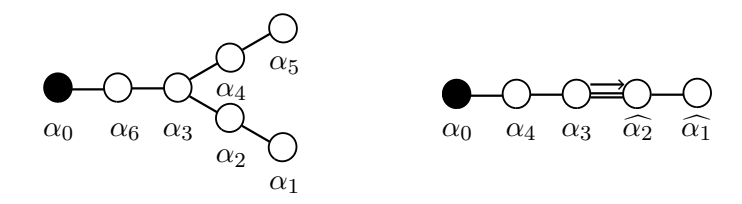


Figure 2. Depiction of the Dynkin diagrams of $\mathfrak{e}_6^{(1)}$ and $\mathfrak{f}_4^{(1)}$, where the affine node is highlighted in black. The later is obtained by folding by the \mathbb{Z}_2 automorphism of \mathfrak{e}_6 . Note that $\mathfrak{f}_4^{(1)}$ is Langland dual to $\mathfrak{e}_6^{(2)}$ given in figure 1.

An interesting example of this question arises in the CHL compactifications of the heterotic string [54]. Beginning with the $E_8 \times E_8$ heterotic theory in 10-dimensions it is possible to perform a circle reduction to obtain a 9-dimensional theory with, for example, E_8 symmetry. In this case the discrete action (3.1) is simply the \mathbb{Z}_2 outer automorphism of the product group $E_8 \times E_8$ which interchanges the two E_8 factors, leaving a single E_8 gauge group in 9-dimensions. The question of how this apparent global symmetry is gauged might be somewhat opaque within the 10-dimensional heterotic theory. However the local nature is clearly visible from the viewpoint of 11-dimensional heterotic M-theory [55] in which this \mathbb{Z}_2 symmetry is realized as a discrete automorphism of the S^1/\mathbb{Z}_2 geometry itself which interchanges the two E_8 -fixed planes (i.e. the 9-dimensional theory is found from compactification on a Mobius strip [56]). As an important final note on this example, it is useful to observe that this symmetry only appears at special/tuned (i.e. higher codimensional) loci within the moduli space of the heterotic compactification (or heterotic M-theory). At generic points in the moduli space the two E_8 bundles are not symmetric. It is only by moving to a special locus where the gauge connections, etc are identical that the symmetry becomes manifest. We will return to this important point in other contexts below.

With these general comments in hand we come now to the question of how can such twisted dimensional reductions be realized in F-theory? There are several immediate observations that can be made — which in turn lead to questions about the nature of any twisting symmetries akin to (3.1) in this context. The first of these is that since we expect this discrete action to be gauged in a compact geometry, it is natural to expect that the symmetry must be realized in some way in the Calabi-Yau geometry of F-theory itself (indeed, in a sense F-theory is just a geometric encoding of field theory information in Calabi-Yau geometry). But that raises the question of how can a twisting symmetry act on the elliptically fibered geometry?

To answer this question it is useful to first recall how diagrams such as in figure 2 are realized in F-theory. To work directly with the Calabi-Yau geometry it is helpful to consider the resolved limit as guide, despite the fact that the physical theory is determined by (singular) Weierstrass models (i.e. thinking of F-theory as a limit of M-theory). In the resolved CY geometry, the Dynkin diagrams of gauge groups are realized geometrically (via blow-ups of degenerate elliptic fibers) as diagrams of affine groups. This affine diagram

is reduced to that of the actual gauge group by the inclusion of a section to the elliptic fibration which intersects one component of the fiber. In the F-theory limit, all components of the fiber that do not intersect the section (i.e. all fibral divisors) are taken to zero size.

In this context we might expect that a twisting symmetry should be visible in the F-theory geometry itself as a discrete automorphism. But at this point several immediate questions arise. The first puzzle is that it is the Dynkin diagrams of affine Lie groups rather than their finite counterparts that arise in the explicit (resolved) elliptically fibered Calabi-Yau geometry. Thus, we must ask how is the discrete action in (3.1) uplifted to the full elliptically fibered geometry? And how does such a symmetry interact with the section (or sections) to the elliptic fibration?

It is clear that any discrete symmetry which "folds" a Dynkin diagram such as in figure 2 realized in an elliptic fibration must act compatibly with section(s) of the fibration. In figure 2 this is straightforward as the affine node "spectates" through the folding, but for some actions on affine diagrams this is not so simple. For example, the \mathbb{Z}_2 action which folds $\mathfrak{e}_7^{(1)}$ to $\mathfrak{e}_6^{(2)}$ identifies the affine node (intersected by the zero-section in an F-theory fiber) with another node as in figure 1. Here the presence of a section intersecting the fibration admitted more than one rational section (which could intersect the diagram in an appropriately symmetric way). It is exactly this latter configuration that we find explicitly realized in the Jacobians of CY genus-one fibrations studied here.

Summarizing the observations above: generic features of the examples we find explicitly realized in (resolved) elliptic Calabi-Yau geometries indicate that

- The twisting symmetries are expected to "lift" to discrete automorphims (i.e. foldings) of the affine Dynkin diagrams realized in the elliptic fibers.
- In order for symmetries to exist which can serve as twisted boundary conditions for the actual (finite) gauge groups, the Mordell-Weil group of the geometry is frequently required to be non-trivial, i.e. there must be more than one rational section. The presence of these sections can "restore" folding symmetries to the fibers that would not otherwise be present with a single rational section.

Due to the geometric relationships between CY genus-one fibrations and their Jacobians, we do not find the standard twisted boundary conditions that arise in gauge theory (for example the $\mathfrak{e}_6 \to \mathfrak{f}_4$ folding in figure 2, though they may exist). Instead, in the explicit CY geometry we find that only foldings such as those in figure 1 can be realized. From the geometric perspective, the appearance of \mathfrak{e}_7 instead of \mathfrak{e}_6 in the Jacobian is perhaps more expected, as its affine extension is the geometric cover for $\mathfrak{e}_6^{(2)}$ fibers. These foldings arise in the context of more complicated geometries with higher rank Mordell-Weil groups and discrete symmetries. As a result, twisted dimensional reductions appear to be part of the rich geometric structure linking genus one fibered Calabi-Yau manifolds and their Jacobian manifolds as described in section 1 and 2.

Finally, similarly to the example of the CHL string mentioned above, it is clear that we may need to tune the F-theory geometry to a special locus in complex structure moduli

space to make any possible discrete twisting automorphisms visible. Here we expect that these tunings may be more difficult to find/engineer explicitly depending on the interplay between the discrete symmetries in (3.1) and the full F-theory gauge group (including non-Abelian and Abelian factors as described by reducible elliptic fibers in the resolved geometry and a higher rank Mordell-Weil group [35]).

3.1 A twisted circle reduction of a $U(1) \times U(1)$ theory

In the sections below we will begin by outlining a twisted dimensional reduction in which the twisting symmetry is made completely manifest in the geometry by restricting ourselves to a highly symmetric point in the complex structure moduli space of the elliptic Calabi-Yau variety. In later sections we will postulate that for many examples milder tunings are possible and can still lead to twisting symmetries involving interchange of rational sections (similar to the freedom studied in [57]).

3.1.1 The Calabi-Yau geometry

Here we briefly review the geometry of a singular elliptic CY variety which leads to an F-theory background with Abelian gauge symmetry $U(1) \times U(1)$.

To begin we recall the logic taken by Morrison and Taylor in [38] in characterizing a geometry with two sections to its elliptic fibration (i.e. Mordell-Weil rank 1) and hence a U(1) gauge symmetry in F-theory. As a starting point, one may consider a genus one fibration defined in an ambient $\mathbb{P}^{1,1,2}_{X,Y,Z}$, defined by (2.12). Fixing s_9 as a constant, redefining and shifting the coordinates X, Y, Z and classes s_i , we can obtain the reduced form of the quartic

$$Z^{2} = s_{1}X^{4} + s_{2}X^{3}Y + s_{3}X^{2}Y^{2} + s_{4}XY^{3} + s_{5}Y^{4}.$$
(3.2)

The s_i are sections of line bundles in the base read off from appendix B as

$$[s_1] \sim 2(c_1 - S_9), \quad [s_2] \sim 2c_1 - S_9, \quad s_3 \sim 2c_1, \quad [s_4] \sim 2c_1 + S_9, \quad [s_5] \sim 2(c_1 + S_9),$$

with S_9 some line bundle class⁶ defined in the base B_2 of the genus one fibration $\pi: X_{CY} \to B_2$ and c_1 the anti-cannonical class of B_2 . This genus one fibration degenerates over higher codimensional loci in the base (in particular the I_2 loci) where the discrete singlets $\mathbf{1}_1$ are located (see [38] for an explicit discussion).

The Jacobian of this geometry, is a hypersurface in $\mathbb{P}^{2,3,1}_{X,Y,Z}$ given as

$$y^{2} = x^{3} - s_{3}x^{2}z^{2} + (s_{2}s_{4} - 4s_{1}s_{5})xz^{4} - (s_{2}^{2}s_{5} + s_{1}s_{4}^{2} - 4s_{1}s_{3}s_{5})z^{6}$$
(3.4)

from which we can read off the Weierstrass coefficients

$$f = \left(s_2 s_4 - \frac{1}{3} s_3^2 - 4 s_1 s_5\right) \tag{3.5}$$

$$g = \left(-s_1 s_4^2 + \frac{1}{3} s_2 s_3 s_4 - \frac{2}{27} s_3^3 + \frac{8}{3} s_1 s_3 s_5 - s_2^2 s_5\right). \tag{3.6}$$

⁶The line bundle S_9 is only restricted by the conditions that all $[s_i]$ are all effective sections.

It should be noted that at the singlet locus, the discriminant becomes singular (and the genus-one fibration reducible).

The geometry given above can be U(1) enhanced by tuning in a section. There are actually two inequivalent ways of doing so. We call the enhancement $U(1)_a$ and $U(1)_b$ that are given by setting

$$U(1)_a: s_1 \to d_1^2/4 \qquad U(1)_b: s_5 \to d_5^2/4.$$
 (3.7)

The above factorizations make sense, as s_1 and s_5 are both elements of even classes in the base and therefore d_1 and d_5 are integral. We can directly see that the above factorization yields another section in the genus one geometry e.g. in the first enhancement as

$$\frac{1}{4}(d_1X^2 - 2Z)(d_1X^2 + 2Z) = s_2X^3Y + s_3X^2Y^2 + s_4XY^3 + s_5Y^4$$
(3.8)

where we have two sections at $Z = \pm \frac{1}{2} d_1 X^2$. So now we have a section and thus, this quartic equation is in birational to the Weierstrass model. The same factorization above happens for the U(1)_b.

Finally, a $U(1)_a \times U(1)_b$ model (our goal in this section) is then given as

$$Z^{2} = \frac{1}{4}(d_{1}^{2}X^{4}) + s_{2}X^{3}Y + s_{3}X^{2}Y^{2} + s_{4}XY^{3} + \frac{1}{4}(d_{5}^{2}Y^{4}).$$
 (3.9)

The above geometry admits a symmetry under the exchange

$$d_1 \leftrightarrow d_5 \qquad s_2 \leftrightarrow s_4 \qquad X \leftrightarrow Y \tag{3.10}$$

while keeping s_3 and Z fixed. This is only possible for the line bundle choices $S_9 = 0$ (but of course for many choices of base manifold, B_2 , in particular for every weak Fano base). As we will see in future sections this type of tuned Weierstrass model (and its symmetries) is similar in spirit to the Jacobians varieties of genus-one fibered manifolds with twisted fibers studied in this work.

3.1.2 Field theory: twisted dimensional reduction

With the geometry above in hand as a background for F-theory, we can consider the compactification of the resulting six-dimensional $U(1) \times U(1)$ gauge theory on a circle. We will consider giving a vev to a scalar field ϕ_{q_1,q_2} charged under both U(1) factors and including Wilson lines ξ_1 and ξ_2 in both gauge factors. The Fourier expansion of the scalar field, and the mass term for the associated modes are then very similar to (2.1) and (2.2) above.

$$\phi_{q_1,q_2}(x,y) = \sum_{n \in \mathbb{Z}} \phi_{q_1,q_2,n}(x) e^{2\pi i n y \tau}$$

$$m_n = |n\tau + q_1 \xi_1 + q_2 \xi_2|$$
(3.11)

For simplicity let us consider the special case where one gives an expectation value to a field where $q_1 = q_2 = q$ which we will denote simply by ϕ . We will also specialize to the case where $\xi_1 = \xi_2 = \xi$. In such an instance, the mass in (3.11) simplifies and we can isolate a special case of backgrounds.

The analysis of the unbroken five-dimensional gauge group in this case mirrors the situation of a single six-dimensional U(1). Taking $\xi = -k/2q$ we find from (3.11) that the massless mode is n = k. This mode transforms under the symmetries as

$$\phi_n \to e^{i((\theta_1 + \theta_2)q + \psi n)} \phi_n \tag{3.12}$$

where θ_1 and θ_2 are the parameters of the two six-dimensional U(1)'s and ψ is that of the KK gauge factor. The expectation value of ϕ_n is therefore invariant if the following condition holds for some $\gamma \in \mathbb{Z}$.

$$q(\theta_1 + \theta_2) + n\psi = 2\pi\gamma \tag{3.13}$$

Clearly, we will always have a U(1) × U(1) symmetry simply by taking $\gamma = 0$ and $\psi = -q/n(\theta_1 + \theta_2)$. As before, to complete the analysis we simply need to decide if any non-zero values of γ are not identified with the $\gamma = 0$ case (and so are not part of the continuous symmetry group already identified).

The gauge parameters are identified under

$$\theta_1 \approx \theta_1 + 2\pi\alpha_1, \ \theta_2 \approx \theta_2 + 2\pi\alpha_2, \ \psi \approx \psi + 2\pi\beta.$$
 (3.14)

Therefore we have the following identification.

$$q(\theta_1 + \theta_2) + n\psi \approx q(\theta_1 + \theta_2) + n\psi + 2\pi(q(\alpha_1 + \alpha_2) + n\beta)$$
(3.15)

Comparing (3.15) and (3.13), we see that values of γ for which $\gamma = q(\alpha_1 + \alpha_2) + n\beta$ for some α_1 , α_2 and β can be identified with zero. Since $\alpha_1 + \alpha_2$ is still just some general integer, as α was in the proceeding analysis, the answer is unchanged. The full gauge group seen in five-dimensions is thus $U(1) \times U(1) \times \mathbb{Z}_{\gcd(q,n)}$.

Where this simple example of a $U(1) \times U(1)$ reduction differs from the analysis with a single abelian factor is in the possibility of there being additional symmetries of the system which can be used as boundary conditions in the circle reduction. In the proposal we present in this paper this symmetry is an emergent one, only appearing on special loci in the moduli space of the Calabi-Yau manifold (i.e. the tuning given in (3.7) for this example). For those choices of complex structure there exists a \mathbb{Z}_2 symmetry which exchanges the two U(1) factors in six-dimensions as described in the previous subsection. If we use such a symmetry as a boundary condition in traveling once around the S^1 upon which we are compactifying, then the analysis of the nature of the five-dimensional theory changes.

A symmetry of the type described in the previous paragraph leaves fields of the form $\phi_{q,q}$ invariant. Therefore the mode expansions (3.12) is unchanged in this case. The symmetry does identify θ_1 and θ_2 mod 2π at the point where the boundary condition is applied, however, and if we assume that these have no y dependence, then they are set equal mod 2π everywhere. We are thus left with a U(1) × $\mathbb{Z}_{\gcd(q,n)}$ theory in five-dimensions.

It is useful to also briefly review the fate of the particle spectrum on dimensional reduction. From fields of type $\phi_{Q,Q}$ in six-dimensions which were not those which for which there was an expectation value we obtain degrees of freedom of charge 2Q under the low

energy U(1). From the field of this type which we gave a vev, we of course obtain an uncharged degree of freedom. In order for the symmetry which we have used as a boundary condition to exist, fields of type ϕ_{q_1,q_2} must always be paired with fields of type ϕ_{q_2,q_1} in the six-dimensional spectrum. This is automatic when starting with six-dimensional theories of course, but the entire discussion here is essentially unchanged in compactifying from four-dimensions where this requirement becomes non-trivial. The symmetry identifies the fields in these pairs, and as such, each pair gives rise to a single field of charge $q_1 + q_2$ in five-dimensions.

As a final comment, it should be noted that we could give an expectation value to a pair of fields of the form ϕ_{q_1,q_2} and ϕ_{q_2,q_1} instead of the case of equal charges under the two six-dimensional U(1)'s described above. In such a case, the mode expansion (3.12) is more complicated as the boundary condition transforms one field into the other as the S^1 is traversed. We have the following.

$$\phi_{q_1,q_2} = \sum_{n \in \mathbb{Z}} \phi_n(x) e^{\pi i n y \tau} ,$$

$$\phi_{q_2,q_1} = \sum_{n \in \mathbb{Z}} \phi_n(x) e^{\pi i n (y+1) \tau} .$$
(3.16)

The mass of the KK mode ϕ_n is then given by the following expression.

$$m_n = \left| \frac{n}{2} \tau + q_1 \xi + q_2 \xi \right| . \tag{3.17}$$

By choosing $\xi = -k/(2(q_1 + q_2))\tau$ we can therefore ensure that the mode n = k is massless. Under the symmetries present in the system, this mode transforms as follows.

$$\phi_n \to \phi_n e^{i(q_1\theta_1 + q_2\theta_2 + \frac{n}{2}\psi)}. \tag{3.18}$$

Thus the condition that we have an unbroken symmetry is simply,

$$q_1\theta_1 + q_2\theta_2 + \frac{n}{2}\psi = 2\pi\gamma , \qquad (3.19)$$

for $\gamma \in \mathbb{Z}$. Since the symmetry operation equates $\theta_1 = \theta_2 \mod 2\pi$ the $\gamma = 0$ possibility here leads to a U(1) symmetry in the five-dimensional theory. The gauge parameters are identified under 2π shifts as in (3.15), and as such, while non-vanishing values for γ are potential elements of a discrete symmetry group, they will be identified with a vanishing transformation if the following condition holds.

$$2\alpha_1 q_1 + 2\alpha_2 q_2 + \beta n = 2\gamma \tag{3.20}$$

The integer on the left hand side of this expression is always a multiple of

$$\gcd(2q_1, 2q_2, n) = \gcd(\gcd(2q_1, 2q_2), n) = \gcd(2\gcd(q_1, q_2), n). \tag{3.21}$$

Therefore (3.20) has a solution iff γ is a multiple of lcm (gcd(2 gcd(q_1, q_2), n), 2) /2. Finally, then we arrive at a symmetry group for the compactified theory of,

$$U(1) \times \mathbb{Z}_{lcm(gcd(2 gcd(q_1, q_2), n), 2)/2}$$
 (3.22)

The discussion of the U(1) charges of the matter spectrum in this case is identical to that seen in the cases where $\phi_{q,q}$ was given an expectation value.

3.2 A non-Abelian twisted circle reduction: the $E_7 \times \mathrm{U}(1)/\mathbb{Z}_2$ theory

With the observations of the previous sections in hand, we can return now to the geometry mentioned in section 1. In the CY geometry defined by (1.4) we see a smooth, genus one fibered CY 3-fold with $\mathfrak{e}_6^{(2)}$ fibers which yields an elliptically fibered Jacobian geometry (as given by (1.4)) with $\mathfrak{e}_7^{(1)}$ fibers. We expect these geometries to be part of a single group of CY torsors and that the 5D M-theory vacua should be related to circle compactifications of the 6D F-theory. We will explore the structure of the genus one geometry and its associated 5D M-theory physics in section 4, but to begin we will consider briefly the 6D F-theory background and the associated circle reduction (which is dual to M-theory on the genus one geometry in 5D). Keeping the connection between the genus-one geometry and its Jacobian in mind, we can try to understand how the 6D/5D theories are related. In particular, we hope to shed some light on the difference between the 6D and 5D gauge groups.

It is worth briefly taking stock of the ingredients at our disposal. As reviewed in previous sections, for ease of description, we begin with a 6D F-theory compactification defined via a Weierstrass model with $(E_7 \times \mathrm{U}(1))/\mathbb{Z}_2$ symmetry. How would this theory reduce to a $F_4 \times \mathrm{U}(1)$ theory upon circle reduction? As in section 2 we expect that the F-theory compactified on S^1 vacuum could include

- 1. Vevs for matter with a profile along the circle (as in (2.1))
- 2. Gauge fields (i.e. fluxes) around the circle (i.e. (1.1))
- 3. Non-trivial boundary conditions (i.e. "twisting" of the circle reduction as in (1.2))

Considering the form of the genus one geometry and its Jacobian (with $E_7 \times \mathbb{Z}_2$ symmetry) we expect the first two elements of the list above to be present. The first of these is necessary in that a matter field vev for a U(1) charged field (as we will see in section 4, $\langle \mathbf{1}_2 \rangle \neq 0$ for the present example) is required to break the 6D U(1) symmetry to the finite group \mathbb{Z}_2 seen in the Jacobian. Likewise, we expect non-trivial gauge flux along the circle in order for the theory to be dual to M-theory on a genus one fibration (see [31, 32]).

However it is clear that these two ingredients alone are not enough. Given the 6D E_7 symmetry visible in the Jacobian it is clear that only U(1)-charged matter (i.e. E_7 singlets) can possibly be given a vev. Likewise with the allowed matter vevs, purely Abelian circle fluxes could not change the rank of the gauge group. Thus, these possibilities alone could not lead to the correct 5D gauge group to match M-theory compactified on the twisted genus one geometry. As a result, we must consider the third item in the list above and the possibility of a "twisted" reduction of F-theory as described in previous subsections.

As described in the start of this section, the key question in this context is what is the F-theory origin of the twisting symmetry of (1.2)? As discussed previously, the resolution of this singular elliptic fibration sketched in (1.4) displays the affine algebra $\mathfrak{e}_7^{(1)}$. Taken in isolation from the rest of the geometry, this affine Dynkin diagram admits an outer automorphism $\tilde{\sigma}_2$ of order two. Modding the diagram by this outer automorphism leads to $\mathfrak{e}_6^{(2)}$ (i.e. finite gauge group F_4) which is depicted in figure 1.

Importantly, as noted in section 1 these "folded" Dynkin diagrams (here $\mathfrak{e}_6^{(2)}$) appear to arise in the fibers of a compact, genus one fibered CY threefold which admits an $E_7 \times \mathbb{Z}_2$

Weierstrass model as its Jacobian in the 6-dimensional theory. This is intriguing structure as the diagram for the *affine* $\mathfrak{e}_7^{(1)}$ admits such a \mathbb{Z}_2 , but of course its finite counterpart \mathfrak{e}_7 does not. Thus, the central puzzles to be addressed include the following:

- Can we perform a twisted dimensional reduction to connect a 6D Weierstrass model with our "folded fiber" genus one geometry in 5D?
- Does the finite Z₂ symmetry which "twists" E₇ → F₄ under a dimensional reduction appear as a true symmetry of the elliptic fibers (of the Jacobian Weierstrass model) which produces the folded (i.e. genus one) threefold? Is this symmetry apparent not just in an action on fibers, but on the full 6D theory/geometry? What is the action on the physical theory?

In trying to address these questions we will begin by using the full, smooth resolved CY Jacobian geometry to explore the structure of possible twisting symmetries, realizing that we must take a singular limit (by blowing down all reducible curves in the fibers that do not intersect the zero section) in order to discuss the 6D F-theory physics. It should be emphasized that in this context we are only using the symmetries of the resolved Jacobian as a guide to the symmetries of 6-dimensional theory, since in the (singular) Weierstrass limit these symmetries may not be apparent due to some Kähler moduli being taken to the zero-volume limit. Note that this is the same logic that allowed us to deduce the \mathbb{Z}_2 action on the U(1) × U(1) theory in section 3.1.

As we will see below, a complete answer to the above questions proves to involve a number of subtle aspects and it is beyond the scope of the present work. However, we will attempt to sketch some of the ideas and the obstacles that arise in fully determining the effective physics of the reduction.

In the resolved geometry, the diagram above makes it clear that the $\mathfrak{e}_7^{(1)}$ fiber could admit an appropriate \mathbb{Z}_2 folding to correspond to the desired $\mathfrak{e}_6^{(2)}$ fiber in the 5D genus one geometry. However, as discussed in the previous section this apparent symmetry is manifestly broken in the full geometry if there exists only a *single* section to the elliptic fibration which would intersect the affine node (α_0 above). However, the folding symmetry could possibly exist if there were to exist *two rational sections* s_0, s_1 to the elliptic fibration (i.e. Mordell-Weil rank 1) and those sections intersected appropriate (i.e. symmetric) nodes in the affine fiber appropriately as shown below:

$$(\alpha_7)$$

$$(\alpha_0)(\alpha_6)(\alpha_5)(\alpha_4)(\alpha_3)(\alpha_2)(\alpha_1) .$$

$$\downarrow \qquad \qquad \downarrow \qquad \qquad \qquad \downarrow \qquad \qquad \qquad$$

In this case, the \mathbb{Z}_2 automorphism that folds the fiber would only be a true automorphism of the (resolution of the) F-theory Weierstrass model at a higher-codimensional locus in moduli space. For example, it could arise if the geometry were fully symmetric under the interchange of the two rational sections (similar to the geometry in section 3.1). It is natural to ask whether this can be achieved by tuning non-Abelian symmetry into a model such as that given in (3.9)? Unfortunately, In this context we find that the geometry

becomes too singular for a purely field theoretic analysis. More precisely, tuning the Weierstrass model given in section 3.1 to achieve a $E_7 \times \mathrm{U}(1)$ symmetry leads to vanishings of $(f,g,\Delta) \geq (4,6,12)$ at points. This implies that the theory contains so-called "SCFT loci" and is not described purely as an ordinary perturbative field theory. Importantly, such geometric limits are likely still be within the realm of "good" string vacua, but we are not able to write down a purely perturbative field theoretic circle reduction of the form shown in section 3.1.2 in this setting.

Alternatively, the higher codimensional locus that makes manifest the \mathbb{Z}_2 twisting symmetry should be obtainable by a suitable tuning of the resolution of the Jacobian CY 3-fold given in (1.4). Unfortunately, without knowing the particular form of the \mathbb{Z}_2 symmetry this is difficult to reverse engineer.

There is a final observation that can be made regarding the possible geometric origin of the \mathbb{Z}_2 folding symmetry. In the resolved geometry of the Jacobian CY 3-fold, either of the two rational sections can be chosen as the zero section. The resulting Weierstrass models that arise from blowing down fibral components not intersecting the chosen section are identical. Moreover, the action of this interchange changes the Dynkin weights as expected for the \mathbb{Z}_2 folding symmetry of the Affine Dynkin diagram and acts on the U(1) charged matter as charge conjugation. This action (combined with the action of R-symmetry on the hypermultiplets) leads to an apparent symmetry of the 6D theory. Moreover, in the 5D theory, this can be directly seen when constructing the two corresponding Shioda maps that are required to compute the U(1) charges: their forms, in terms of the weights α_i is given as

$$\sigma(s_1) = [s_1] - [s_0] + \frac{1}{2}(3\alpha_1 + 4\alpha_2 + 5\alpha_3 + 6\alpha_4 + 4\alpha_5 + 2\alpha_6 + 3\alpha_7), \qquad (3.24)$$

$$\sigma(s_1') = [s_0] - [s_1] + \frac{1}{2}(3\alpha_0 + 4\alpha_6 + 5\alpha_5 + 6\alpha_4 + 4\alpha_3 + 2\alpha_2 + 3\alpha_7). \tag{3.25}$$

From the above form we find that U(1) charges flip sign under exchange, which as expected, implements a charge conjugation operation. The symmetry of this interchange in the 5D theory provides a hint that this symmetry may survive under the M-theory to F-theory uplift.

We view the observations above as suggestive of the origin of the twisting symmetry in 6D, but due to the higher co-dimensional nature of this symmetry in the F-theory moduli space (and the potential presence of (4,6,12) points), there is no clear path to obtain its explicit action, and as a result it is beyond the scope of the present work to solve. For now, we turn our attention to the 5-dimensional theory and relationships between twisted and untwisted genus one fiberations in the 5D M-theory geometries.

4 Phases and lifts of $\mathfrak{e}_6^{(2)}$ in 5D

In this section we discuss the geometry of an $\mathfrak{e}_6^{(2)}$ twisted algebra in a torus fibered threefold. The geometric origin of such a fibre is the fact that affine $\mathfrak{e}_7^{(1)}$ (unlike its finite sub-algebra) admits a \mathbb{Z}_2 outer automorphism. Using a genus-one fibration we can therefore engineer a monodromy in the base of the fibration that folds by this automorphism, which yields $\mathfrak{e}_6^{(2)}$ as shown in figure 1. The key ingredient to achieve such a monodromy, is to start with a torus fibration that does not have a section but a two-section. We will also show, that

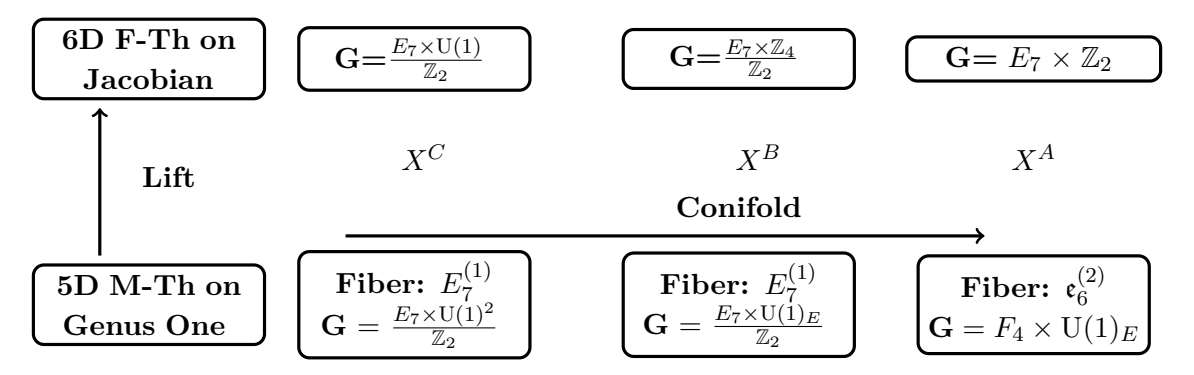


Figure 3. M-and F-theory compactifications of three types of geometries X^I , connected via geometric transitions. For $I \neq C$, the threefolds have a non-trivial TS group III, which results in disconnected 5D vacua.

this monodromy is missing in the respective Jacobian sketched in (1.3), precisely due to the presence of the section, such that those types of fibres evade the famous Koraira/Tate classification of singular fibers.

Below, we will study the intersection matrix of the fibral curves of $\mathfrak{e}_6^{(2)}$ type inside the genus one fibered manifold (over a compact two-fold base) in some detail. We also discuss the structure of the Jacobian and its type III^* fiber structure. By directly studying the geometry, we compute the light 5D BPS states in the M-theory compactification in both theories explicitly for a general base.

Finally, it is possible to explore other genus one fibered geometries, related to $\mathfrak{e}_6^{(2)}$ by geometric transitions as sketched in figure 3. Such geometric transitions usually have an interpretation in terms of Higgs transitions across special loci in the Coulomb branch moduli space. Identifying the massless matter multiplets is more intricate in the present case, which we comment on below.

4.1 The geometry of $\mathfrak{e}_6^{(2)}$

To engineer the $\mathfrak{e}_6^{(2)}$ fibration we require a 2-section model to realize the folded fiber type. To obtain such a model we employ a quartic fiber model [38] that was already introduced in the section 1. We repeat the respective hypersurface equation here for convenience, as

$$p = s_1 X^4 + s_2 X^3 Y + s_3 X^2 Y^2 + s_4 X Y^3 + s_5 Y^4 + s_6 X^2 Z + s_7 X Y Z + s_8 Y^2 Z + s_9 Z^2,$$
(4.1)

where we can fix $s_9 = 1$ globally and with the monodromy divisor for the 2-section X = 0

$$\overline{D}_{2,X} = s_8^2 - 4s_5. (4.2)$$

In order to engineer an $\mathfrak{e}_6^{(2)}$ type of fiber over the base divisor $\mathcal{Z} := z = 0$, we treat the s_i of (4.1) as the generalization of the Tate coefficients in the quartic genus-one model. All of those sections are associated to certain line-bundles⁷ that are given in appendix B. Similarly

⁷Sometimes care has to be taken, that the s_i do not become constants. In such situations the multi-section may split into multiple one-sections and Abelian gauge enhancement may occur [45].

to the Tate-model, we engineer singularity by imposing certain vanishing orders of the s_i in codimension one. In order to do so, we factor powers of the line bundle z out of the s_i as

$$s_i \to d_i z^{n_i}$$
, such that $[d_i] \sim [s_i - n_i \mathcal{Z}]$, (4.3)

which characterises the singularity in the genus-one fiber at the vanishing locus of z. We package those vanishing orders into the generalized Tate-vector \vec{n} . For an elliptic fibration those singularities are classified, but for a genus-one model this remains an open problem.⁸ A toric classification has been given in [58] in terms of tops, introduced in [59] which we are using throughout this work. In this section it is our goal to engineer what we call a III^* non-split singularity that corresponds to an $\mathfrak{e}_6^{(2)}$ resolution, specified by the Tate vector

$$\vec{n} = \{3, 3, 2, 1, 0, 2, 1, 0\}$$
 (4.4)

Note that this factorization is specifically chosen such that the monodromy divisor (4.2) intersects \mathcal{Z} generically. The resolution (following [58]) is given via the following four additional coordinates g_1, g_2, k_1, l_1 given in the toric hypersurface⁹

$$p = d_1 f_2^3 g_2^2 h_1 X^4 + d_2 f_2^3 g_1^2 g_2^3 h_1^3 k_1^3 X^3 Y + d_3 f_2^2 g_1^2 g_2^2 h_1^2 k_1^2 X^2 Y^2 + d_4 f_2 g_1^2 g_2 h_1 k_1 X Y^3$$

$$+ d_5 g_1^2 Y^4 + d_6 f_2^2 g_1 g_2^2 h_1^2 k_1^2 X^2 Z + d_7 f_2 g_1 g_2 h_1 k_1 X Y Z + d_8 g_1 Y^2 Z + Z^2$$

$$(4.5)$$

which admits the following Stanley-Reisner ideal¹⁰

$$SRI: \{YX, Yf_2, Yg_2, Yh_1, Yk_1, Zg_1, Xg_1, Xg_2, Xh_1, Xk_1, f_2h_1, f_2k_1, g_2k_1\}.$$
 (4.6)

In our toric description, the base divisor \mathcal{Z} is then given via the projection

$$\pi: X_3: (f_2, g_1, g_2, h_1 k_1) \to \mathcal{Z} = f_2 g_2^2 h_1^3 k_1^4 g_2^2.$$
 (4.7)

The intersections of the fibral curves is depicted in figure 4. Note that we have highlighted when multiple curves are part of a fibral divisor, e.g. when the self-intersection is -4 instead of -2. E.g. the fibral intersection $D^{i,j} = D_i \cdot D_j$ and the Cartan matrix $\mathfrak{C}^{i,j} = -2\frac{D^{i,j}}{D^{ii}}$ is given as

$$D = \begin{pmatrix} -4 & 2 & 0 & 0 & 0 \\ 2 & -4 & 2 & 0 & 0 \\ 0 & 2 & -4 & 2 & 0 \\ 0 & 0 & 2 & -2 & 1 \\ 0 & 0 & 0 & 1 & -2 \end{pmatrix} \quad \text{and} \quad \mathfrak{C} = \begin{pmatrix} 2 & -1 & 0 & 0 & 0 \\ -1 & 2 & -1 & 0 & 0 \\ 0 & -1 & 2 & -2 & 0 \\ 0 & 0 & -1 & 2 & -1 \\ 0 & 0 & 0 & -1 & 2 \end{pmatrix}$$
(4.8)

Those fibral curves are given as the expressions

$$\mathbb{P}_{\pm,0}^{1} : \{p = f_{2} = 0\} : d_{5}g_{1}^{2} + d_{8}g_{1}Z + Z^{2}
\mathbb{P}_{\pm,1}^{1} : \{p = g_{2} = 0\} : d_{5}g_{1}^{2} + d_{8}g_{1}Z + Z^{2}
\mathbb{P}_{\pm,2}^{1} : \{p = h_{1} = 0\} : d_{5}g_{1}^{2} + d_{8}g_{1}Z + Z^{2}
\mathbb{P}_{3}^{1} : \{p = k_{1} = 0\} : d_{5}g_{1}^{2} + d_{1}h_{1} + d_{8}g_{1}Z + Z^{2}
\mathbb{P}_{4}^{1} : \{p = g_{1} = 0\} : 1 + d_{1}f_{2}^{3}g_{2}^{2}h_{1}.$$
(4.9)

⁸At present even a classification of genus-one fiber models and the range of possible N-sections is not known. The state of the art is the 5-section model presented in [37].

⁹See [34, 60] for a discussion of related techniques used here.

¹⁰Note that we have resolved the ambient space, such that the singular point X = Y = 0 is absent.

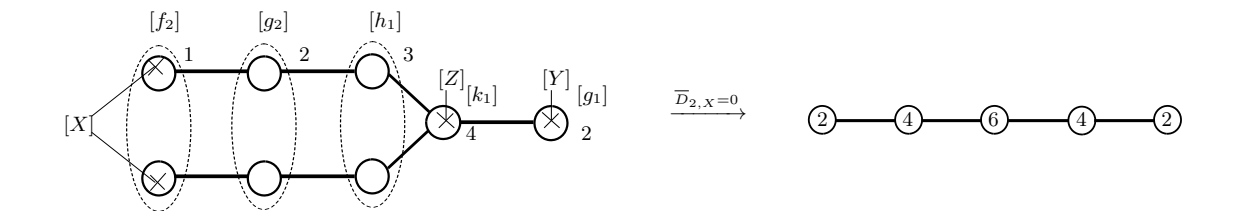


Figure 4. Depiction of the $\mathfrak{e}_6^{(2)}$ fiber. On the left, fibral divisors, curves, intersections and Kac labels are depicted. Crossing the 2-section monodromy divisor $\overline{D}_{2,X}$, interchanges the two fibral curves in $[f_2]$, $[g_2]$ and $[h_1]$. At $\overline{D}_{2,X} = 0$ the fiber degenerates into a multiplicity two fiber, depicted on the right.

Importantly inside of $\mathbb{P}^1_{\pm,j}$ with j=0,1,2 we find two curves that are interchanged along the monodromy divisor (4.2) of the 2-section X=0. This is also clear by inspection of the intersection picture given in figure 4. There we find that the 2-section X intersects each of the two curves of $\mathbb{P}^1_{\pm,0}$, inducing a monodromy action on the respective curves as well. From the intersection picture we find the affine Cartan matrix of $\mathfrak{e}^{(2)}_6$.

An important consequence for this type of geometries is the appearance of multiple fibers [22, 30, 61, 62]: these appear exactly at the smooth codimension two degeneration loci where the monodromy divisor $\overline{D}_{2,X} = 0$ intersects the base curve of the type III^* fiber \mathcal{Z} . In order to see this, recall that the generic fiber \mathcal{E} over \mathcal{Z} becomes reducible and degenerates into

$$[\mathcal{E}] \to [f_2] + 2[g_2] + 3[h_1] + 4[k_1] + 2[g_1],$$
 (4.10)

where the multiplicity factors are the respective Kac labels. Now at the codimension two intersection locus with $\overline{D}_{2,X} = 0$ the fibral curves in $[f_2], [g_2]$ and $[h_1]$ degenerate into a single curve of multiplicity two as depicted on the right side of figure 4. Hence the whole fiber becomes

$$[\mathcal{E}] \xrightarrow{\overline{D}_{2,X}=0} 2 \cdot ([f_2] + 2[g_2] + 3[h_1] + 2[k_1] + [g_1]),$$
 (4.11)

that is a non-reduced fiber of multiplicity two. Note again, that those multiplicity two fibers appear over smooth points in B_2 and hence are of very different kind than those discussed in [22, 30, 61, 62]. More generally, the presence of those multiple fibers implies that the group of CY torsors does not reduce to the TS group $\mathrm{III}(X^A/B_2)$ but the Weil-Châtalet group $WC(X^A/B_2)$ [28].

Similar degeneration structures also appear for non-simply laced groups, at the loci where two fibral curves are interchanged. The important difference in the present case is that this monodromy action can never involve a section, as these are just a single point. A section, in turn, must intersect a multiplicity one fibral curve, typically the affine node. Hence an elliptic fibration can never have a monodromy action on the affine node of some ADE fiber and therefore can only lead to untwisted algebras.

Having discussed the geometry of a non-trivial $WC(X^A/B_2)$ element we can discuss the geometry of the Jacobian $J(X^A/B_2)$. The singular Jacobian is obtained, by employing

the tuning as given by the generalized Tate-Vector in (4.4) and substituting it into the Jacobian map given in appendix B of [45]. To compare the fiber structures over \mathcal{Z} , we only give the relevant leading order Weierstrass coefficients as

$$f = z^3 d_1 \overline{D}_{2,X} + \mathcal{O}(z^4), \quad g = z^5 d_1 P_{(4d)} + \mathcal{O}(z^6), \quad \Delta = 4z^9 d_1^3 \overline{D}_{2,X}^3 + d_1^2 \mathcal{O}(z^{10}).$$
 (4.12)

Note that we find a type III^* fiber, just as in the genus-one geometry, i.e. an \mathfrak{e}_7 singularity. This may come as a surprise as one could have expected a IV^* split singularity here, i.e. an \mathfrak{e}_6 instead, as this is the field theory lift of an $\mathfrak{e}_6^{(2)}$ reduction. Instead the Jacobian yields the geometric cover of the twisted algebra. Interestingly the monodromy divisor of the genus one fibration appears at leading order of the discriminant in (4.12) and leads to local matter fields. Unlike in the genus-one fibration, we can not expect the monodromy divisor to lead to a non-simply laced type of group in the Jacobian, simply because E_7 does not possess an outer automorphism, only its affine extension does. Consequently we find the genus-one fibration and its Jacobian do not have the same number of Kähler moduli similar to the cases discussed in [20, 21, 47] which had multiple fibers as well. It appears that this may be a common feature in the presence of non-trivial Weil-Châtelet groups.

Note that we use the typical polynomial map from the genus-one fibration to the Jacobian, which might not see potential non-polynomial deformations. Indeed, such deformations are often times present, which we will discuss in section 7 in more detail.

4.2 Geometric state counting

Having discussed the difference in codimension one structure between the genus-one threefold and its Jacobian, we now compute the number of charged states for each geometry. We will focus in particular on those states that carry non-trivial representations under the maximal 5D finite sub-group $\mathfrak{f}_4 \subset \mathfrak{e}_6^{(2)}$ and ignore massive singlet states in the rest of this work. We wish to return for a complete discussion of all such states in future work.

State counting in the $\mathfrak{e}_6^{(2)}$ genus-one fibration. Having discussed the general features of the genus-one geometry, we turn now to the generic matter spectrum of the $\mathfrak{e}_6^{(2)}$ fibration. To do so, we first need to understand which line bundles the s_i , and upon tuning the d_i , are sections of. These are determined by the line bundles/divisor classes summarized in appendix B and tuning by the generalized Tate-Vectors in (4.3). From the resolved geometry as well as its Jacobian we find a non-minimal singularity over $z = d_1 = 0$ that exhibits a vanishing order $\operatorname{ord}_{\operatorname{van}}(f, g, \Delta) = (4, 6, 12)$. Those points are generally associated to superconformal matter, i.e. E-string theories associated with tensionless strings in the spectrum. To avoid further complications we use the line bundle class \mathcal{S}_7 dependency of $[d_1]$ to restrict to fibrations where such loci are absent by demanding

$$[z] \cdot [d_1] = 4c_1 \cdot \mathcal{Z} - 2\mathcal{S}_7 \cdot \mathcal{Z} - 3\mathcal{Z}^2 = 0.$$
 (4.13)

¹¹For non-simply laced groups, the monodromy divisor also appears at leading order in Δ but does not directly imply localized matter there.

In this way we can solve for the intersection $S_7 \cdot Z$, which yields the intersections

$$[d_8] \cdot \mathcal{Z} = S_7 \cdot \mathcal{Z} = 2c_1 \cdot \mathcal{Z} - \frac{3}{2}\mathcal{Z}^2 = 4(1-g) + \frac{1}{2}\mathcal{Z}^2, \tag{4.14}$$

with g being the genus of the curve $\mathcal{Z} \subset B_2$. Throughout this work we implicitly assume the base B_2 to be smooth and hence all base divisors to be Cartier [63] resulting in integral intersection numbers. It may therefore seem puzzling to find a factor $\frac{1}{2}$ factor in the intersection formula (4.14). However as we explicitly assumed a smooth base, we should view this ocurance rather as a geometric condition that forces \mathcal{Z}^2 to be an even self-intersection. This condition has also been found in [19]. In section 4.3 we give a physical interpretation of this phenomenon which is related to 56-plets that are not pseudo-real and must therefore appear in pairs of half-hypers.

To compute the multiplicity of BPS particles, charged under the physical gauge group inside $\mathfrak{e}_6^{(2)}$, we need to compute the moduli spaces of divisors D that collapse to curves \mathcal{Z} . The collapsing \mathbb{P}^1 's are wrapped by M2 branes in M-theory which yield states in the 5D theory. In order to do so we adopt the geometric framework pioneered in [64–66] and [46]. The main complication to consider is the monodromy under which the fibral \mathbb{P}^1 's are branched in the base. Before computing the exact moduli spaces we want to find the respective weights of the states. To do so we start with the covering algebra and then implement the monodromy in a second step. In our case, we have an \mathfrak{e}_7 cover and the M2 states that wrap those shrinkable curves form the adjoint representation. We write those curves schematically as $\mathcal{C} = \sum_i a_i \mathcal{C}_i$ for $i = 1 \dots 8$. The curves satisfy the $\mathcal{C}_i \cdot \mathcal{C}_j = -\mathfrak{C}_{i,j}(\mathfrak{e}_7^{(1)})$ being the affine Cartan matrix. In the following we write those curves graphical as

$$C = a_1 - a_2 < \frac{a_3 - a_4 - a_5}{a_6 - a_7 - a_8} \tag{4.15}$$

We can then generate the 126 curves with $a_i \ge 0$ and $C^2 = -2$ that generate the roots of \mathfrak{e}_7 following [46].

In the next step we implement the monodromy on the 126 curves. In order to do so, we need to decompose all curves into orbits under the \mathbb{Z}_2 action

$$\mathbb{Z}_2: \mathcal{C}_5 \leftrightarrow \mathcal{C}_8, \qquad \mathcal{C}_4 \leftrightarrow \mathcal{C}_7, \quad \mathcal{C}_3 \leftrightarrow \mathcal{C}_6,$$
 (4.16)

and group them into the invariant curves such as

$$\mathcal{C} = (\mathcal{C}_1, \mathcal{C}_2, \mathcal{C}_3 + \mathcal{C}_6, \mathcal{C}_4 + \mathcal{C}_7)_{(\mathcal{C}_5 + \mathcal{C}_8)}, \tag{4.17}$$

with the combination $C_5 + C_8$ denoting the affine curve. We have summarized this split in table 1 for several example curves. Shrinking all but the affine curve yields a maximal $\mathfrak{f}_4 \times \mathfrak{u}_{1,E} \in \mathfrak{e}_6^{(2)}$ sub-algebra. We can verify this explicitly when computing the representations and multiplicities of states obtained by M2 branes that wrap the collapsing fibral \mathbb{P}^1 's. First note that the moduli space of a degree d branched curve \overline{g} can be computed via the Riemann-Hurwitz (RH) theorem

$$\overline{g} - g = (d-1)(g-1) + \frac{1}{2}\deg(R).$$
 (4.18)

Mono	# Curves	Example Curve	\mathfrak{f}_4 weight	χ
Inv	24	$1 - 1 < \frac{0 - 0 - 0}{0 - 0 - 0}$	$(-1, -1, 2, 0)_0$	g
\mathbb{Z}_2	24	$1-1 < \frac{1-0-0}{0-0-0} + 1-1 < \frac{0-0-0}{1-0-0}$	$(-1,0,0,1)_0$	\overline{g}
\mathbb{Z}_2	24	$0-1 < \frac{1-0-0}{1-1-1} + 0-1 < \frac{1-1-1}{1-0-0}$	$(1,0,-1,1)_{-1}$	\overline{g}
\mathbb{Z}_2	3	$1-2 < \frac{2-1-1}{1-1-0} + 1-2 < \frac{1-1-0}{2-1-1}$	$(0,0,0,0)_1$	\overline{g}

Table 1. Schematic reduction of the 126 curves of \mathfrak{e}_7 roots into \mathbb{Z}_2 invariant linear combinations, their $\mathfrak{f}_4 \subset \mathfrak{e}_6^{(2)}$ charges and respective moduli spaces dimension χ computed in (4.20).

Here g denotes the genus of the curve $\mathcal{Z} \subset B_2$, d denotes the order of the cover and $\deg(R)$ the degree of the ramification. The degree $\deg(R)$ can be computed from the intersection of the monodromy divisor with \mathcal{Z} as

$$\deg(R) = [\overline{D}_{2,X}] \cdot [\mathcal{Z}] = 2[d_8] \cdot [\mathcal{Z}], \qquad (4.19)$$

given in (4.14) and in our case we have d=2. Putting it all together we get

$$\overline{g} - g = 3(1 - g) + \frac{1}{2} \mathcal{Z}^2.$$
 (4.20)

Now we can read off the associated 5D states, when the respective curves collapse. We first consider the shrinkable curves, given by those that admit trivial affine weight, depicted by the 24 + 24 curves in the first and second row of table 1. Upon including the four invariant Cartan generators those make up the **52**-dimensional adjoint representation of \mathfrak{f}_4 . In total those curves contribute a 5D vectormultiplet and g hypermultiplets in the adjoint representation [64].

Note that the moduli space of the of the 24 \mathbb{Z}_2 branched states, computed in (4.20) is \overline{g} -dimensional. Hence there are still $\overline{g} - g$ massless hypermultiplets that did not get paired up to the adjoint representation. Those left-over states are completed to 26_0 -plet charged hypermultiplets, upon adding two uncharged fields. The later ones are counted as complex structure deformations on the CY geometry (see section 7 for more details).

The other representations work similarly: there are 24 non-shrinkable curves that admit an affine charge and weights of the 26_1 with multiplicity \overline{g} . Note that two singlets from the last row in table 1 are needed to complete the 24 states to a full 26_1 -plet. Summarizing the hypermultiplet sector in terms of geometric data we then have

$$n_{\mathbf{52}_{0}} = g$$
,
 $n_{\mathbf{26}_{0}} = \overline{g} - g = 3(1 - g) + \frac{1}{2}Z^{2}$, (4.21)
 $n_{\mathbf{26}_{1}} = \overline{g} = 3(1 - g) + \frac{1}{2}Z^{2} + g$.

The residual charged singlets are given as

$$n_{\mathbf{1}_1} = \overline{g} = 3(1-g) + \frac{1}{2}\mathcal{Z}^2 + g.$$
 (4.22)

Note again that all fields, that have a non-trivial $\mathfrak{u}_{1,E}$ charge should be regarded as having a shifted KK-momenta and thus, stay massive at the origin of the \mathfrak{f}_4 Coulomb branch. Evidently, the above formula does not satisfy the 6D anomaly cancellation condition for an \mathfrak{f}_4 algebra by exactly one

$$n_{26_0} + n_{26_1} = 5(1-g) + \mathcal{Z}^2 + 1.$$
 (4.23)

As the 6D lift of the above theory is not an \mathfrak{f}_4 however there is no direct reason to expect such a cancellation to occur. In fact, in our construction we argue that the correct lift is given by the Jacobian, i.e. an \mathfrak{e}_7 theory with a matter spectrum that we will discuss momentarily. It is important to remark, that our results are different than the interpretation provided in [46, 61], where it was proposed that the maximal finite subgroup, \mathfrak{f}_4 in our case, would lift to 6D. It turns out however, that there do exist distinct but related geometries which exhibit $\mathfrak{f}_4^{(1)}$ fibers instead of $\mathfrak{e}_6^{(2)}$ that do lift to Jacobians with F_4 gauge symmetry in 6D, as we discuss in section 7.

Comparison with $\mathfrak{e}_6 \to \mathfrak{e}_6^{(2)}$ reduction. The typical way in which a 5D twisted theory with \mathfrak{f}_4 symmetry is obtained in the literature [7, 19, 67], is by starting from a 6D \mathfrak{e}_6 gauge theory and performing a twist by an outer automorphism (as in figure 2) when compactifying on a circle. In contrast to this, we find an \mathfrak{e}_7 theory in the Jacobian, instead of \mathfrak{e}_6 . Despite this difference however, we find the $\mathfrak{e}_6 \subset \mathfrak{e}_7$ subgroup to be acted upon as in the "usual" twisted reduction. In the following we show that the spectrum agrees between these two viewpoints.

To begin we will consider a 6D \mathfrak{e}_6 gauge theory. In order to make contact with our geometric formulas, we will express the number of 6D hypermultiplets in terms of the standard formulas that include the self-intersection and the genus g of the curve \mathcal{Z} that a stack of 7-branes with \mathfrak{e}_6 world-volume gauge theory wraps. Assuming a geometric engineering of such a symmetry in F-theory the massless hypermultiplet spectrum can be expressed as

$$n_{27} = 6(1-g) + \mathcal{Z}^2, \quad n_{52} = g.$$
 (4.24)

This 6D theory is the starting point for a twisted compactification. The \mathbb{Z}_2 twist σ appearing in (1.2) acts as the outer automorphism of \mathfrak{e}_6 by exchanging the two legs of the \mathfrak{e}_6 Dynkin diagram as shown in figure 2. This acts as complex conjugation on the representations

$$\sigma: \mathbf{27} \leftrightarrow \overline{\mathbf{27}}.$$
 (4.25)

Upon the S^1 reduction we impose σ twisted boundary conditions when going around the circle. This effectively shifts the KK-tower by a half-integer multiple and leaves a \mathfrak{f}_4 finite

sub-algebra in 5D. For an integer-spaced KK tower we obtain the decomposition of the adjoint [7, 19] as

$$78 \to 52_0 \oplus 26_{\frac{1}{2}}$$
, (4.26)

where the subscript denotes the shifted KK-charge. Since a 6D hyper contains a fundamental and its conjugate, we can take a pair of them and mod by the σ upon the circle reduction. This condition requires an even amount of 6D hypermultiplets which in terms of the F-theory geometry requires \mathcal{Z}^2 to be even. Note that this is exactly the geometric condition we found in the section before.¹² Decomposing a pair upon the σ -quotient one obtains

$$(\mathbf{27} \oplus \overline{\mathbf{27}}) \to (\mathbf{26}_0 \oplus \mathbf{26}_{\frac{1}{2}} \oplus \mathbf{1}_{\frac{1}{2}} \oplus \mathbf{1}_0). \tag{4.27}$$

The subscript denotes the shifted KK-mass of the fields. As discussed before, we expect those fields to stay massive, as e.g. the $26_{\frac{1}{2}}$ vectormultiplets. Collecting the multiplicities of 5D hypermultiplets in terms of the geometric data of the \mathfrak{e}_6 theory we find

$$n_{26_0} = 3(1-g) + \frac{1}{2}\mathcal{Z}^2, \qquad n_{26_{\frac{1}{2}}} = 3(1-g) + \frac{1}{2}\mathcal{Z}^2 + g, n_{1_{\frac{1}{2}}} = n_{1_0} = 3(1-g) + \frac{1}{2}\mathcal{Z}^2, n_{52_0} = g,$$

$$(4.28)$$

where we added the contribution of fundamentals from 6D adjoint hypermultiplets.

Upon rescaling the shifted KK-charges by two, to obtain the same charge normalization as used in our geometric derivation, we find full agreement of the multiplicities (4.21). Moreover, we also find a prediction for the amount of additional neutral singlets $n_{\mathbf{1}_0}$ in the geometry that we were not able to obtain from in the geometric computations. Those later ones we identify as complex structure moduli specific non-polynomial realized complex structure deformations, that we will discuss in more detail in section 7.

While the state counting coincides with those of a typical $\mathfrak{e}_6 \to \mathfrak{e}_6^{(2)}$ twisted reduction, the \mathfrak{e}_7 in the Jacobian suggests a potential different 6D uplift in our case. Note however, that the 6D \mathfrak{e}_7 is always Higgsable to the desired \mathfrak{e}_6 . Hence, it might be that the Jacobian map that we used in this work might somehow implicitly require those complex structure deformations to acquire non-trivial values and hence breaks $\mathfrak{e}_7 \to \mathfrak{e}_6$ in the Jacobian. As discussed in section 3 we expect the 6D \mathbb{Z}_2 twisting symmetry to be of more intricate origin in the elliptic fibered geometry. But as seen above, its action on the \mathfrak{e}_6 subgroup of \mathfrak{e}_7 must be consistent with that given above.

Another interesting distinction between the reduction proposed in this work and the standard \mathfrak{e}_6 construction is their relationships to the IIB axio-dilaton τ : as the genus-one fibration admits the same τ -profile as the Jacobian, the type III^* singularity fixes this value to $\tau = i$. An \mathfrak{e}_6 singularity on the other hand, fixes the coupling to $\tau = e^{-2\pi i/3}$ locally. In this regard, our construction with $\mathfrak{e}_6^{(2)}$ fibers seems to have a different 6D origin to the usual twisted reductions considered in the literature.

¹²Cases with unpaired matter have been considered in [68] and are not described by our geometric setup.

State counting in the $\mathfrak{e}_{7}^{(1)}$ Jacobian. Having analyzed the $\mathfrak{e}_{6}^{(2)}$ fibration, we turn now to its Jacobian given by the Weierstrass model in (4.12). For this we consider the codimension two enhancements of the Weierstrass model of the \mathfrak{e}_{7} divisor $\mathcal{Z}: z=0$ with the monodromy divisor $\overline{D}_{2,X}$ of the genus-one model. At those loci the vanishing orders enhance as

$$z = 0: \text{ ord}_{|\text{van}}(f, g, \Delta) = (3, 5, 9) \xrightarrow{\overline{D}_{2,X} = 0} \text{ ord}_{|\text{van}}(f, g, \Delta) = (4, 5, 10),$$
 (4.29)

i.e. from a type III^* to a type II^* singularity which corresponds to an E_8 . Those enhancement loci we associate with **56**-plet representations. Note that the multiplicity of those states is precisely given by the number of ramification points in the genus-one fibration

$$n_{56} = 2 \cdot [d_8] \cdot \mathcal{Z} = deg(R) = 8(1 - g) + \mathcal{Z}^2,$$
 (4.30)

consistent with the 6D anomalies. Next we should infer the \mathbb{Z}_2 charges of the \mathfrak{e}_7 fundamentals. In order to do so, we would typically use the genus-one fibration and uplift the 5D shifted $\mathrm{U}(1)_E$ charges to discrete ones in 6D. As the genus-one fibration admits a very different 5D gauge group however, we can not use this approach here. In fact, the following two charge assignments are consistent with the pseudo-reality of the states

$$\mathbf{56}_q \text{ with } q = 0, 1 \mod 2.$$
 (4.31)

This is still a non-trivial charge assignment, as there could have been a non-trivial mixing of the \mathbb{Z}_2 discrete gauge symmetry, with the center of \mathfrak{e}_7 , which have lead to fractional charges that are not compatible with the pseudo reality, as we demonstrate in the next sections. It would be interesting however to deduce those discrete charges from first principles.

Toric examples. To be fully concrete, we give explicit toric examples. For the first one, we specify the toric rays that make up the 4D ambient variety in appendix A: the example is a genus-one fibration on an \mathbb{F}_0 base, with an $\mathfrak{e}_6^{(2)}$ on a $\mathbb{Z}^2 = 0$ curve of genus g = 0. The Hodge numbers are computed as

$$(h^{1,1}, h^{2,1}(h_{np}^{2,1}))(X^C) = (7, 95(9)).$$
 (4.32)

We have also added the $h_{np}^{2,1}$ non-polynomial contribution of the complex structure deformations, that we will discuss in more detail in section 7. The resulting 5D theory admits $3 \times 26_0 \oplus 3 \times 26_1$ -plets in its spectrum. The spectrum also contains several I_2 fibers and 95 uncharged singlets. We will not discuss those charged singlets but comment on the 95 complex structures via a Higgs transition in the next section. As expected, we find three Kähler parameters from generic fiber and Hirzebruch base as well as four more from the $\mathfrak{e}_6^{(2)}$.

Consulting the general expressions for the spectrum in (4.28), we find the possibility for a 5D theory with a trivial Higgs branch, i.e. a trivial hypermultiplet spectrum for g = 0 and $\mathcal{Z}^2 = -6$. Indeed, we can engineer a simple toric example, where the genusone fibration has an \mathbb{F}_6 base as given in table 2. The associated threefold \hat{X}^C admits

$X \mid (-1, 1, 0, 0) \mid v_0 \mid (-4)$,	(-5, -2, 0, -2)
$\begin{vmatrix} Y & (-1, -1, 0, 0) \\ Z & (1, 0, 0, 0) \end{vmatrix} \begin{vmatrix} y_1 & (-1)^2 & (-1)^2 \\ y_1 & (-1)^2 & (-1)^2 \end{vmatrix}$	$[0, -10, 1, 0)$ h_1	(-5, -1, 0, -2) (-7, -2, 0, -3) (-9, -3, 0, -4)

Table 2. The toric rays, of an $\mathfrak{e}_6^{(2)}$ genus-one fibration \hat{X}^C over a \mathbb{F}_6 base with f_2 being the affine node.

Hodge numbers

$$(h^{1,1}, h^{2,1}(h_{np}^{2,1}))(\hat{X}^C) = (7, 151(0)).$$
 (4.33)

The structure of the fibration can be readily be read off from the structure of the toric vertices: the \mathbb{F}_6 base is given via the projection onto the last two coordinates of each ray. The identification of base rays are

$$\{x_1; y_0; y_1; f_2, g_1, g_2, h_1, k_1\} \xrightarrow{\pi} \{\hat{x}_1; \hat{y}_0; \hat{y}_1; \hat{x}_0\} \text{ with } \hat{x}_0 = f_2 g_1^2 g_2^2 h_1^3 k_1^4.$$
 (4.34)

The base curves $D_{\hat{y}_i}$ are the respective 0-curves while $D_{\hat{x}_1}$ is the +6 curve and we identify $\mathcal{Z} = D_{\hat{x}_0} : \hat{x}_0 = 0$ as the -6 curve. This example is significant for various reasons: first, it has a trivial \mathfrak{f}_4 charged hypermultiplet spectrum, i.e. a trivial Higgs branch, analogously to the Non-Higgsable cluster theories. Second, this 5D theory makes it clear, that this theory can not be uplifted to 6D with an \mathfrak{f}_4 gauge theory, as the -6 self-intersection would make it impossible to satisfy the 6D gauge anomalies.

4.3 Transitions to $\mathfrak{e}_6^{(2)}$

Another way to understand various 6D and 5D theories is to connect them via geometric transitions. In the following we will carry this out for the $\mathfrak{e}_6^{(2)}$ fibration and its Jacobian. These geometric transitions typically map to chains of Un/Higgsings in the effective theories. We can therefore learn a lot about the (change of) degrees of freedom in the various theories by moving in a larger moduli space. In particular we want to discuss the relationship between the twisted affine fibration and an untwisted one. Hence we need to consider tunings in the complex structure moduli space that result in an unfolding of the fibers and match the geometric quantities to the associated 5D states. Our starting point is therefore a tuning of the geometry that introduces a section to the genus-one fibration such that it becomes birationally equivalent to the Jacobian fibration. This gives us a useful starting point from which we can follow the branching structure in 5D towards the phase with the twisted $\mathfrak{e}_6^{(2)}$.

For this we recall the critical role of the monodromy divisor $\overline{D}_{2,X}$ and its intersection with the curve \mathcal{Z} in the base to produce the affine folding. To unfold the geometry we thus have two options:

1. Tuning the monodromy divisor, such that it does not intersect \mathcal{Z} anymore, resulting in an un-folded genus one fibration with $\mathfrak{e}_7^{(1)}$ fiber. This model might correspond to

the generalized Tate-tuning

$$\vec{n} = \{3, 3, 2, 1, 1, 2, 1, 0\}$$
 (4.35)

2. Tuning the geometry to an elliptic fibration results in a complete removal of the monodromy divisor and adding a two sections via the generalized Tate-vector

$$\vec{n} = \{3, 3, 2, 1, -, 2, 1, 0\} \text{ for } \mathfrak{e}_7^{(1)}.$$
 (4.36)

Here the entry "-" refers to setting the coefficient d_5 to zero globally. Doing so splits the monodromy divisor into a perfect square

$$\overline{D}_{2,X} \xrightarrow{d_5 \to 0} d_8^2$$
. (4.37)

In the following we will discuss a chain of transitions, that will go through both phases. For ease of exposition we start from the tuning to an elliptic fibration, i.e. the second type of tuning.

The $\mathfrak{e}_7^{(1)} \times \mathfrak{u}_1$ model. Using the tuning in eq. (4.36) we obtain a Morrison-Park type of U(1) model. The singular model can directly be mapped into the birational Weierstrass model where we find at leading orders

$$f = z^3 d_1 d_8 + \mathcal{O}(z^4), \qquad g = z^5 d_1 p_4(d_i) + \mathcal{O}(z^6), \qquad \Delta = z^9 d_1^3 d_8^6 + \mathcal{O}(d_1^2 z^{10}).$$
 (4.38)

We can directly infer the gauge group and matter structure from the above model. We find two discriminant components. The first component is given by $z = d_1 = 0$. This is a (4,6) locus which we have tuned to zero via the specialization given in (4.13). The second component is a (4,5,10) locus at $z = d_8 = 0$ where we find matter in the **56** representation which admits a non-trivial charge under the additional $U(1)_{6D}$. By resolving the full geometry, we can compute its charge directly. The $U(1)_{6D}$ symmetry is associated to the higher rank Mordell-Weil group of the geometry which is generated by the two 1-sections

$$s_0: X = 0 \quad \text{and} \quad s_1: e_1 = 0,$$
 (4.39)

as reviewed in section 2. The fully resolved model is then given as the hypersurface

$$p = d_1 f_2^3 f_4^2 g_2^2 g_3 h_1 X^4 e_1 + d_2 f_2^3 f_4^2 g_1^2 g_2^3 g_3^2 h_1^3 h_2^2 l_1^3 X^3 Y e_1^2 + d_3 f_2^2 f_4 g_1^2 g_2^2 g_3 h_1^2 h_2 l_1^2 X^2 Y^2 e_1$$

$$+ d_4 f_2 g_1^2 g_2 h_1 l_1 X Y^3 + d_6 f_2^2 f_4^2 g_1 g_2^2 g_3^2 h_1^2 h_2^2 l_1^2 X^2 Z e_1^2 + d_7 f_2 f_4 g_1 g_2 g_3 h_1 h_2 l_1 X Y Z e_1$$

$$+ d_8 g_1 Y^2 Z + f_4 g_3 k_2 Z^2 e_1 ,$$

$$(4.40)$$

with the Stanley-Reisner ideal

$$SRI = \{XY, e_1Y, f_2Y, f_4Y, g_2Y, g_3Y, k_1Y, h_1Y, h_2Y, XZ, f_2Z, g_1Z, g_2Z, k_1Z, h_1Z, g_1X, e_1g_1, f_4g_1, g_1g_3, g_1h_2, f_4X, g_2X, g_3X, k_1X, h_1X, h_2X, e_1g_2, e_1g_3, e_1k_1, e_1h_1, e_1h_2, f_2g_3, f_2k_1, f_2h_1, f_2h_2, f_4k_1, f_4h_2, g_2h_2, h_1h_2, g_2g_3, g_2k_1\}.$$

$$(4.41)$$

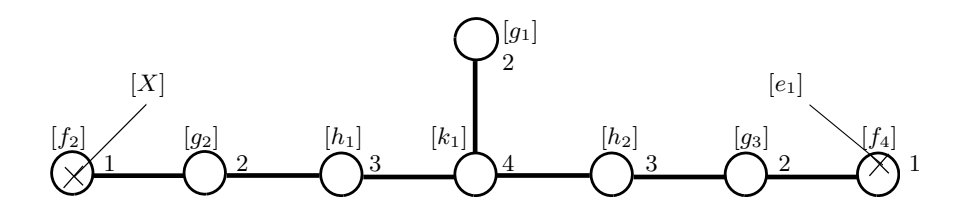


Figure 5. Depiction of the $\mathfrak{e}_7^{(1)}$ fiber and their corresponding fibral divisors. Depicted are also the two section X = 0 and $e_1 = 0$ that intersect the affine and fundamental node respectively.

The fibral divisors f_2 , f_4 , g_1 , g_2 , g_3 , h_1 , h_2 , l_1 resolve the fibral singularity fully and exhibit an intersection picture as depicted in figure 5. The fibral divisors intersect like the affine $\mathfrak{e}_7^{(1)}$ -Cartan matrix as expected, with ordering as

$$\frac{(g_1)}{(f_2)(g_2)(h_1)(k_1)(h_2)(g_3)(f_4)} = \frac{(\alpha_7)}{(\alpha_0)(\alpha_6)(\alpha_5)(\alpha_4)(\alpha_3)(\alpha_2)(\alpha_1)}.$$
 (4.42)

The intersection picture is relevant as the additional section s_1 intersects the fundamental node α_1 of the $\mathfrak{e}_7^{(1)}$ fiber. This signals a non-trivial mixing of the $\mathrm{U}(1)_{6D}$ with the center of \mathfrak{e}_7 which yields the global gauge group

$$G_{6D} = \frac{E_7 \times \mathrm{U}(1)_{6D}}{\mathbb{Z}_2} \,.$$

This is clear, when writing the U(1) generator in terms of the orthogonal divisors. First we note that the naive U(1) generator is generated by the difference of the sections $[e_1] - [X]$. However, this combination is not properly orthogonalized with respect to f_4 , that is the fundamental node α_1 . We thus must therefore orthogonalize the U(1)_{6D} properly by taking the linear combination of fibral divisors

$$\sigma(s_1) = [e_1] - [X] + \frac{1}{2} \underbrace{\sum_{W_C} b_i \alpha_i}_{W_C}, \quad \text{with } b_i = \{3, 4, 5, 6, 4, 2, 3\},$$
 (4.43)

to obtain the actual $U(1)_{6D}$ that is orthogonal to the \mathfrak{e}_7 . The important point is that the linear combination W_C corresponds to the \mathbb{Z}_2 center generator of E_7 . Hence its appearance in the $U(1)_{6D}$ generator implies a global shift by a \mathbb{Z}_2 center values [13, 69] of E_7 . Note that the above configuration admits also a \mathbb{Z}_2 symmetry when interchanging the two sections¹³ and reordering the fibral divisors:

$$\omega: \quad \alpha_0 \leftrightarrow \alpha_1, \alpha_6 \leftrightarrow \alpha_2, \alpha_3 \leftrightarrow \alpha_4 \quad \text{and} \quad s_0 \leftrightarrow s_1.$$
 (4.44)

$$\omega : \sigma(\widetilde{s_1}) = \sigma(\widetilde{s_1}) + \Delta$$

upon relabeling roots and zero-section. The difference term $\Delta = 2(s_0 - s_1) + \frac{3}{2}(\alpha_1 - \alpha_0) + (\alpha_6 - \alpha_2) + \frac{1}{2}(\alpha_5 - \alpha_3)$ vanishes upon the identification of the four classes that are related via the folding procedure.

¹³Similarly, one can obtain the dual Shioda map

From this perspective we directly see that a fundamental **56** must have a $\frac{1}{2}$ -fractional charge under the U(1)_{6D}. Clearly, the U(1)_{6D} get conjugated upon exchanging the Shioda map generator. Hence we have constructed a concrete geometric realization of the section-interchange symmetry, discussed in section 3.2. This can be verified by investigating the explicit degeneration locus of the E_7 fiber over $d_8 = 0$, where **56**-plet states reside. Their charges and multiplicities can then be computed as

$$n_{\mathbf{56}_{\frac{1}{2}}} = 4(1-g) + \frac{1}{2}Z^2,$$
 (4.45)

which we have expressed in terms of geometric intersection numbers. Note that this might look puzzling at first: as **56**-plets are pseudo-real, one typically obtains half-hypermultiplts in 6D. In our case the **56**-plets carry $U(1)_{6D}$ charge and hence renders the states not pseudo-real anymore. We therefore expect to find full hypermultiplets, which is exactly accounted for by the multiplicity formula (4.45).

In an example model over an \mathbb{F}_0 base given in appendix A.2 we find the Hodge numbers

$$(h^{1,1}, h^{2,1})(X^A) = (11, 59). (4.46)$$

We identify the Kähler moduli as the eight from the gauge group and three from the fiber and base respectively. We then identify

$$\mathcal{Z} \sim H_1, \qquad \mathcal{S}_9 \sim 2H_2, \qquad (4.47)$$

and $c_1 \sim 2H_1 + 2H_2$ where $H_{1,2}$ are the hyperplane classes in \mathbb{F}_0 . Using the divisor classes given in appendix B and (4.36) we can then identify $[d_4] \sim 3H_1 + 6H_2$ and $[d_8] \sim 2H_1 + 4H_2$. This allows us to deduce the 6D/5D F/M-theory spectrum which includes the following matter

$$H = 4 \cdot \mathbf{56}_{\frac{1}{2}} \oplus 24 \cdot \mathbf{1}_{2} \oplus 70 \cdot \mathbf{1}_{1} \oplus 60 \cdot \mathbf{1}_{0}, \qquad T = 1, \qquad V = \mathbf{133} \oplus \mathbf{1}.$$
 (4.48)

The $\mathfrak{e}_{7}^{(1)}$ genus-one model. The next step in the chain towards the $\mathfrak{e}_{6}^{(2)}$ theory is to remove the sections. This can be done via a conifold transition which does not affect the $\mathfrak{e}_{7}^{(1)}$ fiber but only the additional $U(1)_{6D}$ part as reviewed in section 2.2. From a geometric point of view, we simply change the generic fiber structure from an $Bl^{1}\mathbb{P}_{112}^{2}$ to \mathbb{P}_{112}^{2} which does not affect the E_{7} fiber itself. This is associated to a Higgsing on a field which is a hypermultiplet with charges $\mathbf{1}_{2}$ and a non-trivial KK charge. The resulting resolved genus-one fibration X^{B} is given via the hypersurface

$$\begin{split} p &= d_1 f_2^3 f_4^2 g_2^2 g_3 h_1 X^4 + d_2 f_2^3 f_3 f_4^2 g_1^2 g_2^3 g_3^2 h_1^3 h_2^2 k_1^3 X^3 Y + d_3 f_2^2 f_3 f_4 g_1^2 g_2^2 g_3 h_1^2 h_2 k_1^2 X^2 Y^2 \\ &\quad + d_4 f_2 g_1^2 g_2 h_1 k_1 X Y^3 + d_5 f_2 g_1^4 g_2^2 g_3 h_1^3 h_2^2 k_1^4 Y^4 + d_6 f_2^2 f_4^2 g_1 g_2^2 g_3^2 h_1^2 h_2^2 k 1^2 X^2 Z \\ &\quad + d_7 f_2 f_4 g_1 g_2 g_3 h_1 h_2 k_1 X Y Z + d_8 g_1 Y^2 Z + d_9 f_4 g_3 h_2 Z^2 \,, \end{split} \tag{4.49}$$

with the following Stanley-Reisner ideal

$$SRI: \{YX, Yf_2, Yf_4, Yg_2, Yg_3, Yh_1, Yh_2, Yk_1, Zf_2, Zg_1, Zg_2, Zh_1, Zk_1, k_1h_1, Xg_1, f_4g_1, g_1g_3, g_1h_2, Xg_2, Xg_3, Xh_1, Xh_2, Xk_1, f_4h_1, f_4h_2, f_4k_1, f_2g_3, f_2h_1, f_2h_2, f_2k_1, g_2h_2, g_3k_1, g_2k_1\}.$$

$$(4.50)$$

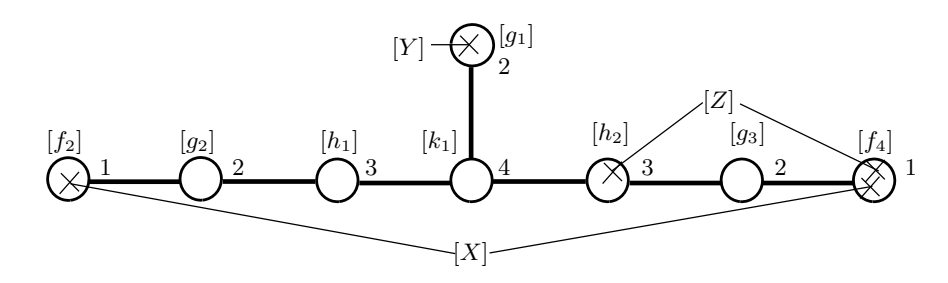


Figure 6. Depiction of the $(E_7 \times \mathbb{Z}_4)/\mathbb{Z}_2$ Dynkin diagram obtained by unfolding $\mathfrak{e}_6^{(2)}$. We depict the divisor classes of the respective \mathbb{P}^1 's as well as their Dynkin multiplicity and intersections with the two sections [X] and [Y] as well as the 4-section [Z]. The affine node is given by the fibral curve at $f_2 = 0$.

Note that the fiber model is the quartic model which we obtain by adding the monomials d_5Y^4 after removing the MW generator given by the divisor $e_1 = 0$. The intersection picture is summarized in figure 6 which yields the expected $\mathfrak{e}_7^{(1)}$ shape. As a result of the conifold, the two 1-sections s_0 and s_1 of the Morrison-Park model have merged into a single 2-section $s_0^{(2)}: X = 0$ that maintains their intersections with the fiber as shown in figure 6. However as we identify the class of the 2-section with the generator of generic fiber class which contains the $\mathfrak{u}_{1,KK}$ we find that it is not orthogonalized to the \mathfrak{e}_7 fibral divisors. This is not surprising when recalling that the 5D U(1)_E is a linear combination of KK U(1) and the massive $\mathfrak{u}_{1,6D}$ which mixed with the center of E_7 . Hence the orthogonalized 2-section analog in the genus-one fibration is given as

$$\sigma(s_0^{(2)}) = [X] + \frac{1}{2}W_C, \qquad (4.51)$$

shifted by the same center Wilson line combination W_C as in (4.43). In the above linear combination we have fixed the $\mathfrak{u}_{1,E}$ charges and its mixture with the KK-tower. E.g. since X=0 is a two-section we have

$$\sigma(s_0^{(2)})[T^2] = 2. (4.52)$$

Thus an M2 brane state that wraps the a fibral curve and the generic torus n times yields 5D particle with $\mathfrak{u}_{1,E}$ charges q+2n. The above structure is in fact useful to deduce the discrete charges q in the 6D (and Jacobian) compactification as we discuss next.

Shrinking all nodes but the affine f_2 we can map the configuration into the Jacobian, i.e. the singular Weierstrass form. At leading order in z we still find the form to be given as (4.38).

In the following we investigate the locus of the \mathfrak{e}_7 fundamentals (inside $d_8 = 0$) in a bit more detail. In order to discuss the degeneration at this codimension two locus we list all eight fibral curves of $\mathfrak{e}_7^{(1)}$ in detail as

$$\mathbb{P}_{\alpha_0} : f_2 = 0 = d_9 f_4 + d_8 g_1 ,$$

$$\mathbb{P}_{\alpha_1} : f_4 = 0 = d_4 f_2 g_2 + d_5 f_2 g_2^2 g_3 + d_8 Z ,$$

$$\mathbb{P}_{\alpha_2} : g_3 = 0 = d_4 g_2 h_1 k_1 + d_8 Z ,$$

$$\mathbb{P}_{\alpha_3} : h_2 = 0 = d_1 g_3 + d_4 k_1 + d_8 Z,
\mathbb{P}_{\alpha_4} : k_1 = 0 = d_8 g_1 + d_1 g_3 h_1 + d_9 g_3 h_2,
\mathbb{P}_{\alpha_5} : h_1 = 0 = d_8 g_1 + d_9 g_3,
\mathbb{P}_{\alpha_6} : g_2 = 0 = d_8 g_1 + d_9 f_4 g_3,
\mathbb{P}_{\alpha_7} : g_1 = 0 = 1 + d_1 f_2^3 g_2^2 h_1.$$
(4.53)

Some curves above become reducible when imposing $d_8 = 0$ where curves split as

$$\mathbb{P}^{1}_{\alpha_{i}} \xrightarrow{d_{8}=0} \sum_{i} \mathbb{P}^{1}_{i,j}. \tag{4.54}$$

Indeed, we find the curves to degenerate into 9 distinct curves with an intersection structure which resembles the affine E_8 Dynkin diagram as given in figure 7. This is in fact also what we expect from the Jacobian, which highlights again the close connection between the two (non-birational equivalent) geometries.

We can use the resolved geometry to deduce the properties of the 5D theory on the Coulomb branch. We do so by considering M2 branes that wrap the reducible fibral curves and compute their charges under the Cartan subalgebra. This allows us to compute E_7 weights and $U(1)_E$ charges by considering the following set of intersections

$$(f_4, g_4, h_2, k_1, h_1, g_2, g_1 | f_2)_{\sigma(s_n^2)} \cdot \mathbb{P}^1_{i,j}$$
 (4.55)

We pick two of the reducible curves, given in figure 7 and compute the intersections

$$\mathbb{P}^{1}_{1,1}: \qquad (-1,1,0,0,0,-1,0|1)_{\left(\frac{1}{2}\right)}, \tag{4.56}$$

$$\mathbb{P}^1_{2,1}: (1,-1,0,0,1,-1,0|1)_{(\frac{1}{2})}.$$
 (4.57)

Note that we have also highlighted non-trivial charges under the affine node f_2 , which is non-trivial for both curves. The above charges are weights of an **56** representation with $\mathfrak{u}_{1,E}$ charges $q=\frac{1}{2}$ as expected.

When taking the singular limit, the above genus-one fibration admits the 5D gauge group $G_{5D} = (E_7 \times \mathrm{U}(1)_E)/\mathbb{Z}_2$. The global shift by W_C effectively mixes the E_7 center with $\mathrm{U}(1)_E$ similar to the case of the Shioda map [51]. This non-trivial global structure lifts in a non-trivial way to the 6D theory as the $\mathfrak{u}_{1,E}$ contains the massive $\mathfrak{u}_{1,6D}$ and in particular its discrete remnant. Recall that the 6D theory is obtained from the Higgsing on a $\mathfrak{1}_2$ state, which breaks the $\mathfrak{u}_{1,6D}$ to a \mathbb{Z}_2 subgroup. The non-trivial center mixing however changes this group to

$$G_{5D} = (E_7 \times \mathrm{U}(1)_E)/\mathbb{Z}_2 \xrightarrow{\text{F-theory lift}} G_{6D} = \frac{E_7 \times \mathbb{Z}_4}{\mathbb{Z}_2},$$
 (4.58)

(see [70] for related effects). This global structure is compatible with the 6D charge assignment

$$\mathbf{56}_{\frac{1}{2}}, \quad \mathbf{1}_{1},$$
 (4.59)

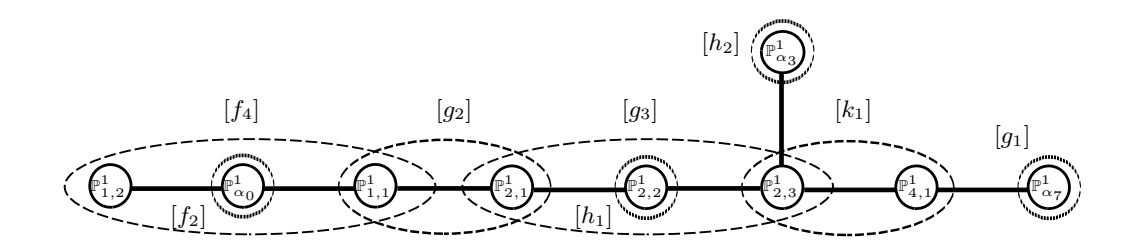


Figure 7. The fiber structure over \mathcal{Z} and $d_8 = 0$ where $\mathbf{56}_{\frac{1}{2}}$ matter resides. The fiber admits an E_8 structure consistent with the expectation of the Jacobian.

given that they are taken mod 2, even though that the \mathfrak{e}_7 fundamentals have a fractional charge. Furthermore these discrete charges make clear that the \mathfrak{e}_7 fundamentals are not pseudo-real and thus not half hypermultiplets, consistent with the count of their multiplicities (4.45).

When performing the transition from X^A to X^B as shown in figure 8, the U(1) generator gets eaten by the $\mathbf{1}_2$ Higgs fields. The remaining degrees of freedom of the same charge become neutral singlets. This can be seen in the example geometry, which admits Hodge numbers

$$(h^{1,1}, h^{2,1})(X^B) = (10, 82). (4.60)$$

Note the decrease in Kähler parameters in X^B compared to X^A (see (4.46)) agrees with the breaking of U(1)_{6D} and the enhancement of 23 complex structure parameters can be explained by the 24 $\mathbf{1}_2$ fields.

Transition to \mathfrak{e}_6^{(2)}. The geometry X^B provides a key step in our goal of engineering a transition to the $\mathfrak{e}_6^{(2)}$ fibration. In terms of the singular geometries this is due to the fact that the order two monodromy divisor does not intersect the \mathfrak{e}_7 singularity, while it does in the $\mathfrak{e}_6^{(2)}$. This can also be observed by comparing the vanishing orders in the two relative singular genus-one geometries (i.e. one can compare the Tate-vectors in (4.4) with (4.35)). The $\mathfrak{e}_6^{(2)}$ leaves the monodromy divisor invariant, while the \mathfrak{e}_7 tuning does not.

In the following we want to discuss the geometric transition and match it to the 5D field theory. The two types of states of relevance, are the scalars in the 5D vector multiplets, that break the theory to a (partial) Cartan subgroup and parametrize the Coulomb branch, and the $\mathbf{56}_{\frac{1}{2}}$ -plets whose VEV parametrize the Higgs branch of the \mathfrak{e}_7 theory. A straight forward way to obtain the \mathfrak{f}_4 theory from \mathfrak{e}_7 , is via the non-Levi type branching as given as

$$e_7 \times \mathfrak{u}_{1,E} \to \mathfrak{f}_4 \times \mathfrak{su}_2 \times \mathfrak{u}_{1,E} \to \mathfrak{f}_4 \times \widehat{\mathfrak{u}}_{1,E},$$
 (4.61)

which can be attributed to a VEV in the $(1,4)_{\frac{1}{2}} \in \mathbf{56}_{\frac{1}{2}}$. This however raises an immediate puzzle: in order to trigger the Higgsing on the $\mathbf{56}_{\frac{1}{2}}$ -plets, we require those fields to be massless.

Those states however admit a $\mathfrak{u}_{1,E}$ charge, and hence one expects them to admit a non-trivial mass, proportional to the $\mathfrak{u}_{1,E}$ Coulomb branch parameter. As the $\mathfrak{u}_{1,E}$ Coulomb branch parameter is proportional to the inverse of the 6D circle radius. It cannot be taken

to zero size at finite distance in the moduli space.¹⁴ However, the fact that we can perform an infinitesimal deformation in complex structure moduli space to go from the singular X^B geometry to X^C suggests that those states should be massless.

We do not resolve the above puzzle here, instead we bypass it by a different mechanism to obatin a massless Higgs field. Instead of a simple complex structure deformation in the singular limit, we first move on the 5D Coulomb branch by performing a particular resolution of the singular fiber. Thus we break the gauge algebra to $\mathfrak{e}_7 \to \mathfrak{e}_6 \times \mathfrak{u}_1$ which then will allow us to obtain massless states, that can be given a vev.

In geometry this branch corresponds to only shrinking the \mathfrak{e}_6 sub-diagram inside of the affine $\mathfrak{e}_7^{(1)}$ given in figure 6, keeping the affine and fundamental nodes at finite sizes. The resulting 5D theory admits an $\mathfrak{e}_6 \times \mathfrak{u}_{1,A} \times \mathfrak{u}_{1,E}$ gauge algebra and the \mathfrak{e}_7 representations decompose as

$$\mathbf{133}_{0} \to \mathbf{78}_{0,0} \oplus \mathbf{27}_{\frac{2}{3},0} \oplus \overline{\mathbf{27}}_{-\frac{2}{3},0} \oplus \mathbf{1}_{0,0}, \mathbf{56}_{\frac{1}{2}} \to \mathbf{27}_{-\frac{1}{3},\frac{1}{2}} \oplus \overline{\mathbf{27}}_{\frac{1}{3},\frac{1}{2}} \oplus \mathbf{1}_{-1,\frac{1}{2}} \oplus \mathbf{1}_{1,\frac{1}{2}}.$$

$$(4.62)$$

As expected only 5D states with trivial $\mathfrak{u}_{1,A} \times \mathfrak{u}_{1,E}$ charges are massless which again is not possible at a generic point in moduli space. The masses of the resulting particles becomes

$$m_{\mathbf{27}_{-\frac{1}{3},\frac{1}{2}}} = \left| -\frac{1}{3}\xi_A + \frac{1}{2}\tau \right|.$$
 (4.63)

Hence when taking the linear combination

$$\hat{\mathfrak{u}}_{1,E} = \frac{3}{2} \mathfrak{u}_{1,A} - \mathfrak{u}_{1,E} \,, \tag{4.64}$$

there is a combined CB parameter

$$\hat{\xi} = \frac{3}{2}\xi_A - \xi_E \,. \tag{4.65}$$

Setting $\hat{\xi} = 0$ makes the $27_{-\frac{1}{3},\frac{1}{2}}$ plets massless. Now we are in the position to give those states a vev and break the gauge symmetry. The resulting gauge theory breaking is then given as $\mathfrak{e}_6\mathfrak{u}_{1,A} \times \mathfrak{u}_{1,E} \to \mathfrak{f}_4 \times \hat{\mathfrak{u}}_{1,E}$. Note that the $\mathfrak{e}_6 \to \mathfrak{f}_4$ folding inside of the \mathfrak{e}_7 resembles nicely the geometry action of the $\mathfrak{e}_7^{(1)} \to \mathfrak{e}_6^{(2)}$ fiber. After collecting the charges under the massless \mathfrak{u}_1 generator, we can obtain the multiplicities of the massless \mathfrak{f}_4 BPS states in terms of the \mathfrak{e}_7 ones as

$$n_{26_0} = n_{56_{1/2}} + n_{133_0} - 1, (4.66)$$

which matches the geometric computation. Similarly, the massive 26_1 plets are given as

$$n_{26_1} = n_{56_{1/2}} + 2n_{133_0}. (4.67)$$

The above expression however, deviates from the geometric computation of 26_1 multiplicities, performed in the $\mathfrak{e}_6^{(2)}$ theory by over counting by one. This suggests that one more massive field should decouple in the transition. It would be interesting to investigate this miss-match in future work.

¹⁴Recall that Higgsing from the $\mathfrak{e}_7 \times \mathfrak{u}_{1,6D}$ theory has fixed the U(1)_{6D} Coulomb branch parameter to $\xi_{6D} = \tau/2$. This also implies that $\mathbf{56}_{\frac{1}{2}}$ must be massive at the origin of the \mathfrak{e}_7 Coulomb branch as well.

We can proceed similarly with the $\hat{\mathfrak{u}}_{1,E}$ -charged singlets. However we want to focus in particular on the change of neutral singlets $\mathbf{1}_0$, as those contribute to the change in complex structure moduli $h^{2,1}$ which is easy to match across the transition. E.g. there are neutral fields $2\mathbf{7}_{-\frac{1}{3},\frac{1}{2}} \to 2\mathbf{6}_0 \oplus \mathbf{1}_0$ upon the breaking to $\mathfrak{f}_4 \times \hat{\mathfrak{u}}_{1,E}$ that contribute uncharged singlets to the geometry. However further singlet contributions are more subtle and deserve a more detailed discussion: recall that the shifted KK symmetry is given as $\mathfrak{u}_{1,E} = \mathfrak{u}_{1,6D} - 2\mathfrak{u}_{1,KK}$. Thus before Higgsing, a singlet state with charges $\mathbf{1}_{-1,\frac{1}{2}} \in \mathbf{56}_{\frac{1}{2}}$ under $\mathfrak{u}_{1,A} \times \mathfrak{u}_{1,E}$ is accompanied with a KK-tower $\mathbf{1}_{-1,\frac{1}{2}+2n}$ having KK momenta n. Upon the Higgs transition such singlet towers therefore change into of $\mathbf{1}_{-2+2n}$ under the unbroken $\hat{\mathfrak{u}}_{1,E}$. This is important as there is a mode in the tower with n=-1 that is neutral and massless and therefore contributing to $h^{2,1}$ in the geometry X^A of the $\mathfrak{e}_6^{(2)}$ theory.

The second source of neutral singlets are the massless representations $\mathbf{26}_0$. Recall that those hypermultiplets admit only 24 non-trivial weights and two more trivial ones that contribute to $h^{2,1}(X^A)$ each. (see section 7 for more details). Hence, each $\mathbf{56}_{\frac{1}{2}}$ KK-tower of states, contributes four neutral singlet components upon the Higgsing. Finally we need to take the 7 neutral states in any $\mathbf{133}$ hypermultiplet that reduce to just 4 in $\mathbf{52}$ and therefore need to be subtracted. Also recall, that there are the Goldstone modes $\mathbf{26}_0 \oplus \mathbf{1}_0$ that need to be removed and thus, subtract three more neutral fields.

Summing up all contributions, we obtain the following change in neutral charged fields

$$\Delta \mathbf{1}_0 = -3 \cdot n_{133_0} - 3 + 4 \cdot 56_{1/2} = 13(1 - g) + 2\mathcal{Z}^2 - 6g, \qquad (4.68)$$

which is identified with the change in complex structure moduli upon the conifold transition.

The above considerations are confirmed in the example geometries. Recall the Hodge numbers of the two geometries are

$$(h^{1,1}, h^{2,1}): (10,82) \to (7,95).$$
 (4.69)

As the respective gauge algebras are over $\mathcal{Z}^2 = 0$ of genus g = 0, we find exactly the difference of 13 complex structure moduli that was expected.

Another puzzle remains, the Higgs transition in the 6D theory associated to the Jacobian geometry appears to be more subtle than that realized in the 5D genus one geometries. When making the transition from the Jacobian of X^B to that of X^C we find the codimension one structure unchanged i.e. the E_7 singularity is preserved. At codimension two however, the locus of **56**-plets has changed to the intersection locus with the two section monodromy divisor. In particular we find that the **56**_q-plets should now be counted as half-hypers which implies a change in the discrete \mathbb{Z}_2 charge to q = 0 or q = 1 but not $q = \frac{1}{2}$. This furthermore implies a subtle modification of the global gauge group structure in the 6D theory as

$$G_{6D} = \frac{E_7 \times \mathbb{Z}_4}{\mathbb{Z}_2} \to G_{6D} = E_7 \times \mathbb{Z}_2.$$
 (4.70)

It would be interesting to explore the origin of the corresponding transition and its relation to the 5D twisted reduction in more detail in the future.

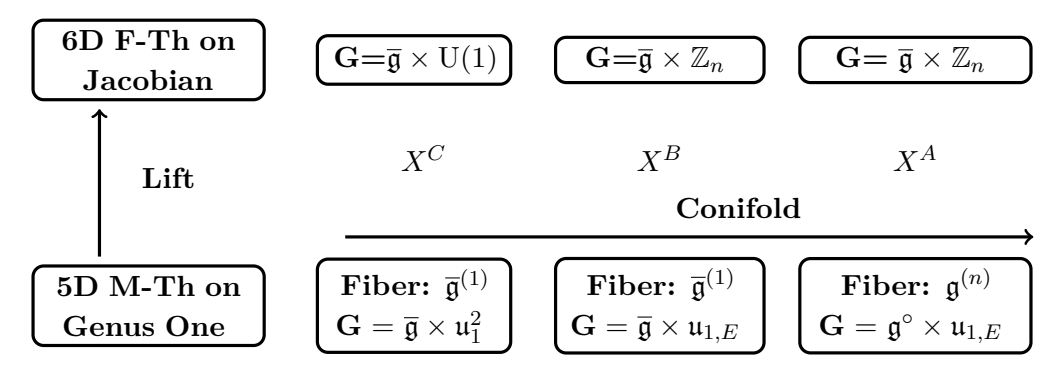


Figure 8. The chain F/M-theory vacua on torus fibered threefolds X^I , highlighting the 6D gauge symmetry G and 5D fiber structures.

s_1	s_2	s_3	s_4	s_5	s_6	s_7	s_8	s_9	f	g	$ \Delta $	Genus-1 Fiber	Jac Fiber
0	0	0	0	1	1	1	1	1	2	3	6	$\mathfrak{g}_2^{(1)}$	$\mathfrak{g}_2^{(1)}$
0	0	0	0	0	1	1	1	1	2	3	6	$\mathfrak{su}_3^{(2)}$	$\mathfrak{g}_2^{(1)}$
0	0	0	0	0	0	0	0	1	0	0	2	$\mathfrak{su}_2^{(1)}$	$\mathfrak{su}_2^{(1)}$

Table 3. Tunings of sections in the quartic genus one model (4.1) for $\mathfrak{su}_3^{(2)}$ fibers and related models. The fiber structure in genus-one and Jacobian is given in the two rightmost columns.

5 More twisted affine fibrations

In this section we will follow the same approach used in section 4 to study the $\mathfrak{e}_6^{(2)}$ geometry and discuss further examples of twisted fibers. We will consider the twisted algebras $\mathfrak{su}_3^{(2)}$ and $\mathfrak{so}_8^{(3)}$. For each we will discuss the structure of their Jacobians and the general conifold relations as given in figure 8.

5.1 The geometry of $\mathfrak{su}_3^{(2)}$

In this section we describe the geometry of the $\mathfrak{su}_3^{(2)}$ fiber. Its fiber structure is given on the left of figure 9. When interpreted as a fiber graph, we see that its geometric cover is that of an $\mathfrak{so}_8^{(1)}$ with a degree 4 folding acting on the four outer nodes. More precisely, the folding proceeds by its $\mathbb{Z}_2 \times \mathbb{Z}_2$ center. In order to perform this geometric action, we require a four-section with the appropriate monodromy. One such example can be found in a manifold with CICY genus-one fiber given by $\mathbb{P}^3[2,2]$ [49]. Luckily, there is a simpler model which allows us to resolve the singularity in a single hypersurface: the model is the quartic fibration given in (4.1). Besides the two 2-sections X, Y there is also a 4-section Z = 0 that brings with it the right monodromy.

To proceed, we employ the same algorithm used to analyze the geometry in section 4: we need to tune an I_0^* type of singularity over Z=0 in the quartic model and let it intersect the order four monodromy divisor. This monodromy divisor can be found by first considering the four-section Z=0 which yields

$$\sigma_4: \{Z=p=0\}: s_1X^4 + s_2X^3Y + s_3X^2Y^2 + s_4XY^3 + s_5Y^4$$
 (5.1)

and then finding its discriminant locus

$$\overline{D}_{4,Z} = 2s_2^3(2s_4^3 - 9s_3s_4s_5) + 2s_1s_2s_4(-9s_3s_4^2 + 40s_3^2s_5 + 96s_1s_5^2)
+ 27s_2^4s_5^2 + s_2^2(-s_3^2s_4^2 + 4s_3^3s_5 + 6s_1s_4^2s_5 - 144s_1s_3s_5^2)
+ s_1(4s_3^3s_4^2 + 27s_1s_4^4 - 16s_3(s_3^3 + 9s_1s_4^2)s_5 + 128s_1s_3^2s_5^2 - 256s_1^2s_5^3).$$
(5.2)

Proceeding further, in table 3 we have summarized the vanishing of the generalized Tate-coefficients and the resulting fiber structures in the quartic threefold and its Jacobian fibration. Hence the singular genus-one $\mathfrak{su}_3^{(2)}$ is given via the tuning

$$s_i \to z^{n_i} d_i$$
, with $\vec{n} = (0, 0, 0, 0, 0, 1, 1, 1, 1)$. (5.3)

Note that we are required to keep the s_9 section explicitly at this point to be able to perform the tuning.

The twisted affine fiber is given by the second row of table 3. The tuning is chosen so that it respects the generic four-monodromy locus. The resolved quartic hypersurface is then given as

$$p = d_1 X^4 + d_2 X^3 Y + d_3 X^2 Y^2 + d_4 X Y^3 + d_5 Y^4 + d_6 f_1 g_1 X^2 Z + d_7 f_1 g_1 X Y Z + d_8 f_1 g_1 Y^2 Z + d_9 f_1 Z^2.$$
 (5.4)

The geometry can be fully analyzed given the Stanley-Reisner ideal

$$SRI: \{YXZ, Zg_1\}, \tag{5.5}$$

and the two fibral divisors are explicitly given as

$$\mathbb{P}_{0,i}^{1}: \{p = f_{1} = 0\}: d_{1}X^{4} + d_{2}X^{3}Y + d_{3}X^{2}Y^{2} + d_{4}XY^{3} + d_{5}Y^{4}, \qquad i = 1 \dots 4,
\mathbb{P}_{1}^{1}: \{p = g_{1} = 0\}: d_{1}X^{4} + d_{2}X^{3}Y + d_{3}X^{2}Y^{2} + d_{4}XY^{3} + d_{5}Y^{4} + d_{9}f_{1}.$$
(5.6)

Note that the four \mathbb{P}^1 s inside of $f_1 = 0$ admit an S_4 symmetry and take the very same form as the four-section Z = 0 and hence, experience the same mondromy effect.

In order to obtain the correct gauge algebra factor of the quartic model we need to choose the fibration so that upon factorizing the divisor $\mathcal{Z}: z=0$, the residual d_9 polynomials becomes a constant. For this we set

$$[z \ d_9] \sim c_1 - \mathcal{S}_7 + \mathcal{S}_9 \,, \tag{5.7}$$

and solving for $S_7 \sim c_1 + S_9 - Z$. In what follows we will then set $d_9 = 1$.

The fibral graphs and intersections with the 2-sections and 4-section is given in figure 9. Note again, that we obtain an order two multiple fiber, over each intersection locus of $\overline{D}_{4,Z}$ with the fibral curve \mathcal{Z} as depicted in figure 9.

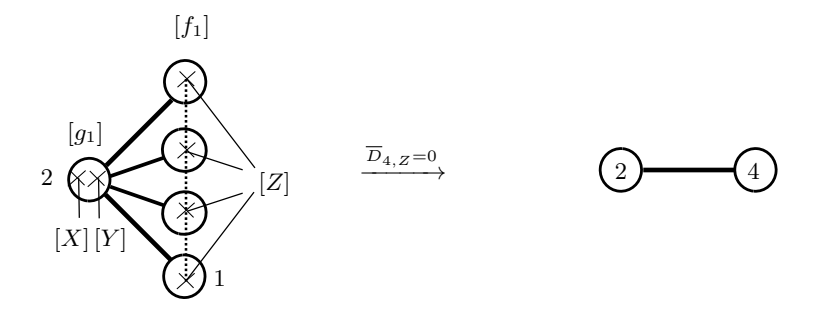


Figure 9. Depiction of an $\mathfrak{su}_3^{(2)}$ fiber. The two two-sections X,Y both intersect the middle node. All four fibral curves in $[f_1]$ are permuted by the four-section Z. At the intersection with the monodromy divisor the fiber degenerates to a multiplicity two fiber.

5.1.1 Counting states in the $\mathfrak{su}_3^{(2)}$ genus-one model

As in the previous section, we turn our attention now to the BPS states. To count the states, within the twisted affine fiber we split up all curves of the \mathfrak{so}_8 cover into orbits of the Eigenspaces of the monodromy action. The starting point are curves \mathcal{C} of self-intersection -2 that are linear combinations $\mathcal{C} = \sum_i a_i \mathcal{C}_i$ for $i = 0 \dots 4$ where the basis curves \mathcal{C}_i intersect as nodes of the affine Dynkin diagram $\mathfrak{so}_8^{(1)}$. Graphically we write those curves as

$$C_i = a_0 - a_2 - a_4$$
, with $a_i \in \mathbb{N}$ and $i = 0 \dots 4$. (5.8)

In this way we setup the 24 states that make up the W bosons of the adjoint of the covering \mathfrak{so}_8 . In the second step, we incorporate the \mathbb{Z}_4 action that fixes \mathcal{C}_2 but rotates the other \mathcal{C}_i . The invariant combination of curves is then given by the collection $(\mathcal{C}_2, \mathcal{C}_1 + \mathcal{C}_3 + \mathcal{C}_4 + \mathcal{C}_5)$ which we will also use in order to compute the weights of states via the intersections of the covering algebra. Then within the 24 states, we need to collect together the Eigenspaces under the action and split them up into shrinkable and non-shrinkable curves. The result is given in table 4.

The permutation action σ_4 acts on the outer roots as

$$\sigma_4: \quad 4. -0 - 1. , \\
3.$$
(5.9)

where we have chosen the i-th root to be permuted to i+1 under the \mathbb{Z}_4 we quotient by.¹⁵ We find two $\mathbf{2}_{\frac{1}{2}}$ doublets as well as two types of singlets as shown in table 4. Note that one of the singlets is only an order two ramified curve under the order four action.

In order to compute the moduli space dimensions, we need the divisor class of the monodromy divisor. In order to deduce it, we first note that the ramification divisor is

¹⁵Note that there might be other potential subgroups of the S_4 symmetry to quotient by and an interesting point for future research (see. e.g. [71] for S_3 example of \mathfrak{so}_8).

Mono	#Curves	Example Curve	$\mathfrak{su}_2 \subset \mathfrak{su}_3^{(2)}$ weight	χ
Inv	2	$0 \\ 0 - 1 - 0 \\ 0$	(-2)	g
\mathbb{Z}_4	2	$\begin{array}{cccccccccccccccccccccccccccccccccccc$	(-1)	g '
\mathbb{Z}_4	2	$\begin{matrix} 0 & 1 \\ 1 - 1 - 0 + 0 - 1 - 0 \\ 0 & 0 \\ 0 & 0 \\ + 0 - 1 - 0 + 0 - 1 - 1 \\ 1 & 0 \end{matrix}$	(-1)	g '
\mathbb{Z}_4	1	$ \begin{array}{cccccccccccccccccccccccccccccccccccc$	(0)	g '
\mathbb{Z}_2	1	$ \begin{array}{cccccccccccccccccccccccccccccccccccc$	(0)	$\overline{g}\prime$

Table 4. Schematic splitting of the 24 curves of \mathfrak{so}_8 roots into \mathbb{Z}_4 invariant curves, their $\mathfrak{su}_2 \subset \mathfrak{su}_3^{(2)}$ charges and respective moduli space dimensions χ computed in (5.13).

associated to the base line bundle class

$$[\overline{D}_{4,Z}] \sim 2[d_1] + 4[d_4],$$
 (5.10)

and we further observe

$$[d_1] \sim 2c_1 - 2S_9 + \mathcal{Z}$$
 $[d_4] \sim 2c_1 + S_9 - 2\mathcal{Z}$. (5.11)

Plugging those in, we find that S_9 cancels out and we obtain

$$[\overline{D}_{4,Z}] \sim 12c_1 - 6\mathcal{Z}. \tag{5.12}$$

Intersecting the monodromy divisor $\overline{D}_{Z,4}$ with \mathcal{Z} yields the points of ramification that we need to compute the moduli spaces of fibered \mathbb{P}^1 's. There we count the moduli spaces g' and \overline{g}' for degree 4 and 2 covered curves respectively which are given as

$$g' = 9(1-g) + 3Z^2 + g$$
, $\overline{g}' = 11(1-g) + 3Z^2 + g$. (5.13)

When adding up, the non-trivial representations, we obtain

$$n_{3_0} = g$$
, $n_{2_{\frac{1}{2}}} = 18(1-g) + 6\mathcal{Z}^2 + 2g$, (5.14)

$$n_1 = 20(1-g) + 6\mathcal{Z}^2 + 2g.$$
 (5.15)

Note that all states carry a non-trivial $\mathfrak{u}_{1,E}$ charge and are therefore generically massive.

Comparison with $\mathfrak{su}_3 \to \mathfrak{su}_3^{(2)}$ reduction. In pure field theories, the 5D $\mathfrak{su}_3^{(2)}$ theories have been observed to arise from an outer automorphism twisted 6D theory with a \mathfrak{su}_3 gauge algebra. The autormorphism acts as complex conjugation among the fundamental representations, and leaves an \mathfrak{su}_2 maximal sub-algebra. Similarly to the examples given in section 4 we will observe below that the Jacobian admits an \mathfrak{g}_2 gauge algebra instead of \mathfrak{su}_3 . Thus, we expect that the genus one geometry we outline here will arise from a circle reduction of a 6D \mathfrak{g}_2 F-theory background, but that the twisting symmetry will act on the $\mathfrak{su}_3 \in \mathfrak{g}_2$ sub-algebra as in the usual gauge-theoretic twisted reductions.

The decomposition of the fields under the twisted reduction ¹⁶ results in

$$\mathbf{8} \to \mathbf{3}_0 \oplus \mathbf{2}_{\frac{1}{4}} \oplus \mathbf{2}_{\frac{3}{4}} \oplus \mathbf{1}_{\frac{1}{2}} \quad \text{and} \quad (\mathbf{3} \oplus \overline{\mathbf{3}}) \to \mathbf{2}_{\frac{1}{4}} \oplus \mathbf{2}_{\frac{3}{4}} \oplus \mathbf{1}_0 \oplus \mathbf{1}_{\frac{1}{2}}. \tag{5.16}$$

The subscript \mathbf{R}_s denotes the shifted KK charge q = s + n and KK-momentum n typically used in the literature.

Recollecting the 5D multiplicities of states, we write the 6D spectrum in geometric terms as

$$n_{\mathbf{3}_0} = 18(1-g) + 6\mathcal{Z}^3, \qquad n_{\mathbf{8}} = g.$$
 (5.17)

Since $\mathbf{2}_{\frac{1}{4}}$ states are in the same tower as $\mathbf{2}_{\frac{3}{4}}$ we can simply sum them up to obtain the multiplicity of

$$n_{2\frac{1}{4}} = 18(1-g) + 6\mathcal{Z}^2 + 2g.$$
 (5.18)

Finally we need to match the normalization of the shifted KK-charges with those used for our intersections. In order to do so, we need to multiply the above shifted KK-charges by two to obtain a match of both multiplicities.

Similar as in the $\mathfrak{e}_6^{(2)}$ case, we also obtain a prediction for the neutral singlets that are inherited from the fundamentals, given as

$$n_{\mathbf{1}_0} = \frac{n_{\mathbf{3}}}{2} = 9(1-g) + 3\mathcal{Z}^2.$$
 (5.19)

The states above in (5.19) we will interpret as non-polynomial deformations of the toric hypersurface in section 7.

State counting in the $\mathfrak{g}_2^{(1)}$ Jacobian. Lets compare those computations with that of the Jacobian which admits an unaltered 6D uplift. Similar as for the $\mathfrak{e}_6^{(2)}$ geometry, we expect to find a generic I_0^* fiber i.e. a \mathfrak{g}_2 . Indeed at leading order of the Weierstrass form along the singularity at z=0 we find

$$f = -z^{2} \frac{1}{3} (d_{3}^{2} + d_{2}d_{4} - 4d_{1}d_{5}) + \mathcal{O}(z^{3}),$$

$$g = -z^{3} \frac{2}{27} (2d_{3}^{3} - 9d_{2}d_{3}d_{4} + 27d_{1}d_{4}^{2} + 27d_{2}^{2}d_{5} - 72d_{1}d_{3}d_{5}) + \mathcal{O}(z^{4}),$$

$$\Delta = z^{6} \overline{D}_{4,Z} + \mathcal{O}(z^{7}).$$
(5.20)

¹⁶Note that our shifted KK charge for the fundamentals differ from those, given in [19].

Table 5. Toric rays, of a genus-one fibration over \mathbb{F}_3 base, with $\mathfrak{su}_3^{(2)}$ where the ray f_1 yields the affine node.

with $\overline{D}_{4,Z}$ the monodromy divisor. In the Jacobian we find over z=0 simply an I_0^* non-split fiber, i.e. an \mathfrak{g}_2 singularity. The monodromy divisor takes on a similar role as in the genus-one fibration but in this case, it only rotates three of \mathfrak{so}_8 outer roots, instead of four. Hence the fibral \mathbb{P}^1 's undergo a degree d=3 monodromy. This is important to compute the moduli spaces of the curves that yields $n_7=(\overline{g}-g)$ fundamental hypermultiplets of \mathfrak{g}_2 . Using the same amount of ramification points as for $\mathfrak{su}_3^{(2)}$ but this time d=3 in the RH theorem yields the multiplicities

$$n_{14} = g, n_7 = 10(1-g) + 3Z^2, (5.21)$$

which satisfies the \mathfrak{g}_2 anomalies in 6D.

Toric examples. In the following we discuss two concrete toric examples. The first threefold, admits a \mathbb{P}^2 base with an $\mathfrak{su}_3^{(2)}$ over a $\mathbb{Z}^2 = +1$ curve of genus g = 0. The toric rays are given in appendix A and the respective Hodge numbers are computed as

$$(h^{1,1}, h^{2,1}(h_{np}^{2,1})) = (3, 107(12)). (5.22)$$

Note that the number of Kähler parameters matches the expectation. The charged spectrum comes with multiplicities

$$n_{\mathbf{3}_0} = 0, \qquad n_{\mathbf{2}_{\frac{1}{2}}} = 24.$$
 (5.23)

We will return to the model above, when discussing another transition to an actual $\mathfrak{su}_2^{(1)}$ fiber, which shares the very same Hodge numbers as the model above in section 7.

Finally we also present the geometry that correspond to the twisted reduction of a non-Higgsable \mathfrak{su}_3 theory. From a 6D perspective, this comes when g=0 and $\mathcal{Z}^2=-3$. From the general considerations we find, that we should also find no $\mathfrak{su}_3^{(2)}$ particles. Such an example can easily be constructed, over an \mathbb{F}_3 base. The toric rays for this model are given in table 5 and the Hodge numbers can be computed as

$$(h^{1,1}, h^{2,1}(h_{np}^{2,1})) = (4, 130(0)), (5.24)$$

admitting the four expected Kähler parameters and notably only polynomial complex structure deformations.

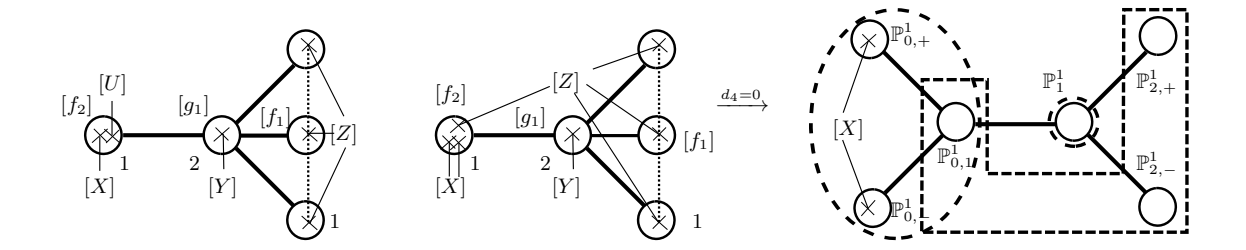


Figure 10. Summary of three fiber structures. On the left is the \mathbf{g}_2 fiber in the elliptic model and in the middle in the genus-one model and their intersections. Shown are the two-sections X, Y and the four-section Z = 0. On the right is the \mathfrak{so}_{10} degeneration shown where matter is localized.

5.1.2 Transitions to $\mathfrak{su}_3^{(2)}$

In the following we explore various transitions towards the 5D $\mathfrak{su}_3^{(2)}$ theory. We have observed already, that this theory admits a $\mathfrak{g}_2 \times \mathbb{Z}_2$ theory in its Jacobian. We therefore tune the theory to an $\mathfrak{g}_2 \times \mathfrak{u}_{1,6D}$ in 6D via various transitions.

Geometrically, the way this fibration is constructed follows the same approach as in the $\mathfrak{e}_6^{(2)}$ theory, by having a monodromy that acts non-trivially an the affine node.

The $\mathfrak{g}_2 \times [\mathrm{U}(1)_{6D} \to \mathbb{Z}_2]$ transition. The basis for the $\mathfrak{su}_3^{(2)}$ model was the existence of the 4-section monodromy divisor that folds the $\mathfrak{so}_8^{(1)}$ covering fiber. We will not present a complete such unfolding, but only a deformation which grants us a section and hence an elliptic model. As the generic fiber description is the same as in the $\mathfrak{e}_6^{(2)}$ model.

For this we can start with an $\mathfrak{g}_2 \times \mathfrak{u}_{1,6D}$ 6D theory by using the tuning given by general Tate-vector¹⁷ specified in table 3 and at the same time tuning d_5 to zero globally.

The resolved hypersurface is given as

$$p = d_1 f_2^3 U^3 X^4 + d_2 f_2^2 U^2 X^3 Y + d_3 f_2 U X^2 Y^2 + d_4 X Y^3 + d_6 f_1 f_2^2 q_1 U^2 X^2 Z + d_7 f_1 f_2 q_1 U X Y Z + d_8 f_1 q_1 Y^2 Z + d_9 f_1 U Z^2.$$
 (5.25)

The zero-section is again denoted by U = 0 and the second section by X = 0. The above fiber is of \mathfrak{g}_2 type as can be seen from the fibral curves and their intersections using the

$$SRI: \{YX, YU, Yf_2, e_1Z, e_1U, e_1f_1, e_1g_1, e_1f_2, XZ, Zg_1, Zf_2, Xf_1, f_1f_2, Xg_1\}.$$
 (5.26)

This leads to the following form of fibral curves:

$$\mathbb{P}_{i}^{1}:[f_{1}]: d_{1}U^{3} + d_{2}U^{2}Y + d_{3}UY^{2} + d_{4}Y^{3}, \qquad i = 1, 2, 3,
\mathbb{P}_{2}^{1}:[g_{1}]: d_{9}f_{1}U + d_{1}f_{2}^{3}U^{3} + d_{2}f_{2}^{2}U^{2}Y + d_{3}f_{2}UY^{2} + d_{4}Y^{3},
\mathbb{P}_{0}^{1}:[f_{2}]: d_{8}g_{1} + d_{9}U + d_{4}X.$$
(5.27)

$$\vec{n} = \{3, 2, 1, 0, -, 2, 1, 0, 0\}$$

in the quartic model. Consistently, this tuning also leaves $\overline{D}_{3,Z}$ invariant.

¹⁷Note that we have used f_1 as the affine coordinate to make contact with the $\mathfrak{su}_3^{(2)}$ geometry. The affine coordinate however is given as f_2 , which can equally well be given by the tuning

The divisor $f_1 = 0$ itself is a cubic polynomial that decomposes into three irreducible curves \mathbb{P}^1_i , that are interchanged by the monodromies. Note that Z = 0 is a 3-section in the MP model but will become a 4-section in the quartic genus-one fibration.

The intersections in the fiber are depicted in figure 10. To compute the spectrum it is convenient to map the geometry into the Weierstrass form which we sketch to leading orders here

$$f = -\frac{1}{3}(d_3^2 - 3d_2d_4)z^2 + \mathcal{O}(z^3),$$

$$g = -\frac{1}{27}(2d_3^3 - 9d_2d_3d_4 + 27d_1d_4^2)z^3 + \mathcal{O}(z^3),$$

$$\Delta = z^6d_4^2\overline{D}_{3,Z} + \mathcal{O}(z^7),$$
(5.28)

with $\overline{D}_{3,Z}$ the \mathbb{Z}_3 monodromy divisor of the three-section Z=0, that also permutes the three \mathbb{P}^1 's in $f_1=0$. Its polynomial equation is explicitly given as

$$\overline{D}_{3,Z} = \left(-d_2^2 d_3^2 + 4d_1 d_3^3 + 4d_2^3 d_4 - 18d_1 d_2 d_3 d_4 + 27d_1^2 d_4^2\right). \tag{5.29}$$

Precisely due to the reason that $\overline{D}_{3,Z}$ is not a perfect cube leads to the non-split type I_0^* fiber. From the intersections with the additional section, we find the U(1) Shioda map to be simply given as

$$\sigma(s_1) = [X] - [U]. \tag{5.30}$$

Unlike to the other examples there is no geometric mixing of the U(1) with the \mathfrak{g}_2 center at this point as this is simply trivial. The presence of the extra U(1) leads to the expectation of non-trivial charged matter. The first source is non-localized matter induced by the monodromy locus $\overline{D}_{3,Z}$ but we also find a (2,3,7) enhancement locus over $z=d_4=0$. In the resolved model we find the curves \mathbb{P}_2^1 to split into two curves which thus gives the fiber the topology of $\mathfrak{so}_{10}^{(1)}$ as depicted in figure 9. One of these components, e.g. $g_1=U=0$ contains the zero-section and admits the following intersections with the Cartan generators $(f_1,g_1,f_2)_{\sigma(s_1)}$

$$(1, -1; 1)_1 \ni \mathbf{7}_1, \tag{5.31}$$

i.e. a weight from the fundamental of \mathfrak{g}_2 with non-trivial U(1) charge.

When Higgsing to the genus-one model, the \mathfrak{g}_2 stays basically as it is, so we will not discuss matter multiplicities up to this point.

When performing the conifold transition to the genus-one geometry we blow down U and add the deformation term $d_5f_1g_1^2Y^4$ to the hypersurface. This results in changing Z=0 and X=0 into a four- and a two-section respectively. This is reflected by the change in the intersection picture depicted in the middle of figure 10 for which we used the fibral Stanley-Reisner ideal

$$SRI = \{YX, Yf_2, Zg_1, Xf_1\}. \tag{5.32}$$

In analogy to the procedure before we use the two-section X=0 as the analog of the zero-section. As all of its strains intersect the affine node $\mathbb{P}^1_{\alpha_0}$ only, we do not have to

node	Irredu	icible compon	ents over $d_4 = 0$
	\mathbb{P}^1_0 $]$ $\mathbb{P}^1_{0,1}:f_2$ ($f: f_1 \cap (f_2 \pm pY)$
$\mathbb{P}^1_2 : [g_1$	$] \mid \mathbb{P}_2^1 : g_1 \cap$	$(d_9f_1+d_1f_2^3+d_1f_2^2+d_$	$+ d_2 f_2^2 Y + d_3 f_2 Y^2)$
$\mathbb{P}^1_0: [f_2]$	$[\mathbb{P}^1_{0,1}:f_2$ ($\cap f_1 \qquad \mathbb{P}^1_{0,\pm}:$	$f_2 \cap (f_0 g_1 \pm q Z)$

Table 6. The codimension two irreducible components of the fiber at $d_4 = 0$, where \mathfrak{g}_2 fundamentals $\mathbf{7}_1$ are located. Their intersection picture is given on the right of figure 10.

orthogonalize it with respect to other \mathfrak{g}_2 Cartan generators, just as in the case before. Hence we use X as the discrete Shioda map generator itself which in order to compute the 6D discrete \mathbb{Z}_2 charges or 5D KK charges. Lets investigate the reducible fibers below in codimension one, for which we find

$$\mathbb{P}^{1}_{\alpha_{1},i}: \quad [f_{1}] \cap d_{1}f_{2}^{3} + d_{2}f_{2}^{2}Y + d_{3}f_{2}Y^{2} + d_{4}Y^{3}, \qquad i = 1, 2, 3,
\mathbb{P}^{1}_{\alpha_{2}}: \quad [g_{1}] \cap d_{9}f_{1} + d_{1}f_{2}^{3}X^{4} + d_{2}f_{2}^{2}X^{3}Y + d_{3}f_{2}X^{2}Y^{2} + d_{4}XY^{3},
\mathbb{P}^{1}_{\alpha_{0}}: \quad [f_{2}] \cap d_{5}f_{1}g_{1}^{2} + d_{4}X + d_{8}f_{1}g_{1}Z + d_{9}f_{1}Z^{2}.$$
(5.33)

From the point of view of the four-section Z=0 it is notable, that the three fibral curve \mathbb{P}^1_i undergo only a \mathbb{Z}_3 monodromy. Indeed one of the four-section strains of Z=0 attaches to the affine node in $f_2=0$. This is also reflected in the Jacobian of the genus-one model which at leading order is exactly the same as given in (5.28). Hence we also find the same degeneration locus over $d_4=0$ again. This is the important locus that triggers the 5D Higgs transition to the $\mathfrak{su}_3^{(2)}$ theory so we will discuss it in a bit more detail. Moving onto the locus $d_4=0$, the fibral curves split as summarized in table 6. When investigating the curve $\mathbb{P}^1_{0,\pm}$, we find the M2 brane states to support the following weights

$$\mathbb{P}^1_{0,+}: (1,0;-1)_1 \ni \mathbf{7}_1, \tag{5.34}$$

Similar as in $U(1)_{6D}$ phase, the new fibral component gives rise to a charged fundamental. When lifting to 6D, the charge under $U(1)_E$ becomes a \mathbb{Z}_2 charge, while in the genus-one geometry it combines with the $U(1)_{KK}$ charge.

Up to this point we have not yet computed the multiplicities of the \mathfrak{g}_2 charged states in either geometry. In order to do so, we take f_1 as the affine coordinate that factored out of d_i . The full factorization in terms of the quartic model is given in table 3.

Using the formulas for the classes first, we need to set d_9 to be a constant in order to avoid additional \mathfrak{su}_2 gauge factors. In order to achieve this, we can fix the line bundle classes of the base as

$$S_7 \sim c_1 + S_9 - \mathcal{Z} \,. \tag{5.35}$$

Important for what follows are the classes of the two sections d_1 and d_4 . Those can be deduced to transform in the base classes

$$[d_1] \sim 2c_1 - 2S_9 + \mathcal{Z}, \quad [d_4] \sim 2c_1 + S_9 - \mathcal{Z}.$$
 (5.36)

From this data we can read off the class of the \mathbb{Z}_3 monodromy divisor (5.29) to

$$[\overline{D}_{Z,3}] \cdot \mathcal{Z} = [2d_1 + 2d_4] \cdot \mathcal{Z} = 8c_1 \cdot \mathcal{Z} - 2\mathcal{Z}^2 - 2\mathcal{S}_9 \cdot \mathcal{Z} = 16(1-g) + 6\mathcal{Z}^2 - 2\mathcal{S}_9 \cdot \mathcal{Z}.$$
(5.37)

With this topological information we can compute the multiplicities of the charged matter. First there is as usual the adjoint valued fields counted by the genus of \mathcal{Z} . Then there are the two sources of 7-plets The first source is counted by the intersections of z=0 with $d_4=0$, while the second uses the moduli spaces of the degree three branched curve z=0 via Riemann-Hurwitz. The result is

$$n_{7_1} = [d_4] \cdot \mathcal{Z} = 4(1-g) + \mathcal{S}_9 \cdot \mathcal{Z}, \qquad n_{14_0} = g,$$

 $n_{7_0} = 2(g-1) + \frac{1}{2}R = 6(1-g) + 3\mathcal{Z}^2 - \mathcal{Z} \cdot \mathcal{S}_9.$ (5.38)

Note that there is the additional free line bundle class S_9 which is not fixed. The freedom of tuning this classes and the intersection with Z allows to control the relative difference of charged and uncharged 7-plets.¹⁸ Consistent with gauge anomalies we find that the sum of the representation does not depend on the additional parameter S_9 as it must be

$$n_{7_1} + n_{7_0} = 10(1-g) + 3\mathcal{Z}^3$$
. (5.39)

To illustrate those general considerations, we discuss a concrete toric example in the following For this we fix the base to be \mathbb{P}^2 and the full toric data is given in appendix A. The model admits an \mathfrak{g}_2 over a genus 0 curve with the additional data $\mathcal{Z} \cdot \mathcal{S}_9 = \mathcal{Z}^2 = 1$ and Hodge numbers

$$(h^{1,1}, h^{2,1}) = (4,98). (5.40)$$

Indeed, besides the two classes of fiber and base, there are two more Kähler classes that parametrize the \mathfrak{g}_2 Coulomb branch. Focusing on the \mathfrak{g}_2 charged spectrum, we find

$$n_{7_1} = 5, \qquad n_{7_0} = 8.$$
 (5.41)

Transition to $\mathfrak{su}_3^{(2)}$. With all the details at hand, we can perform the conifold type of transitions. In order to do so, we first need to go to a partial Coulomb branch, as in the $\mathfrak{e}_7 \to \mathfrak{e}_6^{(2)}$ case. The reason is again, that the $\mathbf{7}_1$ states admit a non-trivial $\mathfrak{u}_{1,E}$ charge and therefore do not become massless at the Coulomb branch origin of \mathfrak{g}_2 . While we can break the $\mathfrak{g}_2 \to \mathfrak{su}_2 \times \mathfrak{su}_2$ and then move to the Coulomb branch, followed by a Higgsing.

Instead we break the $\mathfrak{g}_2 \to \mathfrak{su}_2 \times \mathfrak{u}_{1,A}$ such that there is a second CB modulus to make states massless. In geometry, the respective curve in g_1 may be shrunk while f_1 and f_2 stays finite. This realizes an $\mathfrak{su}_2 \times \mathfrak{u}_{1,A} \times \mathfrak{u}_{1,E}$ gauge algebra and the 7 plets decompose to

$$\mathbf{7}_{1} \to \mathbf{2}_{\frac{1}{2},1} \oplus \mathbf{2}_{-\frac{1}{2},1} \oplus \mathbf{1}_{-1,1} \oplus \mathbf{1}_{1,1} \oplus \mathbf{1}_{0,1} ,
\mathbf{7}_{0} \to \mathbf{2}_{\frac{1}{2},0} \oplus \mathbf{2}_{-\frac{1}{2},0} \oplus \mathbf{1}_{-1,0} \oplus \mathbf{1}_{1,0} \oplus \mathbf{1}_{0,0} ,
\mathbf{14}_{0} \to \mathbf{3}_{0,0} \oplus 2 \times \mathbf{2}_{-\frac{1}{2},0} \oplus 2 \times \mathbf{2}_{-\frac{1}{2},0} \oplus \mathbf{1}_{1} \oplus \mathbf{1}_{-1,0} \oplus \mathbf{1}_{0,0} .$$
(5.42)

The class S_9 is constrained by the existence of sections d_i to be effective.

d_1	d_2	d_3	d_4	d_5	d_6	d_7	d_8	d_9	d_{10}	f	g	Δ	Genus-1 Fiber	Jac Fiber
2	2	1	0	2	1	0	1	0	1	3	4	8	$\mathfrak{f}_4^{(1)}$	$\mathfrak{f}_4^{(1)}$
2	2	1	0	2	1	0	1	0	0	3	4	8	$\mathfrak{so}_8^{(3)}$	$\mathfrak{f}_4^{(1)}$
2	1	1	0	1	0	0	1	0	0	3	4	8	$\mathfrak{g}_2^{(1)}$	$\mathfrak{g}_2^{(1)}$

Table 7. Tunings of sections in the cubic genus one model and the resulting fiberes.

In the $\mathbf{1}_{-1,1} \in \mathbf{7}_1$, we find a good Higgs candidate, that leaves the \mathfrak{su}_2 subgroup invariant. This state can become massless when the $\mathfrak{u}_{1,A}$ and $\mathfrak{u}_{1,E}$ CB moduli become the same. Now, we can Higgs on the $\mathbf{1}_{-1,1}$ by giving it a VEV that corresponds to a complex structure deformation of the geometry. Field theoretically, the Higgsing leaves a $\hat{\mathfrak{u}}_{1,E} = \mathfrak{u}_{1,A} + \mathfrak{u}_{1,E}$ symmetry unbroken.

Collecting the $\mathbf{2}_{\frac{1}{2}}$ -plets¹⁹ yields a collection of massive states of multiplicity

$$n_{\mathbf{2}_{\frac{1}{2}}} = 2n_{\mathbf{7}_1} + 2n_{\mathbf{7}_0} + 4n_{\mathbf{14}_0},$$
 (5.43)

which matches the geometric computation but over counts by two.

In a similar way, also the charged and neutral singlets can be counted. Especially the later ones correspond to complex structure moduli, which can be used to predict the change in $h^{2,1}$ upon the conifold transition, given as

$$\Delta h^{2,1} = 2n_{7_1} - 1. (5.44)$$

Note that the $\mathbf{7}_0$ and $\mathbf{14}_0$ representations already contain one and two neutral singlets respectively before and after the transition that are included in the overall count already. Importantly, we must also count the $\mathbf{1}_2$ -plets that originiated from the $\mathbf{7}_1$ -plets, as neutral states that contribute to $h^{2,1}$. This is again due to the fact, that the whole tower of KK states, is given as $\mathbf{1}_{2+2n}$ and hence, for n=-1, there is a zero mode that contributes a neutral singlet.

When comparing the amount of complex structures upon the $\mathfrak{g}_2^{(1)} \to \mathfrak{su}_3^{(2)}$ deformation, we find the Hodge numbers

$$(h^{1,1}, h^{2,1}) = (4,98) \to (3,107),$$
 (5.45)

where we have $\Delta h^{2,1} = 2n_{7_1} - 1 = 9$ as expected from the above field theory arguments.

5.2 The geometry of $\mathfrak{so}_8^{(3)}$

In this section we describe the geometry of the twisted $\mathfrak{so}_8^{(3)}$ algebra. This geometry can be interpreted as the twisted compactification of an \mathfrak{so}_8 by its order three automorphism, which admits a \mathfrak{g}_2 invariant sub-algebra. However, when viewed as a fiber graph, the $\mathfrak{so}_8^{(3)}$ Cartan matrix admits reversed arrows when compared to $\mathfrak{g}_2^{(1)}$. Hence its geometric cover is rather that of an $\mathfrak{e}_6^{(1)}$ affine Dynkin diagram folded by its order three automorphism.

¹⁹Note that $2_{\frac{3}{2}}$ are part of the same KK-tower and are therefore counted as the same representation.

To engineer a geometry with such an order three (affine) automorphism, we are therefore required to consider genus-one fibrations with a three-section. We must therefore depart from the quartic fiber model, that worked well in the models before, but not in this case.

The simplest choice for a three-section genus-one model is the cubic fibration, where the fiber is represented as a generic degree three polynomial, given as

$$p = s_1 u^3 + s_2 z^2 u^2 v + s_3 u v^2 + s_4 v^3 + s_5 u^2 w + s_6 u v w + s_7 v^2 w + d_8 u w^2 + s_9 v w^2 + s_{10} w^3,$$
(5.46)

in $\mathbb{P}^2_{u,v,w}$. To promote the genus-one curve to a fibration, the s_i must become sections of line bundle of the base B_2 which we consider as the generalized Tate-sections of the cubic.

The specific dependencies of those line bundle classes that are in agreement with the CY conditions can be found in appendix B and follow the convention used in [45]. The above model admits a 3-sections, given by the vanishing of any of the toric coordinates which makes the geometry into a genus-one fibration. Following the logic in the sections before, we define the monodromy divisor as the discriminant locus of a three-section. In the following we use u=0 as the reference 3-section, which results in the solutions of the polynomial

$$s_0^{(3)} = s_4 + s_7 w + s_9 w^2 + s_{10} w^3, (5.47)$$

with discriminant locus

$$\overline{D}_{3,u} = 27s_{10}^2 s_4^2 + 4s_{10}s_7^3 - 18s_{10}s_4s_7s_9 - s_7^2 s_9^2 + 4s_4 s_9^3.$$
(5.48)

The line bundle classes of the monodromy divisor can then be read off from appendix B as

$$[\overline{D}_{3,u}] \sim 2\mathcal{S}_9 + 2\mathcal{S}_7 = 2\mathcal{R}. \tag{5.49}$$

The respective 3-section class $\sigma(s_0^{(3)}) = [u]$ is also used to obtain the respective charges under $\mathfrak{u}_{1,E}$ of the 5D states. Due to the usual mixing, KK-tower states admits charges $q_E = q + 3n$ for the *n*-th KK-mode.

Similar as in the quartic, this can be tracked field theoretically by a $\mathfrak{u}_{1,6D}$ Higgsing of a q=3 state, that carries 5D KK-momentum [31, 45].

Using the Artin-Tate algorithm, we can map the cubic into the Weierstrass form (see [45]). Following the usual logics, we need to tune a type IV^* singularity that intersects the monodromy divisor $\overline{D}_{3,u}$ non-trivially. This ansatz is motivated as the geometric cover of $\mathfrak{so}_8^{(3)}$ is $\mathfrak{e}_6^{(1)}$. We again employ a tuning of the $s_i \to d_i z^{n_i}$ in (5.46) and emply the following generalized Tate-vector

$$\vec{n} = \{2, 2, 1, 0, 2, 1, 0, 1, 0, 0\},$$
 (5.50)

which yields an $\mathfrak{so}_8^{(3)}$ singularity. The respective toric resolution requires two more resolution divisors, which yield the toric hypersurface

$$p = d_1 f_1^2 g_1 u^3 + d_2 f_1^2 g_1^2 h_1^2 u^2 v + d_3 f_1 g_1 h_1 u v^2 + d_4 v^3 + d_5 f_1^2 g_1^2 h_1^2 u^2 w + d_6 f_1 g_1 h_1 u v w + d_7 v^2 w + d_8 f_1 g_1 h_1 u w^2 + d_9 v w^2 + d_{10} w^3.$$
 (5.51)



Figure 11. Depiction of the intersection structure of the $\mathfrak{so}_8^{(3)}$ fiber. Numbers denote the multiplicity of the divisor, that coincide with the Kac labels. The three-section u=0 interchanges the three curves in $[f_1]$ and $[g_1]$ along its monodromy divisor. Along its intersection the fiber degenerates into an order three multiple fiber depicted on the right.

Here f_1 replaces the singularity z and g_1, h_1 yield the exceptional divisors. Using the Stanley-Reisner ideal

$$SRI: \{ug_1, uh_1, f_1h_1, wvu, wvf_1, wvg_1, wvh_1\}.$$
 (5.52)

The explicit form of the fibral curves is given as

$$\mathbb{P}^{1}_{\alpha_{0},i}: \quad f_{1} \cap d_{4}v^{3} + d_{7}v^{2}w + d_{9}vw^{2} + d_{10}w^{3},
\mathbb{P}^{1}_{\alpha_{1},i}: \quad g_{1} \cap d_{4}v^{3} + d_{7}v^{2}w + d_{9}vw^{2} + d_{10}w^{3},
\mathbb{P}^{1}_{\alpha_{2}}: \quad h_{1} \cap d_{1}g_{1} + d_{4}v^{3} + d_{7}v^{2}w + d_{9}vw^{2} + d_{10}w^{3}.$$
(5.53)

Note that the first two fibral divisors contain three irreducible curves each that are permuted along the \mathbb{Z}_3 monodromy of the 3-section $\overline{D}_{3,u}=0$ given in (5.48). This allows us to compute the intersections as given in figure 11. Similar to the other twisted algebras before the degeneration picture of the fibral curves, with the monodromy divisor is of central importance: as can be seen from the fibral curves in eq. (5.53), at the intersection point of the curve \mathcal{Z} with the monodromy divisor $\overline{D}_{3,u}$, we find the fiber to degenerate into a degree three multiple fiber. This phenomenon is indicative, that the group of CY-torsors, the Weil-Châtalet group does not simply reduce to the Tate-Shafarevich group.

When compared to the singular Weierstrass model, this structure is absent due to the presence of a section. Here we find at leading orders the Weierstrass coefficients

$$f = \frac{1}{2}z^{3}d_{1}(9d_{10}d_{4}d_{6} - 6d_{10}d_{3}d_{7} + 2d_{7}^{2}d_{8} - d_{6}d_{7}d_{9} - 6d_{4}d_{8}d_{9} + 2d_{3}d_{9}^{2}) + \mathcal{O}(z^{4}),$$

$$g = -\frac{1}{4}z^{4}d_{1}^{2}\overline{D}_{3,u} + d_{1}\mathcal{O}(z^{5}),$$

$$\Delta = \frac{27}{16}d_{1}^{4}z^{8}\overline{D}_{3,u}^{2} + d_{1}^{3}\mathcal{O}(z^{9}),$$

$$(5.54)$$

which yields the expected type $IV^{*,ns}$, i.e. \mathfrak{f}_4 singularity. Just as in the other twisted cases, we find the monodromy divisor $\overline{D}_{3,u}$ of the genus-one fibration, to also appear as a codimension two component in the discriminant in the Weierstrass model. However, note that there is also an E-string component localized over $z=d_1=0$ where the WSF sections vanish to orders (4,6,12). To keep the discussion simple, we want to avoid those additional non-perturbative contributions in the following.

5.2.1 State counting in $\mathfrak{so}_8^{(3)}$ genus-one fibration

Next we compute the number of BPS states that are non-trivially charged under $\mathfrak{so}_8^{(3)}$ from geometry. The discussion is analogous to that in the $\mathfrak{e}_6^{(2)}$ model.

The starting point here are the 72 W-bosons of the adjoint representation of the \mathfrak{e}_6 covering algebra as this is the geometric cover of $\mathfrak{so}_8^{(3)}$. The M2 branes states wrap the curve \mathcal{C} that we are the linear combinations of the base curves \mathcal{C}_i which intersecting as the affine \mathfrak{e}_6 Cartan matrix. We express those curves graphically as

$$C = a_0 - a_1 - a_2 < \frac{a_3 - a_4}{a_5 - a_6}, \tag{5.55}$$

with $a_i \in \mathbb{N}^0$ and start with all combinations that yield the 72 W-roots of the \mathfrak{e}_6 adjoint. In the second step, we implement the \mathbb{Z}_3 monodromy action which is given as

$$\mathbb{Z}_3: \{\mathcal{C}_0 \to \mathcal{C}_4 \to \mathcal{C}_6 \to \mathcal{C}_3\} \text{ and } \{\mathcal{C}_1 \to \mathcal{C}_3 \to \mathcal{C}_5 \to \mathcal{C}_1\}.$$
 (5.56)

An invariant basis of curves under the \mathbb{Z}_3 action is given by the combination²⁰

$$\{C_2, C_1 + C_3 + C_5, C_0 + C_4 + C_6\}.$$
 (5.57)

We can now split up the 72 base curves of \mathfrak{e}_6 into invariant curves under the \mathbb{Z}_3 action and compute their weights. The \mathfrak{g}_2 weights are then computed as

$$\mathcal{C} \cdot (\mathcal{C}_2, \mathcal{C}_1 + \mathcal{C}_3 + \mathcal{C}_5). \tag{5.58}$$

Furthermore it is important to identify shrinkable and non-shrinkable curves, given by a non-trivial combination of affine curves $a_0 + a_4 + a_6$ modulo 3. Those later three numbers also yield the shifted KK-momenta.

Reducing the 72 roots by the \mathbb{Z}_3 monodromy into invariant curves is depicted in table 8. In order to compute the moduli spaces, we first need to compute the intersection of the monodromy divisor with \mathcal{Z} . Before doing so, we need to restrict to the locus without E-strings by demanding $[d_1] \cdot \mathcal{Z} = 0$, which results in the condition

$$(\mathcal{S}_7 + \mathcal{S}_9) \cdot \mathcal{Z} = \mathcal{R} \cdot \mathcal{Z} = 3c_1 \cdot \mathcal{Z} - 2\mathcal{Z}^2. \tag{5.59}$$

From this we can compute the number of ramification points $R = 2\mathcal{R} \cdot \mathcal{Z}$. Using the RH theorem, we can compute the moduli spaces of each of such curve for d = 3 for which we obtain

$$q' = 4(1-q) + \mathcal{Z}^2 + q. (5.60)$$

Computing the moduli spaces \overline{g}' on the other hand is a bit more involved. These elements have a trivial S_3 stabilizer and were for an $g = 0, \mathbb{Z}^2 = 1$ case computed in [46]. In the following we propose to compute the general case as follows: we start with the order three

²⁰For more details, the very same fiber geometry has been discussed in [46] with a \mathbb{P}^2 base.

Mono	#Curves	Example Curve	$\mathfrak{g}_2 \in \mathfrak{so}_8^{(3)}$ weight	χ
Inv	6	$0 - 0 - 1 < \frac{0 - 0}{0 - 0}$	(-3,6)	g
\mathbb{Z}_3	6	$0 - 1 - 0 < \frac{0 - 0}{0 - 0} + 0 - 0 - 0 < \frac{1 - 0}{0 - 0} + 0 - 0 - 0 < \frac{0 - 0}{1 - 0}$	(-2, -3)	g'
\mathbb{Z}_3	6	$0 - 0 - 1 < \frac{1 - 1}{0 - 0} + 1 - 1 - 1 < \frac{0 - 0}{0 - 0} + 0 - 0 - 1 < \frac{0 - 0}{1 - 1}$	(-1,0)	g'
\mathbb{Z}_3	6	$1-1-1 < \frac{1-0}{1-1} + 0 - 1 - 1 < \frac{1-1}{1-1} + 1 - 1 - 1 < \frac{1-1}{1-0}$	(-1, -3)	g _'
\mathbb{Z}_6	1	$ \begin{array}{cccccccccccccccccccccccccccccccccccc$	(0,0)	\overline{g}'
\mathbb{Z}_6	1	$0-1-2 < \frac{2-1}{1-1} + 1-1-2 < \frac{2-1}{1-0} + 0-1-2 < \frac{1-1}{2-1}$ $1-2-2 < \frac{1-1}{1-0} + 1-2-2 < \frac{1-0}{1-1} + 1-1-2 < \frac{1-0}{2-1}$	(0,0)	\overline{g}'

Table 8. Schematic decomposition of the 72 curves of \mathfrak{e}_6 roots into \mathbb{Z}_3 invariant curves, their $\mathfrak{g}_2 \subset \mathfrak{so}_8^{(3)}$ charges and respective moduli space dimensions χ computed in (5.60) and (5.61).

ramified \mathbb{P}^1 's, given by g' and take another order two cover, ramified at the same points. This then yields

$$\overline{g}' = (g' - 1) + \frac{1}{2}R + g',$$
 (5.61)

$$= 13(1-g) + g + 3\mathcal{Z}^2, \qquad (5.62)$$

which reproduces the result given in [46]. We are now in the position to identify the respective 5D states and their representations. First we have the states with trivial weights under $C_0 + C_4 + C_6$ which are hence shrinkable curves. Those 6 + 6 states from the first two rows in table 8, together with the two Cartan generators combine to the vector multiplets of \mathfrak{g}_2 as well as g adjoint charged hypermultiplets. The moduli space of the shrinkable \mathbb{Z}_3 branched states however has dimension g' and thus, additional hypermultiplets in the fundamental of \mathfrak{g}_2 are provided upon adding the neutral hyper. Subtracting the contribution to the g adjoint hypers, we therefore get

$$n_{7_0} = g' - g = 4(1 - g) + \mathcal{Z}^2,$$
 (5.63)

fundamentals with trivial $U(1)_E$ charge. In the last four rows of table 8 we find the non-shrinkable curves, i.e. states that have a non-trivial $U(1)_E$ charge which therefore stay massive at the origin of the \mathfrak{g}_2 Coulomb branch.

Curves in the third and fourth row of table 8 makeup 7_1 and 7_2 -plets respectively. Their multiplicities are given as

$$n_{7_1} = n_{7_2} = g' = 4(1-g) + \mathcal{Z}^2 + g.$$
 (5.64)

When turning to the singlets $\mathbf{1}_1$ and $\mathbf{1}_2$ we again need to take into account, that each of them is needed to complete the shifted 7-plets. Hence we find for both of them

$$n_{1_1} = n_{1_2} = \overline{g}\prime - g\prime = 9(1 - g) + 2Z^2$$
. (5.65)

We summarize the non-trivially charged spectrum under the \mathfrak{g}_2 subgroup as

$$n_{14_0} = g$$
, $n_{7_1} = 4(1-g) + \mathcal{Z}^2$
 $n_{7_1} = n_{7_2} = 4(1-g) + \mathcal{Z}^2 + g$. (5.66)

Comparison with $\mathfrak{so}_8 \to \mathfrak{so}_8^{(3)}$ reduction. An $\mathfrak{so}_8^{(3)}$ theory can be obtained, by starting with an \mathfrak{so}_8 6D theory and mod by the triality symmetry that interchanges vector, spinor and co-spinor representations upon the circle compactification. In geometric terms of an (unfrozen) 6D F-theory model, the mulitplicites of the respective states are given as

$$n_{\mathbf{8}_V} = n_{\mathbf{8}_S} = n_{\mathbf{8}_C} = 4(1-g) + \mathcal{Z}^2, \quad n_{\mathbf{28}} = g.$$
 (5.67)

The twisted compactifiation breaks \mathfrak{so}_8 to its \mathfrak{g}_2 subgroup. The light states then branch to

$$28 \to 14_0 \oplus 7_{\frac{1}{3}} \oplus 7_{\frac{2}{3}}$$
, (5.68)

$$(\mathbf{8}_{V} \oplus \mathbf{8}_{S} \oplus \mathbf{8}_{V}) \to (\mathbf{7}_{0} \oplus \mathbf{7}_{\frac{1}{2}} \oplus \mathbf{7}_{\frac{2}{2}} \oplus \mathbf{1}_{0} \oplus \mathbf{1}_{\frac{1}{2}} \oplus \mathbf{1}_{\frac{2}{2}}),$$
 (5.69)

where the subscript denotes the usual shifted KK-charge. Collecting the multiplicities of \mathfrak{g}_2 charged states in terms of geometric data, we find

$$n_{\mathbf{7}_0} = 4(1-g) + \mathcal{Z}^2, \qquad n_{\mathbf{7}_{\frac{1}{3}}} = n_{\mathbf{7}_{\frac{2}{3}}} = 4(1-g) + \mathcal{Z}^2 + g,$$
 (5.70)

which matches the geometric count upon rescaling the KK-charges to our geometric conventions. This perspective also gives a prediction for additional singlet states, counted as

$$n_{\mathbf{1}_0} = 4(1-g) + \mathcal{Z}^2. (5.71)$$

In section 7 we will come back to those states and interpret them, as parts of the complex structure moduli space, not realized as polynomial deformations of the CY hypersurface equation.

State counting in the $\mathfrak{f}_4^{(1)}$ Jacobian. The Jacobian of the $\mathfrak{so}_8^{(3)}$ model lifts to the geometric cover, which is a generic Type $IV^{*,ns}$ singularity, as given in (5.54). This can be readily seen by noting, that the monodromy divisor of the genus-one model $\overline{D}_{3,u}$ appears at leading order at the discriminant as well as the g coefficient of the discriminant. Hence g/z^4 at z=0 is not a perfect square by construction and therefore the fiber is non-split. Note also once again, the appearance of the E-string points at $z=d_1=0$ which we have switched off by fixing the base line bundle intersections accordingly.

We continue to compute the spectrum in a similar way as in the cases before. Here the appearing monodromy is only of degree d=2 and split the \mathfrak{e}_6 adjoint as

$$78 \to 52 \oplus 26$$
. (5.72)

The multiplicity of the adjoint is simply given by the genus g of \mathcal{Z} and the fundamentals originate from degree 2 ramified curves. Their moduli spaces are just computed as before,

\mathbb{F}_4 Base	
$r_1 (-1 -1 0 1)$	$\mathfrak{su}_3^{(2)}$ Fiber
$ y_0 (8,8,-1,-4) $	$g_1 (1,0,0,-2) $
$ y_1 (-7,-8,1,0) $	$ h_1 (1,0,0,-3) $
$ f_1 (1 \ 0 \ 0 \ -1)$	
	$\begin{bmatrix} x_1 & (-1, -1, 0, 1) \\ y_0 & (8, 8, -1, -4) \end{bmatrix}$

Table 9. Toric rays, of an $\mathfrak{so}_8^{(3)}$ genus-one fibration \hat{X}^C over a \mathbb{F}_4 base with f_1 being the affine node.

using the RH theorem using $R = [\overline{D}_{3,u}] \cdot \mathcal{Z}$. Upon absorbing $g \times 26$ -plets to complete the adjoint of \mathfrak{f}_4 we are left with the following spectrum

$$n_{52} = g, n_{26} = (g-1) + \frac{1}{2}R = 5(1-g) + \mathcal{Z}^2,$$
 (5.73)

which is exactly what one expects from an anomaly free \mathfrak{f}_4 gauge group in 6D. Note also, that we can not infer the potential discrete charges for the \mathfrak{f}_4 fundamentals directly from the genus-one fibration.

Toric examples. We close by presenting two explicit toric examples. The first one is an $\mathfrak{so}_8^{(3)}$ on a $\mathcal{Z}^2 = -1$ curve within a dP_1 base. The toric divisors are given in appendix A. The Hodge numbers are given as

$$(h^{1,1}, h^{2,1}(h_{nn}^{2,1})) = (5,71(6)). (5.74)$$

We find the 1+2+2 expected Kähler parameters that originate from fiber, base and the \mathfrak{g}_2 Cartan generators as well as six non-toric polynomial deformations. The non-trivial \mathfrak{g}_2 charged spectrum is given as

$$n_{7_0} = n_{7_1} = n_{7_2} = 3. (5.75)$$

Another interesting example, is to have a trivial \mathfrak{g}_2 hyerpmultiplet sector, which can be achieved by having \mathcal{Z} being a curve of self-intersection $\mathcal{Z}^2 = -4$ and genus g = 0 (see (5.70)).

Such geometry is nothing but the \mathfrak{so}_8 non-Higgsable cluster theory after a twisted reduction. The minimal compact base, that hosts such a curve is therefore \mathbb{F}_4 . It is then straightforward to find a toric realization of $\mathfrak{so}_8^{(3)}$ over the -4 curve. The toric rays that engineer the respective polytope are given in 9. The polytope data one can compute the Hodge numbers to

$$(h^{1,1}, h^{2,1}(h_{np}^{2,1})) = (5,92(0)). (5.76)$$

The five Kähler moduli can again be attributed to three classes coming from fiber and base, and two more from the \mathfrak{g}_2 . Also note, that the geometry does not posses any non-polynomial complex structure deformations. We will come back to this point in section 7 and propose a physics explanation for that.

5.2.2 Transitions to $\mathfrak{so}_8^{(3)}$

In the following we want to use geometric transitions to connect other torus-fibered threefolds with enhanced gauge symmetries to the $\mathfrak{so}_8^{(3)}$ model.

In order to do so, we employ the toric tunings of the generalized Tate-vectors as summarized in table 7 and first start with an enhanced singularity which engineers an \mathfrak{f}_4 in the Jacobian and genus-one model with a three-section. It is straightforward to unhiggs the \mathbb{Z}_3 to an $\mathfrak{u}_{1,6d}$ by tuning the section d_{10} to zero globally (see [31, 45] for more details). We will skip this part, for brevity and keep in mind that the \mathfrak{f}_4 singularity is simply a spectator of this transition, similar to the unhiggsings of $\mathbb{Z}_2 \to \mathfrak{u}_{1,6D}$ we encountered in the examples before. Recall however, that the resulting 5D $\mathfrak{u}_{1,E}$ is a linear combination of the 6D \mathbb{Z}_3 with the KK U(1).

When compared to the $\mathfrak{so}_8^{(3)}$ geometry, the main difference is the additional tuning

$$d_{10} \to z d_{10}$$
 (5.77)

Due to this, the type IV^* singularity in the genus-one model is not intersected by the order three monodromy divisor $\overline{D}_{3,u}$ in (5.48) and hence, does not experience the full monodromy but only a subgroup thereof. This can be observed by noting, that the monodromy divisor $\overline{D}_{3,u}$ splits over z=0 as

$$\overline{D}_{3,u} \to d_9^2 \overline{D}_{2,u}$$
, with $\overline{D}_{2,u} = d_7^2 - 4d_4d_9$. (5.78)

The appearance of the $\overline{D}_{2,u}$ divisor intersecting z=0, highlights the fact that the type IV^* singularity is folded to an \mathfrak{f}_4 . This can be explicitly seen in the resolved genus-one fibration which is given as

$$p = d_1 f_1^2 f_2 g_1 u^3 + d_2 f_1^2 f_2^2 g_1^2 g_2^2 h_1^2 u^2 v + d_3 f_1 f_2^2 g_1 g_2^2 h_1 u v^2 + d_4 f_2^2 g_2^2 v^3 + d_5 f_1^2 f_2 g_1^2 g_2 h_1^2 u^2 w + d_6 f_1 f_2 g_1 g_2 h_1 u v w + d_7 f_2 g_2 v^2 w + d_8 f_1 g_1 h_1 u w^2 + d_9 v w^2 + d_{10} f_1 g_1^2 g_2 h_1^3 w^3,$$
 (5.79)

where the additional exceptional coordinates g_1, h_1, g_2, f_2 are required. Computing their intersections can be done, when employing the Stanley-Reisner ideal

$$SRI: \{wf_2, wg_2, vf_1, vg_1, vh_1, ug_1, ug_2, uh_1, f_1g_2, f_1h_1, f_2h_1, wvu\}.$$
(5.80)

The fibral intersections are summarized in figure 12. We find that this figure corresponds to a folding along two legs of the \mathfrak{e}_6 cover. The respective fibral curves are given as

$$\mathbb{P}_{\alpha_0}^1 : f_2 \cap d_{10} f_1 g_1^2 g_2 + d_8 f_1 g_1 u + d_9 v ,
\mathbb{P}_{\alpha_1}^1 : g_2 \cap d_1 f_2 g_1 + d_8 g_1 h_1 + d_9 v ,
\mathbb{P}_{\alpha_2}^1 : h_1 \cap d_1 g_1 + d_4 g_2^2 + d_7 g_2 w + d_9 w^2 ,
\mathbb{P}_{\alpha_3,\pm}^1 : g_1 \cap d_4 f_2^2 g_2^2 + d_7 f_2 g_2 w + d_9 w^2 ,
\mathbb{P}_{\alpha_4,\pm}^1 : f_1 \cap d_4 f_2^2 + d_7 f_2 w + d_9 w^2 .$$
(5.81)

Note that the fibral divisors $f_1 = 0$ and $g_1 = 0$ consist both of two fibral curves, that are interchanged along $\overline{D}_{2,u}$. Note again, that we took f_1 as the singular divisor upon which

node	Irred	lucible components over $d_9 = 0$
$\mathbb{P}^1_{\alpha_0}:[f_2]$	$\mathbb{P}^1_{0,1}: f_2 \cap f_1$,	$\mathbb{P}^1_{0,2}: f_2 \cap g_1, \mathbb{P}^1_{0,3}: f_2 \cap (d_{10}g_1g_2 + d_8u)$
$\mathbb{P}^1_{\alpha_1}:[g_2]$	$\mathbb{P}^1_{1,1}:g_2\cap g_1,$	$\mathbb{P}^1_{1,2}:g_2\cap (d_1f_2+d_8h_1)$
$\mathbb{P}^1_{\alpha_2}:[h_1]$	$\mathbb{P}_2^1: h_1 \cap d_1g_1 +$	$+d_4g_2^2 + d_7g_2w$
$\mathbb{P}^1_{\alpha_3}:[g_1]$	$\mathbb{P}^1_{0,2}:g_1\cap f_2,$	$\mathbb{P}^1_{1,2}: g_1 \cap g_2, \mathbb{P}^1_{3,2}: g_1 \cap (d_4 f_2 g_2 + d_7 w)$
$\mathbb{P}^1_{\alpha_4}:[f_1]$	$\mathbb{P}^1_{0,1}:f_1\cap f_2$	$\mathbb{P}^1_{4,1}: f_1 \cap (d_4f_2 + d_7w)$

Table 10. The codimension two irreducible components of the fibre at $d_9 = 0$, where \mathfrak{f}_4 fundamentals 26_1 are located. Their intersection picture is given on the right of figure 12.

we tuned the model, although here f_2 yields the affine node. However, independent of which node we use to map into the singular Weierstrass model, it leads in both cases to the following form

$$f = \frac{1}{2}z^{3}d_{1}(9d_{10}d_{4}d_{6} - 6d_{10}d_{3}d_{7} + 2d_{7}^{2}d_{8} - d_{6}d_{7}d_{9} - 6d_{4}d_{8}d_{9} + 2d_{3}d_{9}^{2}) + \mathcal{O}(z^{4}),$$

$$g = \frac{1}{4}z^{4}d_{1}^{2}d_{9}^{2}\overline{D}_{2,u} + d_{1}\mathcal{O}(z^{5}),$$

$$\Delta = \frac{27}{16}z^{8}d_{1}^{4}d_{9}^{4}(\overline{D}_{2,u})^{2} + d_{1}^{3}\mathcal{O}(z^{9}).$$

$$(5.82)$$

It is straight forward to see, that also the Jacobian admits an \mathfrak{f}_4 singularity over z=0 as long as the polynomial $\overline{D}_{2,u}$ does not become a perfect square at z=0. As the genus-one fibration does not posses multiple fibers, it admits the same type of fiber structure as its Jacobian. We can therefure use the Weierstrass form, to deduce codimension two singularities, which should lead to charged matter in both models. First we find an E-string locus over $z=d_1=0$, which was also present in the $\mathfrak{so}_8^{(3)}$ model. The second component at the locus $z=d_9=0$ yields a vanishing order (3,5,9) singularity, which is an E_7 point where we expect to find matter. Finally, we also have the monodromy divisor appearing. Indeed, apart from $d_1=z=0$, we find the other two loci to yield reducible fibers whose intersections are depicted in figure 12.

In order to compute the charges under $\mathfrak{u}_{1,E}$ in the genus-one geometry, we pick u=0 as the reference 3-section class and orthogonalize the other generators to obtain the discrete Shioda map as

$$\sigma(u) = [u] + 2[g_2] + 4[h_1] + 3[g_1] + 2[f_1], \qquad (5.83)$$

which is constructed such, that all three intersection points of $\sigma(u)$ intersect only $f_2 = 0$. Over $z = d_9 = 0$ we expect to find charged fundamentals, which we will verify in the following. To do so, we impose $d_9 = 0$, which results in the fibral curves to split into various fibral \mathbb{P}^1 s. The irreducible curves are given in table 10.

The intersections of the curves are summarized in figure 12 and admits the shape of $E_7^{(1)}$, just as suggested by the Jacobian. These components are of importance as they get wrapped by M2 branes giving rise to multiplets that trigger the Higgsing in 5D to the $\mathfrak{so}_8^{(3)}$

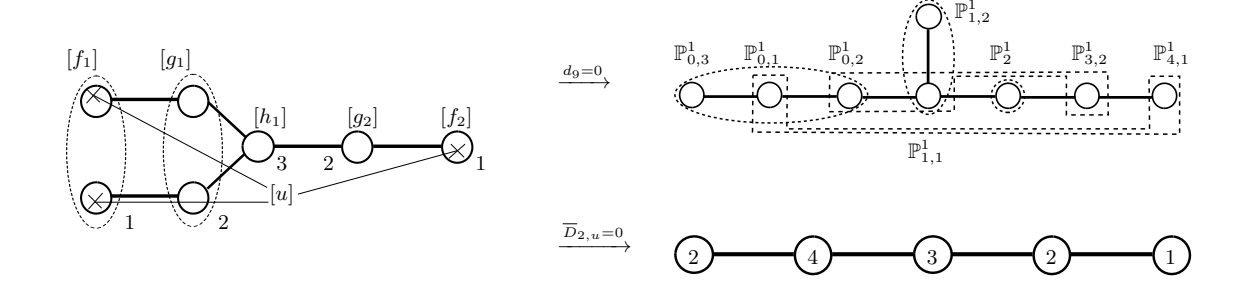


Figure 12. Depiction of the $\mathfrak{f}_4^{(1)}$ fiber in the cubic model and its intersections with the three-section [u]. There are two loci, where the fiber degenerates further, depicted on the right. Multiplicities of fibral curves are highlighted below.

fiber geometry, by effectively folding the third leg of the $\mathfrak{e}_6^{(1)}$. Computing intersections of the reducible fibral curves and the divisors allows to deduce weights of the hypermultiplets at the Coulomb branch. We obtain the weights by intersection with the fibral divisors $(g_2, h_1, g_1, f_1)_{(\sigma)}$. In the following we pick the curve $\mathbb{P}^1_{1,2}$ and compute the weights

$$\mathbb{P}^{1}_{1,2} \cdot (g_2, h_1, g_1, f_1)_{(\sigma)} : (-1, 0, 1, 0)_{(1)}, \tag{5.84}$$

which indeed are weights of an **26**₁-plet. The U(1)_E charge is given by $\sigma(u)$ which lifts to the \mathbb{Z}_3 charge in the 6D F-theory lift.

The second type of matter originates from the monodromy divisor $\overline{D}_{2,u}$, leading to non-localized \mathfrak{f}_4 fundamentals. Due to the geometric origin in the $\mathfrak{e}_6/\mathfrak{f}_4$ adjoint, they must have a trivial $\mathfrak{u}_{1,E}$ -charge.

We can then continue by counting the multiplicities of those states in terms of intersections of line bundles of the base. There are two line bundle classes S_7 and S_9 as before. Demanding absence of E-string points, fixes the sum of the intersections (5.59), analogous to the $\mathfrak{so}_8^{(3)}$ model.

To compute the multiplicity of 26_1 -plets we simply take the intersection of $d_9 = 0$ with \mathcal{Z} which hence results in

$$n_{\mathbf{26}_1} = \mathcal{S}_9 \cdot \mathcal{Z} \,. \tag{5.85}$$

The second source of the **26**₀-plets originates from the monodromy divisor that yields the ramification points $\mathcal{R} = \overline{D}_{2,u} \cdot \mathcal{Z}$ which is used in the RH theorem, resulting in

$$n_{26_0} = 5(1-g) + \mathcal{Z}^2 - \mathcal{S}_9 \cdot \mathcal{Z},$$
 (5.86)

where we have used (5.59).

The sum of the two contributions of fundamentals is given as

$$n_{26_0} + n_{26_0} = 5(1-g) + \mathcal{Z}^2,$$
 (5.87)

consistent with the 6D gauge anomalies of \mathfrak{f}_4 . This result is expected, as the theory admits no twisted algebras and hence a 6D SUGRA lift with the same gauge algebra structure. In that lift, only the $\mathfrak{u}_{1,E}$ charges turn into \mathbb{Z}_3 discrete charges.

Similar to the \mathfrak{g}_2 model in the section before, the $\mathcal{S}_9 \cdot \mathcal{Z}$ intersection may result in different numbers of charged and uncharged fundamental multiplets depending on the chosen compactification.

Before discussing the Higgsing in the next section, we present a concrete toric example. The base is a dP_1 , where the \mathfrak{f}_4 is placed over the $\mathcal{Z}^2 = -1$ curve of genus g = 0. The toric rays that of the 4D polytope that underlie the CY hypersurface are summarized in appendix A. The Hodge numbers are given as

$$(h^{1,1}, h^{2,1}(h_{np}^{2,1})) = (7,67(4)). (5.88)$$

Indeed, we find three Kähler parameters of fiber and base, and four more that correspond to the \mathfrak{f}_4 Cartan generators. Analysis of the geometry reveals the intersection number $S_9 \cdot Z = 2$ by finding the class of the section d_9 which yields the spectrum

$$n_{26_0} = n_{26_1} = 2. (5.89)$$

Higgsing to $\mathfrak{so}_8^{(3)}$. To Higgs to the twisted algebra $\mathfrak{so}_8^{(3)}$ and its \mathfrak{g}_2 finite sub-algebra, we can employ the group theory decomposition

$$\mathfrak{f}_4 \times \mathfrak{u}_{1,E} \to \mathfrak{g}_2 \times \mathfrak{su}_2 \times \mathfrak{u}_{1,E} \,,$$
 (5.90)

and then in the second step to break $\mathfrak{su}_2 \times \mathfrak{u}_{1,E}$. A related type of breaking, that resembles the same type of breaking directly in the 5D Coulomb branch is given as follows: starting off with the maximal enhanced gauge algebra $\mathfrak{f}_4 \times \mathfrak{u}_{1,E}$ that we constructed in the geometry before, we move to a partial Coulomb branch by keeping the curves inside of the fibral divisor f_1 and f_2 finite. On this locus in the Kähler moduli space, there is a breaking as

$$\begin{array}{|c|c|c|c|c|}\hline
\mathbf{f}_{4} \times \mathbf{u}_{1,E} & \mathbf{so}_{7} \times \mathbf{u}_{1,A} \times \mathbf{u}_{1,E} \\
\hline
\mathbf{52}_{0} & \mathbf{21}_{(0,0)} \oplus \mathbf{8}_{(1,0)} \oplus \mathbf{8}_{(-1,0)} \oplus \mathbf{7}_{(2,0)} \oplus \mathbf{7}_{(-2,0)} \oplus \mathbf{1}_{(0,0)} \\
\hline
\mathbf{26}_{0} & \mathbf{8}_{(1,0)} \oplus \mathbf{8}_{(-1,0)} \oplus \mathbf{7}_{(0,0)} \oplus \mathbf{1}_{(-2,0)} \oplus \mathbf{1}_{(2,0)} \oplus \mathbf{1}_{(0,0)} \\
\hline
\mathbf{26}_{1} & \mathbf{8}_{(1,1)} \oplus \mathbf{8}_{(-1,1)} \oplus \mathbf{7}_{(0,1)} \oplus \mathbf{1}_{(-2,1)} \oplus \mathbf{1}_{(2,1)} \oplus \mathbf{1}_{(0,1)}
\end{array} (5.91)$$

This group theory breaking is clear from geometry, simply by observing that we shrunk an $\mathfrak{so}_7 \subset \mathfrak{f}_4^{(1)}$ sub diagram.

On this more generic point in the CB moduli space, we may identify the $\mathbf{8}_{-1,1} \in \mathbf{26}_1$ as the Higgs candidate to break \mathfrak{so}_7 down to \mathfrak{g}_2 . Note that this constrains the line bundle \mathcal{S}_9 and in particular its intersection with \mathcal{Z} to be non-trivial for the respective Higgs to exist and the transition to be possible.

This path in the CB moduli space, allows to find the locus, where the $\mathbf{8}_{-1,1}$ -plets become massless in order to allow for a non-trivial VEV that triggers the respective Higgsing. At a generic point of the 2D Coulomb branch the 5D **8**-plet admits the mass

$$m_{8-1,n} = |-\xi_A + \tau(1+3n)|,$$
 (5.92)

with ξ_A and τ being the CB parameters of $\mathfrak{u}_{1,A} \times \mathfrak{u}_{1,E}$. The respective state becomes massless, when choosing $\xi_A = \tau$ and picking the n = 0 KK-mode. Upon this choice of

Coulomb branch parameters one obtains the new unbroken generator $\hat{\mathfrak{u}}_{1,E} = \mathfrak{u}_{1,A} + \mathfrak{u}_{1,E}$. Upon the Higgsing, we collect all states with non-trivial charges as

$$n_{21_0} = n_{52_0} = g$$
,
 $n_{7_0} = n_{26_0} + n_{26_1} - 1 + n_{52_0} = 4(1 - g) + \mathcal{Z}^2$, (5.93)
 $n_{7_1} = n_{7_2} = n_{26_0} + n_{26_1} + 2n_{52_0} = 5(1 - g) + \mathcal{Z}^2 + 2g$,

which matches the geometric computation, but over counts the multiplicity of massive states by one.

Note that the states recombine exactly in such a way, that the dependence on the class S_9 drops out.

Having identified the Higgs particles, we can also obtain predictions for the change in complex structure moduli upon the transition. Care needs to be taken when doing so as the 26_0 contains already two uncharged states, just as 7_0 of \mathfrak{g}_2 that contribute to $h^{2,1}$. Taking this into account, we simply obtain

$$\Delta h^{2,1} = 3n_{26_1} - 2 = 3S_9 \cdot \mathcal{Z} - 2. \tag{5.94}$$

Another important detail, that already appeared in the examples before, is the number of neutral fields. I.e. we also find singlets states with $\mathfrak{u}_{1,E}$ $\mathbf{1}_3$ in the transition. However as there is full a KK-tower of such states present, we also should have states, such as $\mathbf{1}_{3+3n}$ with masses $m = |(3+3n)\tau|$. Therefore, for n = -1, there is a zero model that contributes a neutral massless hypermultiplet, which appears as a complex structure modulus in the geometry.

Our general considerations are consistent with the toric examples. Consider for this, the change in Hodge numbers, given as

$$(h^{1,1}, h^{2,1}) = (7,67) \to (5,71).$$
 (5.95)

First we find a rank reduction by 2, consistent with the $\mathfrak{f}_4 \to \mathfrak{g}_2$ reduction in gauge symmetry. Second, there is a change of four complex structure moduli that originate from the $n_{26_1}=2$ Higgs fields.

6 Decoupling gravity and non-compact limits

Up to this point, all the theories studied in this work were associated to compact geometries and hence gravitational theories. This proved useful in understanding symmetries and global constraints arising from the geometry. In this section however, we take a different approach and systematically decouple gravity by taking a decompactification limit of the threefold. The limits are chosen such that the non-compact threefold still admits compact divisors with twisted fibers.

The resulting theory is not a SUGRA, but merely a supersymmetric quantum field theory (SQFT) (which thanks to its origin, is guaranteed to have a consistent UV completion). In particular, we will chose the decompatification limit such that the SQFT flows to a little string theory (LST) in the UV. Analyzing this LST will the provide an additional cross check of our geometric construction.

In order to do so, we exploit two of the striking features of little string theories. First, they admit a continuous global 2-group symmetry [72] and second, they often exhibit T-duality. T-duality in this context refers to the feature that one or multiple theories can share a Coulomb branch upon circle compactification.²¹ In [74] it was proposed that the universal part of the 6D 2-group symmetries should match across T-duality.²² This is very useful as the 2-group symmetries depend on the dual Coxeter numbers $h_{\mathfrak{g}}^v$ of gauge algebra factors that are coupled to the 6D tensors and therefore on the un/twisted affine extension.

The match of the 2-group structure constants among two dual theories therefore provides another robust test of our geometric construction.

6.1 Supergravity phase and T-duality

The starting point of our construction is a compact genus-one fibered threefold X specified by a toric hypersurface in an ambient fourfold, obtained from a regular fine star triangulation of the toric rays given in table 11. The threefold X admits the following Hodge numbers, that can be computed from the structure of the polytope as

$$(h^{1,1}, h^{2,1}(h_{nn}^{2,1}))(X) = (15, 63(3)). (6.1)$$

This geometry admits two toric fibrations that are inherited from the ambient space which can be identified by its 2D relexive sub-polytope structure²³ in Δ . We are then guaranteed to have (at least) one regular fine star triangulation that respects that fibration structure. We will discuss the two fibrations in detail: one is a genus-one fibration and the other an elliptic fibration. The two corresponding 6D theories are therefore (twisted) T-duals.

In the following we use the quiver notation of base curves and their fibers, which is commonly used in the literature (see e.g. [4, 77]). A quiver is written as

$$\dots \stackrel{\mathfrak{g}_i^{(s)}}{n_i} \dots \tag{6.2}$$

where $\mathfrak{g}_i^{(s)}$ an (s) twisted affine algebra sitting over a curve w_i of genus zero and self-intersection $w_i^2 = -n_i$ and two neighbouring curves in the quiver intersect. For more details see [4, 77] for recent reviews. The full structure can readily be obtained from the toric diagram of the base.

The genus-one fibration. The first fibration admits an F_4 ambient space in the (a, b, 0, 0) plane in the enumeration used in [45]. The base is spanned by the primitive rays that have the F_4 ambient space over the generic point. This yields the base divisors $w_{0,0}, w_{1,0}, w_2, y_1, y_{1,0}, y_2, y_3, y_{4,0}$ obtained from the primitive rays of (-, -, c, d) vertices and then constructing a fan from those. The resulting base admits $h^{1,1}(B_2) = 6$ or equivalently

²¹See also [73] for related work.

²²See also [75–77] for a systematic exploration of heterotic LSTs and their T-duals exploiting the match of 2-group structures.

²³The 2D sub-polytope criterion [78] also allows to deduce a triangulation that respects the fibration of the ambient space, although it might lead to a non-reflexive but VEX polytope.

T=5 in six dimensions. In addition there are fibral divisors of $\mathfrak{su}_3^{(1)},\mathfrak{su}_2^{(1)},\mathfrak{su}_2^{(1)}$ and $\mathfrak{e}_6^{(2)}$ -type. This is consistent with the number of Kähler moduli

$$h^{1,1}(X) = 2 + T + \text{rk}(G) = 2 + 5 + 8 = 15.$$
 (6.3)

The full quiver of the model admits the following ring like structure

Red marks the choosen curve, whose volume is send to infinity in the decompactification limit to a little string theory in the next section.

As discussed in section 4, the $\mathfrak{e}_6^{(2)}$ twisted algebra admits a spectrum as follows

$$\mathbf{26}_0 \oplus \mathbf{26}_1 \oplus \mathbf{1}_1 \oplus \mathbf{1}_0 \tag{6.5}$$

This twisted reduction admits a Jacobian fibration with an e_7 gauge algebra and two full hypers in the **56** representation.

The second elliptic fibration. The second torus fibration is given by the second 2D sub-polytope structure and found by projecting onto the (a, 0, 0, d)-slice in the ambient 4D polytope. The 2D sub-polytope that is given by F_6 yields a Morrison-Park model [24, 45] which is elliptic and hence not twisted. As before, the base is found by inspection, resulting in the ring like-quiver

In the LST decompactification limit, the volume of the curve in red is taken to infinite. This curve is dual to the one in the quiver (6.4). Note that there is also a curve with a geometric self-intersection +1, which we denote as -1 in the quiver convention. Due to the presence of a section, the resulting 5D compactification is untwisted and hence we only find untwisted algebras over each curve. The 6D theory admits T = 6 and an $\mathfrak{su}_3 \times \mathfrak{f}_4 \times \mathfrak{u}_1$ gauge algebra, which matches the 15 Kähler moduli of the geometry.

6.2 Little string limit and twisted T-duality

In this subsection we will decouple gravity to obtain an LST. At the level of the quiver, this can be achieved by removing the curve w_2 from the base, such that the resulting intersection form of the residual curves $w_I \cdot w_I = \Omega_{I,J}$ is positive semi-definite [26]. The respective base curve lifts to a toric divisor of the ambient space, given by the ray (1, -1, -1, -1).

Ge	nus 1 fiber
X	(-1,1,0,0)
Y	(-1,-1,0,0)
Z	(1,0,0,0)
$w_{0,0}$	(-1,0,0,-1)
$w_{0,1}$	(-1,-1,0,-1)
$w_{0,2}$	(0,-1,0,-1)
$w_{1,0}$	(0,0,0,1)
$w_{1,1}$	(-1,0,0,1)
w_2	(1, -1, -1, -1)

	Compact curves
y_1	(-3,-1,1,1)
$y_{1,i}$	(-3,0,1,0), (-5,-2,2,0), (-7,-2,3,0), (-9,-3,4,0), (-5,-1,2,0)
y_2	(-7,-3,3,-1) (-5,-2,2,-1)
y_3	(-5,-2,2,-1)
$y_{4,i}$	(-3,-2,1,-1) , $(-3,-1,1,-1)$

Table 11. Toric rays of the compact threefold with inequivalent genus-one and elliptic fibration descending from the ambient space.

The residual toric rays lift to divisors on the full threefold and in fact also to the 4D ambient space²⁴ which yields a non-compact ambient space. This limit is exactly chosen such that it removes the red 0 curves in the quiver diagrams (6.4) and (6.6). While the red curve is completely removed, the neighbouring quiver nodes become non-compact and their fibers become flavor algebra factors that we denote by $[\mathfrak{g}_F^{(s)}]$. The decompactification limit of the threefold is chosen such that the two torus-fibration structures are still part of the non-compact threefold which preserves T-duality for the LSTs.

As there are two LSTs we can compute and match their 2-group structure constants. In order to do so, we first need to compute the little string charges N_I . These are given as the multiplicities of the unique null vector [26] of the intersection form Ω_{IJ}

$$\Sigma_0 = \sum_i N_I w^I \,. \tag{6.7}$$

We summarize the resulting non-compact quiver with its LS charges as the vectors

$$[\mathfrak{su}_2] \ 1 \ {\overset{\mathfrak{e}_6^{(2)}}{4}} \ 1 \ 2 \ {\overset{\mathfrak{su}_2^{(1)}}{2}} [\mathfrak{su}_3], \qquad N_I = (1, 1, 3, 2, 1). \tag{6.8}$$

The above LST admits four compact base curves and twisted fibers of total rank 5 and hence a Coulomb branch of dimension $\dim(CB) = 9$. We have excluded other flavor and matter factors from the quivers, as they are not important for our arguments. The second LST quiver is given as

$$[\mathfrak{su}_3] \ 1 \ {\overset{\mathfrak{f}_4^{(1)}}{5}} \ 1 \ 2 \ 2 \ 2, \qquad N_I = (1, 1, 4, 3, 2, 1).$$
 (6.9)

The theory admits five compact base curves and a rank four gauge group which also yields a Coulomb branch dimension $\dim(CB) = 9$ as expected.

Consistency check from 2-groups. As mentioned above, the fact that these two theories have the same compact geometric origin implies that the two LSTs are (twisted) T-duals.

²⁴More details to the construction can be found in [76].

Beyond that however we can also match the 2-group structure constants characteristic to the LSTs as proposed in [74].

In the following we focus on the universal 2-group structure constants obtained from the mixing of the \mathfrak{u}_1 LST 1-form symmetry and the Poincare and SU(2)-R-symmetry. Their structure constants are computed as [72, 74]

$$\kappa_P = \sum_I N_I (2 - \Omega^{II}), \qquad \kappa_R = \sum_I N_I h_{\mathfrak{g}_I^{(s)}}^v. \tag{6.10}$$

Here $\Omega^{II} = n_I$ and $h^v_{\mathfrak{g}_I^{(s)}}$ being the dual Coxeter number of the s twisted gauge algebra $\mathfrak{g}^{(s)}$ coupled to the curve w^I with string charge N_I . The dual Coxeter number can simply be computed from the sum of the Kac labels of the Dynkin diagram. For $\mathfrak{su}_n^{(1)}$ algebras, the dual Coxeter is given as

$$h_{\text{su}}^v(1) = n$$
. (6.11)

We formally assign the value $h^v = 1$ for curves that are paired to the trivial gauge algebra. Most importantly, the dual Coxeter number is sensitive to a twisted or untwisted affinization of a finite gauge algebra. For the case at hand, there is

$$h_{\mathfrak{e}_{6}^{(2)}}^{v} = 12, \qquad h_{\mathfrak{f}_{4}^{(1)}}^{v} = 9.$$
 (6.12)

Taking the above difference into account, we obtain the matching 2-group structure coefficients in the two theories

$$(\kappa_P, \kappa_R) = (2, 20). \tag{6.13}$$

The above check is highly non-trivial and confirms that the two LSTs are indeed T-dual as implied from geometry.

Untwisting the fiber. At this point one might wonder how the threefold would differ if the $\mathfrak{e}_6^{(2)}$ fiber were to be replaced by a regular $\mathfrak{f}_4^{(1)}$ fiber over the same curve in a genus-one geometry. In such a case at least the number of Kähler moduli would agree, but what about the rest of the theory?

Fortunately, such a geometry exists with polytope vertices given in table 12 and is obtained simply by exchanging the vertex (-9, -3, 4, 0) for (-2, -1, 1, 0). It should be noted that the resulting threefold has not only the same number of Kähler moduli, but also complex structure moduli

$$(h^{1,1}, h^{2,1})(X_2) = (15, 63(2)), (6.14)$$

as the one with $\mathfrak{e}_6^{(2)}$ fiber (however the number of complex structure moduli realized "non-polynomially" has reduced in number).

In this new geometry, the $\mathfrak{e}_6^{(2)}$ fibration over the curve \mathcal{Z} with self-intersection $\mathcal{Z}^2 = -4$ has now changed to an untwisted $\mathfrak{f}_4^{(1)}$ fibration. Upon decoupling gravity the LST quiver for the first genus-one fibration is given as

$$[\mathfrak{su}_2] \ 1 \ \stackrel{\mathfrak{f}_4^{(1)}}{4} \ 1 \ 2 \ \stackrel{\mathfrak{su}_2^{(1)}}{2} [\mathfrak{su}_3], \qquad N_I = (1, 1, 3, 2, 1). \tag{6.15}$$

Ge	nus 1 fiber
X	(-1,1,0,0)
Y	(-1,-1,0,0)
Z	(1,0,0,0)
$w_{0,0}$	(-1,0,0,-1)
$w_{0,1}$	(-1,-1,0,-1)
$w_{0,2}$	(0,-1,0,-1)
$w_{1,0}$	(0,0,0,1)
$w_{1,1}$	(-1,0,0,1)
w_2	(1, -1, -1, -1)

	Compact curves
_	(-3,-1,1,1)
$y_{1,i}$	(-3,0,1,0), (-5,-2,2,0), (-7,-2,3,0), (-5,-1,2,0), (-2,-1,1,0)
y_2	(-7,-3,3,-1)
y_3	(-5,-2,2,-1)
$y_{4,i}$	(-3,-2,1,-1) , $(-3,-1,1,-1)$
3 -,0	

Table 12. Toric rays of the threefold where the $\mathfrak{e}_6^{(2)}$ fiber got exchanged for $\mathfrak{f}_4^{(1)}$. Both geometries share the same Hodge numbers but differ not only in curve structure but also the number of non-polynomial complex structures deformations.

Since the Hodge numbers have not changed, the Coulomb branch dimension of the LST remains the same. As we will explore in more generality in section 7, the $\mathfrak{f}_4^{(1)}$ fiber over the $\mathcal{Z}^2 = -4$ curve admits a single 26_0 -plet only. Although the change in fiber structure was very subtle, the 2-group structure constant κ_R is able to detect it, as the dual Coxeter number of $\mathfrak{f}_4^{(1)}$ is lower than $\mathfrak{e}_6^{(2)}$.

Importantly, the change in the fiber structure has not eliminated the second elliptic fibration and as a result we can discuss the change in the T-dual geometry in this new context as well. Here we find the LST quiver

$$\begin{bmatrix} \mathfrak{su}_3 \end{bmatrix} 1 \overset{\mathfrak{f}_4^{(1)}}{5} 1 2 2, \qquad N_I = (1, 1, 3, 2, 1) . \qquad (6.16)$$

The resulting quiver is similar to the original one given in (6.9). The only difference is that an E-string curve to the right of the 5 curve has been moved down, making it a trivalent vertex.

The change in base curve structure has altered the LST charge vector N_I exactly in such a way that the 2-group structure constants still match in both theories, given as

$$(\kappa_P, \kappa_R) = (2, 17). \tag{6.17}$$

In the following we propose a physical interpretation of the two (dual) transitions as specific Higgs branch deformations. Indeed, in [76], the proposal was made that κ_R should be thought of as a measure of the degrees of freedom of an LST which decrease monotonoically along Higgs branch deformations, analogously to the a-coefficient in an SCFT. This might at first seem puzzling as both geometries admit the very same number of complex structure coefficients. However we have observed that in the untwisted case, one of those deformations changed from non-polynomial to a polynomial deformation. This hints at the possibility that the twisted algebra lives on an enhanced point of symmetry in the moduli space of the theory. In section 7 we will consider this type of transition in further generality. Similarly, for the T-dual theory we have an exotic type of E-string transition, which has changed the number of M-strings, i.e. 2 curves into an E-string.

We close this section by discussing how all of the above theories/geometries can be similarly used to construct twisted 5D SQFTs with an SCFT limit in the UV. The plan we employ is the same as for the LST phase. One simply needs to remove an arbitrary compact base curve from an LST quiver²⁵ to obtain an SQFT that flows to an SCFT.

The two simplest choices are to decompactify the left most 1 curve or rightmost 2 curve in the quiver (6.8) resulting in an SCFT quiver such as

All of the constructions presented in this sections, straightforwardly generalize to the other twisted reductions that we discuss in section 5. In particular many of the explicit toric examples given in appendix A have twisted algebras over 0 curves or shrinkable curves that yield LSTs or SCFTs in their respective decompactification limits.

7 Twisted VS. untwisted genus-one fibers

In the previous section we encountered the possibility of exchanging a twisted algebra with its untwisted counterpart

$$\mathfrak{g} \in \hat{\mathfrak{g}}^{(n)} \text{ and } \mathfrak{g} \in \mathfrak{g}^{(1)}.$$
 (7.1)

In the $\overset{\mathfrak{e}_6^{(2)}}{4} \to \overset{\mathfrak{f}_4^{(1)}}{4}$ case, we noted that the two compact threefolds share some important features, in particular identical Hodge numbers. In this section we will compare twisted and untwisted fibers more systematically and observe that these relationships can be formulated in more generality. In fact in all the examples we have encountered, the geometries with twisted fibrations exhibit "cousins" in the form of untwisted fibrations which share the very same Hodge numbers and can be connected through a geometric transition.

These observations help to resolve a puzzle in the literature: in [46] the geometry of a genus-one fibration with a twisted $\mathfrak{so}_8^{(3)}$ algebra was considered and in that work it was expected to lift to a 6D F-theory with an \mathfrak{g}_2 gauge algebra. It was noted that all gauge and gravity anomalies could be cancelled. In view of the geometries we have seen in the present work, this conclusion may come as a surprise as the Jacobian admits a very different fiber structure and we therefore do not expect such a gauge algebra in the 6D F-theory lift (see section 5.2). The fact that the gauge algebra must change in the 6D lift is further signaled from the 5D BPS state count enumerated throughout this work, which deviates from [46]. In the present work, we find that the twisted algebras do not solve the 6D anomalies if their finite gauge algebra is not altered. At first glance, this may appear as a very unlikely coincidence: how did the lifts of [46], which assumed that the gauge algebra was unaltered between 5D/6D, lead to a seemingly consistent 6D SUGRA theory?

This puzzle is resolved by the geometries we present in this section by noting that most of the twisted algebras we study are closely related to a similar geometry with an untwisted

²⁵As noted in [76] any such removal destroys other inequivalent torus fibration in the geometry.

fiber. These untwisted algebras have the same fiber structure in the Jacobian and complex structure and BPS states consistent with the 6D anomalies as proposed in [46]. This section is therefore devoted to a comparison of these two type of geometries and the transitions among them.

Besides the subtle difference in the fiber structure of the two geometries, there is another similarly subtle difference in the complex structure moduli sector: we find that twisted fibrations generally admit complex structure deformations that are realized as non-polynomial deformations in the toric hypersurface description, as opposed to the untwisted one. Such terms can be conveniently computed via the Batyrev formula from the toric polytope. While this observation might first appear just as a technical detail, we propose a physical interpretation, making those deformations relevant to understand the difference between twisted and untwisted fibers. In order to do so, we first discuss their physical significance in elliptic fibrations.

7.1 Enhanced symmetries and non-poly defs

The number of complex structure moduli and their non-polynomial contributions in toric hypersurfaces can be conventiently computed from the pair of relexive polytopes Δ , Δ^* in the Batryev construction [79]. It is given via the combinatorial formula

$$h^{2,1}(X) = l(\Delta^*) - 4 - \sum_{\Gamma^*} l^{\circ}(\Gamma^*) + \underbrace{\sum_{\Theta} l^*(\Theta) l^*(\Theta^*)}_{h^{2,1}}.$$
 (7.2)

Here $(l^{\circ})l$ counts (interior) points, with Γ^* being edges in Δ^* and Θ^* being codimension two faces of Δ^* with duals Θ . The part $h_{np}^{2,1}$ is the main relevant contribution for us, that counts complex structures without a corresponding hypersurface monomial.

For elliptic fibration such deformations can be given a physical interpretation in the F/M-theory picture. For this we first introduce the neutral components of hypermultiplet fields

$$\delta h_{np}^{2,1}(\mathbf{R}) = \text{Dim}(\mathbf{R}) - H_{ch}(\mathbf{R}). \tag{7.3}$$

 $H_{ch}(\mathbf{R})$ denotes the non-trivial weights of a hypermultiplet representation \mathbf{R} , called the charge dimension of a representation. In the case of the adjoint representation, $H_{ch}(\mathbf{Adj})$ is simply the number of roots and $\delta h_{np}^{2,1}(\mathbf{Adj})$ the number of Cartan generators. As $\delta h_{np}^{2,1}(\mathbf{R})$ are themselves uncharged fields everywhere at the Coulomb branch, they are counted as complex structure moduli in the threefold. In fact there is a natural reason why those contributions should be non-polynomial when giving them a symmetry breaking vev. For adjoint hypermultiplets, such Higgs branches typically breaks to the maximal Cartan sub-algebra as in

$$\mathfrak{su}_2 \to \mathfrak{u}_1 \,, \tag{7.4}$$

via $\mathbf{3} \to \mathbf{1}_1 \oplus \mathbf{1}_{-1} \oplus \mathbf{1}_0$. There are more options for non-simply laced algebras as those typically admit non-trivial (lower dimensional) representations with non-trivial $\delta h_{np}^{2,1}(\mathbf{R})$

besides the adjoint. When those representations acquire non-trivial vevs, a rank preserving Higgsing is possible such as in

$$\mathfrak{g}_2 \to \mathfrak{su}_3 \,, \quad \mathfrak{f}_4 \to \mathfrak{so}_8 \,, \tag{7.5}$$

via the decompositions of the Hypermultiplet representations

$$7 \to 3 \oplus \overline{3} \oplus 1$$
, $26 \to 8_v \oplus 8_s \oplus 8_c \oplus 1 \oplus 1$, (7.6)

that acquire the symmetry breaking vevs. Those vevs sit precisely in the $\delta h_{np}^{2,1}(\mathbf{R})$ parts of \mathbf{R} . As the Higgsing is rank preserving, no Cartan generator becomes massive and the number of neutral fields is preserved, resulting in a conservation of Hodge numbers.

The above considerations are reflected in the geometry of the respective elliptic fibration: e.g. for each **26**-plet representation of an \mathfrak{f}_4 fiber, one finds two $\delta h_{np}^{2,1}$, realized as non-polynomial complex structure deformations. When Higgsing to \mathfrak{so}_8 , the threefolds admits the very same Hodge numbers. The difference however is, that the associated $\delta h_{np}^{2,1}$ deformations became all realized as polynomial deformations. Similarly, when Higgsing \mathfrak{su}_2 on $g \times 3$ -plets, all g non-polynomial deformations become polynomial and the geometry acquires a non-trivial Mordell-Weil rank [38].

Turning this logic upside down, the knowledge about non-polynomial deformations may allow us to track representation content²⁶ of the gauge algebra, directly from geometry. Furthermore it suggests a direct physics interpretation. In the symmetry broken phase, the vevs are moduli that parameterize the (partial) Higgs branch of the two gauge algebras of same rank. As those vevs are moduli, they can take on any non-vanishing value matching the (real part of the) monomial coefficients in the hypersurface. At the locus of enhanced symmetry, the vevs must vanish, matching the absence of the respective polynomial coefficients, while the number of neutral fields is preserved.

We adopt this interpretation of the non-polynomial defs for the twisted algebras in what follows. As already anticipated in section 6, the presence of those non-polynomial deformation is a universal feature for (almost) all twisted fibers. Furthermore it suggests the possibility that they are part of a larger twisted affine type of representation, which can be Higgsed in a rank preserving way to a non-twisted one. Moreover we will use the field theory of twisted compactifications, to match/predict non-poly defs in the compact threefolds. At the same time, their presence yields a criterion when geometric transitions to an untwisted algebra may be possible. These Higgsing transitions/singlets are generically present but with the exception of the twisted versions of 6D non-Higgsable cluster theories $\mathfrak{e}_{6}^{(2)}$ $\mathfrak{su}_{3}^{(2)}$ $\mathfrak{so}_{8}^{(3)}$ $\mathfrak{so}_{8}^{(3)}$ and 4 as already alluded to in section 4 and section 5.

7.2 $\mathfrak{e}_6^{(2)}$ vs $\mathfrak{f}_4^{(1)}$ genus-one fibers

In the following we consider another singular genus-one model which is related to the $\mathfrak{e}_6^{(2)}$ twisted fibration of the quartic which we will call X^D . For this we consider the generalized

 $^{^{-26}}$ Care has to be taken from other sources of such deformations, such as adjoints or empty -2 curves. See for example [80].

Tate-vector

$$n_i = \{3, 2, 2, 1, 0, 2, 1, 0\} , (7.7)$$

which reduces the vanishing order of the X^3Y term in the quartic fiber model by one. From this perspective, the $\mathfrak{e}_6^{(2)}$ model appears as an enhanced singularity.

As we will discuss in the following, the resulting singularity will be of $IV^{*,ns}$ type both in the genus-one and Jacobian fibration. Note that the above tuning is such, that the monodromy divisor $\overline{D}_{2,X} = d_8^2 - 4d_5$ stays un-affected, still intersecting the base divisor \mathcal{Z} non-trivially. When mapping the singular genus-one model, specified by the Tate vector (7.7) to the Jacobian we obtain (at leading order in z) the expressions

$$f = z^{3}\widehat{p} + \mathcal{O}(z^{4}),$$

$$g = z^{4}d_{2}^{2}\overline{D}_{2,X} + \mathcal{O}(z^{5}),$$

$$\Delta = z^{8}d_{2}^{4}\overline{D}_{2,X}^{2} + \mathcal{O}(z^{9}).$$

$$(7.8)$$

As long $\overline{D}_{2,X}|z=0$ does not become a perfect square, which is the case by construction,²⁷ we have a Type IV^* non-split singularity i.e. an \mathfrak{f}_4 in the Jacobian as claimed. Thus we expect an $\mathfrak{f}_4 \times \mathbb{Z}_2$ gauge algebra in the 6D F-theory. We begin by analyzing the spectrum in the Jacobian and then argue that this spectrum coincides with that in the genus-one fibration as well. In order to do so, we first note that the discriminant admits two codimension two components over z=0: first there is the monodromy divisor $\overline{D}_{2,X}$ and the second component $d_2=0$. The later one yields a codimension two vanishing order (3,5,9) which corresponds to an E_7 singularity. The hypermultiplets that are localized here yield 26_1 matter multiplets which we will double check in the genus-one model momentarily.

When computing the multiplicity of states, we first start by being fully general. For this we recall the line bundle classes of the various sections to be given as

$$[d_2] \sim 2c_1 - S_9 - 2\mathcal{Z}, \qquad [d_8] \sim c_1 + S_9,$$
 (7.9)

which are needed to compute the multiplicities of states. Those of the $\mathbf{26}_1$ states are simply evaluated via the intersections $\mathcal{Z} \cdot [d_2]$ whereas the neutral $\mathbf{26}_0$ -plets are non-localized states over the loci where the fibral curves of \mathcal{Z} are branched, which is fixed by the number of ramification points $\mathcal{R} = [\overline{D}_{2,X}] \cdot [\mathcal{Z}]$ in the RH theorem eq. (4.18). Taking the degree of the cover to be d = 2, we find the following multiplicities

$$n_{52_0} = g$$
, $n_{26_1} = 4(1-g) - S_9 \cdot Z$, $n_{26_0} = (1-g) + Z^2 + S_9 \cdot Z$, (7.10)

which admits the additional degree of freedom, to dial the relative multiplicities via the $S_9 \cdot Z$ intersections. Notably, the combined multiplicity of the \mathfrak{f}_4 fundamentals yields

$$n_{26_1} + n_{26_0} = 5(1-g) + \mathcal{Z}^2,$$
 (7.11)

which is consistent with 6D gauge algebra anomaly cancellation conditions (see e.g. [81]).

²⁷The polynomial in f is given as $\hat{p} = d_2 d_7 d_8 - 2d_1 d_8^2 - 2d_2 d_4 + 8d_1 d_5$.

In order to compare the above model with an geometric transition to the $\mathfrak{e}_6^{(2)}$ geometry however, we also need to impose the extra condition that $[d_1] \cdot [\mathcal{Z}] = 0$ which resulted in (4,6,12) points. These points are generally absent in the $\mathfrak{f}_4^{(1)}$ model, but would appear when performing the respective deformation to $\mathfrak{e}_6^{(2)}$. This extra condition removes the degree of freedom and yields

$$S_9 \cdot Z = 2(1-g) + \frac{1}{2}Z^2$$
. (7.12)

Plugging this restrictions into (7.11) gives

$$n_{\mathbf{52}_0} = g, \qquad n_{\mathbf{26}_1} = 2(1-g) + \frac{1}{2}\mathcal{Z}^2, \qquad n_{\mathbf{26}_0} = 3(1-g) + \frac{1}{2}\mathcal{Z}^2.$$
 (7.13)

When compared to the $\mathfrak{e}_6^{(2)}$ multiplicities that were computed in section 4.1, we find the 26_0 -plets to exactly coincide with the multiplicity there, whereas the number of 26_1 is reduced by one.

This computation concludes the f_4 spectrum in the Jacobian. In the following however, we want to double check the claim, that the spectrum coincides with the genus-one model.

For this we consider the resolved genus-one fibration X^D , given as

$$p = d_1 f_2^3 g_2^2 h_1 X^4 + d_2 f_2^2 g_2 X^3 Y + d_3 f_2^2 f_3 g_1^2 g_2^2 h_1^2 X^2 Y^2 + d_4 f_2 f_3 g_1^2 g_2 h_1 X Y^3 + d_5 f_3 g_1^2 Y^4 + d_6 f_2^2 f_3 g_1 g_2^2 h_1^2 X^2 Z + d_7 f_2 f_3 g_1 g_2 h_1 X Y Z + d_8 f_3 g_1 Y^2 Z + f_3 Z^2,$$
 (7.14)

with fibral Stanley Reisner ideal

$$SRI : \{YX, Yf_2, Yg_2, Yh_1, e_1Z, e_1f_2, e_1f_3, e_1g_1, e_1g_2, e_1h_1, Zf_1, f_1f_3, f_1g_2, f_1h_1, Zg_1, Xf_3, f_2f_3, f_3g_2, Xg_1, Xg_2, Xh_1, f_2h_1\}.$$
(7.15)

The base divisor \mathcal{Z} then pulls back to the reducible divisor

$$\mathcal{Z} = f_2 g_2^2 h_1^3 g_1^2 f_3 \,, \tag{7.16}$$

with fibral curves

$$\mathbb{P}_{0,\pm}^{1}: f_{2} \cap d_{5}g_{1}^{2} + d_{8}g_{1}Z + Z^{2},
\mathbb{P}_{1,\pm}^{1}: g_{2} \cap d_{5}g_{1}^{2} + d_{8}g_{1}Z + Z^{2},
\mathbb{P}_{2}^{1}: h_{1} \cap d_{5}f_{3}g_{1}^{2} + d_{2}g_{2} + d_{8}f_{3}g_{1}Z + f_{3}Z^{2},
\mathbb{P}_{3}^{1}: g_{1} \cap f_{3} + d_{1}f_{2}^{3}g_{2}^{2}h_{1} + d_{2}f_{2}^{2}g_{2}Y,
\mathbb{P}_{4}^{1}: f_{3} \cap d_{1}h_{1} + d_{2}Y.$$
(7.17)

In figure 13 we have summarized the fibral intersections of the curves. The monodromy divisor $\overline{D}_{2,X}$ of the 2-section X is again central as it is also the locus along which the two fibral curves in f_2 and g_2 get interchanged.

Note that the 2-section X intersects the node f_2 which is the affine node we associate with the base coordinate z. This however might come as a surprise, as it is f_3 which lifts to an actual F_4 singularity in the genus-one geometry! In fact, when shrinking all but the f_3 node, we need to again orthogonalize the reference 2-section properly with respect to the unbroken gauge group.

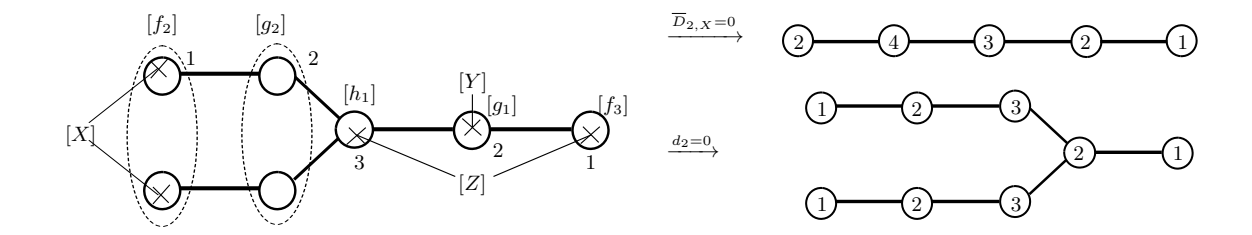


Figure 13. Depiction of the X^D genus-one fibration and its $\mathfrak{f}_4^{(1)}$ fibral structure. Choosing f_2 as the affine node results in an \mathfrak{so}_9 singularity while keeping f_3 finite results in an \mathfrak{f}_4 singularity. The two codimension two degeneration loci shown on the right.

In order to account for both singular limits, we consider the two possible discrete Shioda map combinations

$$\sigma_2(X) = [X], \qquad \sigma_2'(X) = [X] + 2[f_2] + 3[g_2] + 4[h_1] + 2[g_1],$$
 (7.18)

for which we have the intersections

$$\sigma_2(X) \cdot (f_2, g_2, h_1, g_1, f_3) = (2, 0, 0, 0, 0), \text{ and } \sigma'_2(X) \cdot (f_2, g_2, h_1, g_1, f_3) = (0, 0, 0, 0, 2).$$

$$(7.19)$$

While the topology of the resolved fiber is that of $\mathfrak{f}_4^{(1)}$ the two singular limits, keeping either f_2 or f_3 finite, yield an \mathfrak{so}_9 or \mathfrak{f}_4 singularity respectively.²⁸

In order to cross check the computations made in the Jacobian, we investigate the matter loci in the resolved genus-one geometry next. First we recall the codimension two locus $d_2 = 0$. When investigating the fibral curves, we indeed find a split into an E_7 type of fiber, just as in the Jacobian. We can then compute the intersections with the other fibral divisors e.g. for the $\mathbb{P}^1_{2,\pm}$ curve and obtain the intersections

$$\mathbb{P}^{1}_{2,\pm} \cdot (f_2, g_2, h_1, g_1, f_3)_{(\sigma_2, \sigma_2')} = (0, 1, -1, 0, 1)_{(0, -1)}. \tag{7.20}$$

These intersections numbers yield the charges of (massive) 5D particles obtained from M2 branes wrapping the respective curve. When taking f_3 as the affine node and hence finite, such that we obtain the \mathfrak{f}_4 limit we find weights of an $2\mathfrak{6}_1$ just as claimed in the Jacobian fibration. Similarly we find, over $\overline{D}_{2,X}=0$ to support the monodromy divisor that yields the $2\mathfrak{6}_0$ -plets. As opposed to the $\mathfrak{e}_6^{(2)}$ model, the fiber does not become a degree two multiple fiber over such loci as the degree one curve \mathbb{P}_3^1 does not split here. Therefore we expect the Weil-Châtelet group to reduce to the Tate-Shafarevich group $\mathrm{III}(X^D)$, which we take as the main criterion, why Jacobian and genus-one fibration admit the very same $\mathfrak{f}_4^{(1)}$ fiber structure. From this perspective it is also clear, why the matter and its multiplicities in genus-one and Jacobian are the same, with the only difference being that the $2\mathfrak{6}_1$ -states stay massive at the origin of the \mathfrak{f}_4 Coulomb branch.

 $^{^{28}}$ Note however, that both singular limits become identical when being mapped into the singular Weierstrass model.

The spectrum of the $\mathfrak{f}_4^{(1)}$ genus-one geometry X^D appears to be very similar to that of the $\mathfrak{f}_4 \in \mathfrak{e}_6^{(2)}$ geometry X^A albeit the difference in the massive $2\mathfrak{6}_1$ multiplicities. One might then wonder, if and how the two fibrations might be related. This can be deduced by having a closer look at the precise geometry and recalling that we kept different curves finite throughout the transition. In X^A , we kept curves in f_2 finte, which resulted in an \mathfrak{f}_4 singularity, keeping f_2 finite in X^D yields an $\mathfrak{so}_9 \in \mathfrak{f}_4^{(1)}$ singularity. Using the methods from section 4 and section 5 and can indeed compute the shrinkable curves in X^D while keeping f_2 finite resulting 32+4=36 vector multiplets, that make up the adjoint of \mathfrak{so}_9 . Hence when performing the conifold transition from $\mathfrak{f}_4 \in \mathfrak{e}_6^{(2)}$ we rather obtain an \mathfrak{so}_9 via the breaking

$$\mathbf{52}
ightarrow \mathbf{36} \oplus \mathbf{16}$$
 , $\mathbf{26}
ightarrow \mathbf{16} \oplus \mathbf{9} \oplus \mathbf{1}$.

The curious fact however is, that the resulting genus-one fibration admits another limit in the Coulomb branch moduli space of $\mathfrak{so}_9 \times \hat{\mathfrak{u}}_{1,E}$ such that an $\mathfrak{f}_4 \times \mathfrak{u}_{1,E}$ gauge algebra arises with a massless spectrum just as in the $\mathfrak{e}_6^{(2)}$ theory. This on the other hand suggests, that not only Coulomb branch dimension but also the number of complex structure moduli of X^D coincides with that of X^A . This is indeed the case, as we will demonstrate in an example in the following.

Toric example. Let us move from these general considerations to a concrete toric example. The toric rays defining the threefold are given in appendix A and the Hodge numbers can be computed via the Batyrev construction. In our example geometries, we have the same Hodge numbers

$$(h^{1,1}, h^{2,1})(X^A) = (h^{1,1}, h^{2,1})(X^D) = (7,95). (7.21)$$

This seems to be at odds with the fact that we performed a tuning of the generalized Tate coefficients when relating the two theories. The resolution to this puzzle is the fact that not all complex structure moduli in the toric hypersurface equation of X^A are realized as polynomial deformations. Computing the complex structure moduli, and the respective fractions of non-poly deformations of the two geometries, we obtain

$$h^{2,1}(h_{np}^{2,1})(X^A) = 95(9)$$
 and $h^{2,1}(h_{np}^{2,1})(X^D) = 95(6)$. (7.22)

Note that there are several contributions of non-poly deformations in both geometries that need to be discussed. The six deformations in the $\mathfrak{f}_4^{(1)}$ geometry X^D are contributions from the 3×2 neutral components inside the three 26_0 -plets.

For the twisted fiber $\mathfrak{e}_6^{(2)}$ of geometry X^A we have two contributions to the nine non-poly deformations: first there is the contribution of the $3 \times 26_0$ -plets neutral fields, which is the same as in the $\mathfrak{f}_4^{(1)}$ model. We propose that the three missing neutral fields correspond to neutral localized singlets. These can be directly deduced from the twisted reduction of the \mathfrak{e}_6 theory, which we reviewed in section 4. From this 6D origin, we can obtain a prediction for the non-poly deformations as

$$\delta h_{np}^{2,1} = n_{\mathbf{1}_0} + 2n_{\mathbf{26}_0} + 4n_{\mathbf{52}_0} = 9(1-g) + \frac{3}{2}\mathcal{Z}^2 + 4g.$$
 (7.23)

In the case at hand, the curve of consideration admits self-intersection $\mathcal{Z}^2 = 0$ and g = 0, such that we have a match of all non-poly deformations in X^A . Note that this also implies, that an $\mathfrak{e}_6^{(2)}$ on a $\mathcal{Z}^2 = -6$ curve of genus zero does not posses any such singlets. Indeed, the respective genus one model, given in section 4.1 admits 151 complex structure moduli with $h_{np}^{2,1} = 0$.

In analogy to the elliptic threefolds, discussed in the section before, it becomes apparent that those singlets are an integral part of a non-trivial twisted $\mathfrak{e}_6^{(2)}$ representation, and not only its \mathfrak{f}_4 subgroup. Hence, when breaking the $\mathfrak{e}_6^{(2)}$ symmetry via the $\mathfrak{f}_4 \to \mathfrak{so}_9$ chain, it is suggestive that those singlets are not fixed to a vanishing vev any longer which translates to polynomial deformations in the toric hypersurface. We wish to return to this specific point in future work.

7.3 $\mathfrak{so}_8^{(3)}$ vs $\mathfrak{g}_2^{(1)}$ genus-one fibers

We now turn to a genus-one fibration X^D that admits a $\mathfrak{g}_2^{(1)}$ fiber which shares the same Hodge numbers as the genus-one fibration X^A with twisted $\mathfrak{so}_8^{(3)}$ fiber. The singular genus-one model with an $\mathfrak{g}_2^{(1)}$ fiber is obtained via the generalized Tate-vector

$$n_i = \{2, 1, 1, 0, 1, 1, 0, 1, 0, 0\} . (7.24)$$

The $\mathfrak{so}_8^{(3)}$ model, is obtained upon a further tuning of the above vanishing orders to $d_2 \to z \hat{d}_2$, $d_5 \to z \hat{d}_5 z$, $d_6 \to z d_6$. When mapping the respective tuning into the singular Weierstrass model, we obtain at leading orders the Jacobian $J(X^D/B_2)$

$$f = \frac{1}{3}z^{2}(-9d_{10}d_{2}d_{4}d_{5} + 3d_{10}d_{2}^{2}d_{7} - d_{5}^{2}d_{7}^{2} + 3d_{4}d_{5}^{2}d_{9} + d_{2}d_{5}d_{7}d_{9} - d_{2}^{2}d_{9}^{2}) + \mathcal{O}(z^{3}),$$

$$g = z^{3}P + \mathcal{O}(z^{4}),$$

$$\Delta = z^{6}Q^{2}\overline{D}_{3,u} + \mathcal{O}(z^{7}),$$

$$(7.25)$$

with P some longer irrelevant polynomial and Q given as

$$Q = d_{10}d_2^3 - d_4d_5^3 + d_2d_5^2d_7 - d_2^2d_5d_9. (7.26)$$

The resulting singularity is of $I_0^{*,ns}$ type i.e. an $\mathfrak{g}_2^{(1)}$ fiber upon resolution. Note that we also find here the order three monodromy divisor appearing at leading orders of the discriminant. Lets compare this to the fiber structure in the genus-one model X^D after sufficient resolution, which is given as

$$p = d_1 f_1^2 g_1 u^3 + d_2 f_1 u^2 v + d_3 f_0 f_1 g_1 u v^2 + d_4 f_0 v^3 + d_5 f_1 u^2 w + d_6 f_0 f_1 g_1 u v w + d_7 f_0 v^2 w + d_8 f_0 f_1 g_1 u w^2 + d_9 f_0 v w^2 + d_{10} f_0 w^3,$$
 (7.27)

with Stanley-Reisner ideal

$$SRI : \{uf_0, f_0f_1, ug_1, wvu, wvf_1, wvg_1\}.$$
 (7.28)

The intersection picture of the fiber is given in figure 14. The fibral curves are given as

$$\mathbb{P}_{\alpha_0}^1: \quad f_0 \cap d_1 g_1 + d_2 v + d_5 w ,
\mathbb{P}_{\alpha_1}^1: \quad g_1 \cap d_2 f_1 v + d_4 f_0 v^3 + d_5 f_1 w + d_7 f_0 v^2 w + d_9 f_0 v w^2 + d_{10} f_0 w^3 ,
\mathbb{P}_{\alpha_2, i}^1: \quad f_1 \cap d_4 v^3 + d_7 v^2 w + d_9 v w^2 + d_{10} w^3 .$$
(7.29)

where $\mathbb{P}^1_{\alpha_2,i}$ admits 3 components that are interchanged along the $\overline{D}_{3,u}$ monodromy divisor. We conclude that we find a type $I_0^{*,ns}$ fiber in the genus-one model X^D just as in its Jacobian.

It is important to recall that the affine node f_1 in the $\mathfrak{so}_8^{(3)}$ model now hosts the three nodes of the $\mathfrak{g}_{2}^{(1)}$, while the new divisor f_{0} , yields the usual single affine node. Interestingly, we could have also blow-down f_1, g_1 and used f_0 to map the geometry into the Jacobian, which would result in the very same singularity type. As the fiber structure is the same in both models, we can use the Jacobian to find reducible fibers and similarly, we can use the genus-one model to compute the 6D discrete \mathbb{Z}_3 charges of the \mathfrak{g}_2 matter states. To do so, we first note that the discriminant over z=0 factorizes into two components in codimension two. The first component is given by z = Q = 0 where the fiber singularity enhances to vanishing orders (2,3,7), which is an \mathfrak{so}_{10} singularity. The second component in the discriminant is the intersection locus with monodromy divisor $\overline{D}_{3,u}$. The later determines the ramification points that fold the covering \mathfrak{so}_8 to \mathfrak{g}_2 and provide non-localized mater. In this situation, the curves $\mathbb{P}^1_{1,i}$ degenerate to a single curve of degree three as depicted in figure 14. Apparently, the associated genus-one fibration does not admit multiple fibers and hence we expect the $WC(X^D)$ group to reduce to the Tate-Shavarevich group $\mathrm{III}(X^D)$. We can now discuss these two loci in the genus-one model to deduce the respective matter charges.

As we have selected f_0 as the affine component and u = 0 as the reference 3-section, we need to orthogonalize the respective \mathfrak{u}_1 generators, which yields the discrete Shioda map

$$\sigma(s_0^{(3)}) = [u] + (2[f_1] + 3[g_1]), \tag{7.30}$$

which admits the intersections with the fibral divisors as

$$\sigma(s_0^{(3)}) \cdot \{f_0, g_1, f_1\} = \{3, 0, 0\}. \tag{7.31}$$

We can then impose Q = 0 and deduce the reducible components when solving for d_5 . The respective components are summarized in table 13. A graphical representation of the intersections of these irreducible curves is given in figure 14 and we them to have the shape of an affine $\mathfrak{so}_{10}^{(1)}$ Dynkin diagram, consistent with the Jacobian prediction. The weights of particles, obtained from M2 branes wrapping the curve $\mathbb{P}^1_{1,1}$ are computed as

$$\mathbb{P}_{1,1}^{1} \cdot (g_{1}, f_{1})_{\sigma(s_{0}^{(3)})} = (-1, 1)_{-1} \ni \mathbf{7}_{-1}. \tag{7.32}$$

Hence upon the singular limit, those weights are completed to full $\mathbf{7}_{-1}$ -plets with non-trival $\mathfrak{u}_{1,E}$ charge, which lifts to a \mathbb{Z}_3 charge in 6D. The non-localized states, obtained from the monodromy divisor on the other hand, are obtained from the \mathfrak{so}_8 adjoint and hence correspond to uncharged $\mathbf{7}$ -plets.

node	Irreducible components over $Q = 0$
$\mathbb{P}_{\alpha_0}:[f_0]$	$\mathbb{P}_0^1: f_0 \cap (d_1g_1 + d_2v + d_5w),$
$\mathbb{P}_{lpha_1}:[g_1]$	$\mathbb{P}^{1}_{1,1}: g_{1} \cap (d_{2}v + d_{5}w), \qquad \mathbb{P}^{1}_{1,2}: \begin{array}{l} g_{1} \cap (d_{10}d_{2}^{2}f_{0}v^{2} + d_{5}^{2}d_{7}f_{0}v^{2} - d_{2}d_{5}d_{9}f_{0}v^{2} \\ + d_{5}^{3}f_{1} - d_{10}d_{2}d_{5}f_{0}vw + d_{5}^{2}d_{9}f_{0}vw + d_{10}d_{5}^{2}f_{0}w^{2} \end{array}$
$\mathbb{P}_{\alpha_2,i}:[f_1]$	$\mathbb{P}^1_{2,1}: f_1 \cap (d_2v + d_5w) \qquad \mathbb{P}^1_{2,\pm}: f_1 \cap (v + (a_1 \pm a_2)w)$

Table 13. The codimension two irreducible components of the fiber at Q = 0 where \mathfrak{g}_2 charged matter resides. The intersections are depicted in figure 14.

We turn now to the computation of the multiplicity of the states described above. To this end, we compute the intersections that lead to localized 7_1 plets and the 7_0 -plets that originate from the monodromy divisor. Since we took f_0 as our new affine node, we need to change the factorization in the genus-one fibration above. For this we need the classes of the monodromy divisor in the new factorization²⁹ geometry given as

$$[\overline{D}_{3,u}] \sim 2\mathcal{S}_9 + 2\mathcal{S}_7 - 4\mathcal{Z}, \qquad (7.33)$$

as well as the class of

$$[Q] \sim -\mathcal{S}_7 - \mathcal{S}_9 - \mathcal{Z} + 6c_1. \tag{7.34}$$

The number of charged 7_1 is given by

$$n_{7_1} = [Q] \cdot \mathcal{Z} = 12(1-g) - \mathcal{S}_7 - \mathcal{S}_9 + 5\mathcal{Z}^2$$
 (7.35)

The neutral 7-plets are computed from the monodromy divisor and the Riemann-Hurwitz theorem, which yields

$$n_{7_0} = 2(g-1) + \frac{1}{2}R = 2(g-1) + S_7 + S_9 - 2Z^2$$
. (7.36)

Taking the sum of the two representations we obtain

$$n_{7_1} + n_{7_0} = 10(1-g) + 3\mathcal{Z}^2, \quad n_{14_0} = g,$$
 (7.37)

which satisfies the 6D anomalies as expected. Note again, that there is a degree of freedom to tune the relative number of charged and uncharged 7-plets.

In the second step we want to relate the $\mathfrak{so}_8^{(3)}$ and $\mathfrak{g}_2^{(1)}$ models. In order to do so, we need to make sure that there are no (4,6,12) points after tuning, which requires $d_1=z=0$ to be trivial (see section 5.2). This condition can be translates into the following intersection of the line bundle classes

$$(S_7 + S_9) \cdot Z = 3c_1 \cdot Z$$
.

²⁹We read this off from $[d_{10}] \sim 2S_9 - S_7 - Z$, $[d_7] \sim S_7 - Z$ and $[d_2] \sim 2c_1 - S_9$.

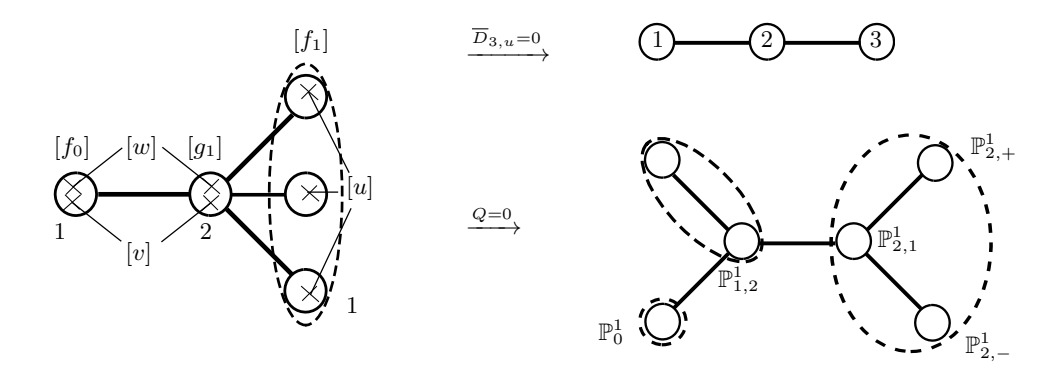


Figure 14. The fiber structure of the $\mathfrak{g}_2^{(1)}$ cubic genus-one fiber and its two degeneration loci.

When using the above constraint and plugging them into the multiplicities of the states we obtain

$$n_{7_0} = 4(1-g) + \mathcal{Z}^2, \qquad n_{7_1} = 6(1-g) + 2\mathcal{Z}^2.$$
 (7.38)

We can now compare the multiplicity of states in the $\mathfrak{g}_2^{(1)}$ cubic genus-one fibration X^D with that of the $\mathfrak{so}_8^{(3)}$ fibration X^A (given in (5.66)) we find perfect agreement for the massless $\mathbf{7}_0$ multiplicities. However, just as in the $\mathfrak{e}_6^{(2)}$ case, there is a difference in the massive $\mathbf{7}$ -plet sector. We remark, that we do not find $\mathbf{7}_2$ states in the $\mathfrak{g}_2^{(1)}$ theory. This can be explained by noting, that the $\mathbf{7}$ -plets are real representations. Thus, when conjugating a $\mathbf{7}_2$ state, it becomes a $\mathbf{7}_{-2}$. Recall that our KK tower is normalized with the three-section as $\mathbf{7}_{-2+3n}$. Hence, when shifting the KK-tower to $n \to n+1$, we find the $\mathbf{7}_2$ states to sit in the same KK-tower as the $\mathbf{7}_1$ states. Therefore the multiplicity given in (7.38) yields the combined multiplicities of massive $\mathbf{7}_1$ and $\mathbf{7}_2$ states.

Similar to the other twisted fibrations, we find the number of massive 7-plets to differ when engineered in their untwisted variants. In particular both the numbers of 7_1 and 7_2 states are each enhanced in the $\mathfrak{so}_8^{(3)}$ model, when compared to those in $\mathfrak{g}_2^{(1)}$.

Similar to the $\mathfrak{e}_6^{(2)} \to \mathfrak{g}_2^{(1)}$ case, there exists a chain of geometric transitions from $\mathfrak{so}_8^{(3)}$ to $\mathfrak{g}_2^{(1)}$. For this we first need to choose the usual $\mathfrak{g}_2 \in \mathfrak{so}_8^{(3)}$ limit when shrinking the curves in g_1, h_1 that yields massless 7_0 -plets which can be used as a Higgs resulting in the familiar breaking $\mathfrak{g}_2 \to \mathfrak{su}_3$ with the branchings $14 \to 8 \oplus 3 \oplus \overline{3}$ and $7 \to 3 \oplus \overline{3} \oplus 1$. After the deformation we replace the \mathfrak{g}_2 singularity by an \mathfrak{su}_3 , which is resolved by f_0 and g_1 which results in the $\mathfrak{g}_2^{(1)}$ diagram given in figure 14. As $\mathfrak{g}_2 \to \mathfrak{su}_3$ deformations preserve the Hodge numbers of the threefolds, we therefore claim that there exists an $\mathfrak{g}_2^{(1)}$ with exactly the same Hodge numbers. We give an example in the following.

Toric examples. In the following we give toric example of a threefold geometry X^D in which the gauge group is supported over a curve of self-intersection $\mathcal{Z}^2 = -1$ and genus 0 within a dP_1 base. The toric rays can be found in table 19 of appendix A. The \mathfrak{g}_2 spectrum is given as

$$n_{7_0} = 3, \qquad n_{7_1} = 2, \tag{7.39}$$

which indeed cancels the 6D \mathfrak{g}_2 anomalies. When compared to the $\mathfrak{so}_8^{(3)}$ model X^A , we find the very same Hodge numbers and a difference only in the non-polynomial complex structure deformations

$$(h^{1,1}, h^{2,1}(h_{np}^{2,1}))(X^A) = (5,71(6)), \text{ and } (h^{1,1}, h^{2,1}(h_{np}^{2,1}))(X^D) = (5,71(3)).$$
 (7.40)

The three non-polynomial deformations in the X^D geometry can be attributed to the singlet in the three $\mathbf{7}_0$ -plets. The very same three $\mathbf{7}_0$ -plets are also present in X^A where three additional non-poly deformations are present. Analogously to the $\mathfrak{e}_6^{(2)}$ model, we propose those contributions to the additional singlets from the twisted reduction. In particular, we expect to find the total contribution of non-polynomial deformations

$$\delta h_{np}^{2,1} = n_{10} + n_{70} + 2n_{140} = 12(1-g) + 3\mathcal{Z}^2 + 2g, \qquad (7.41)$$

in the $\mathfrak{so}_8^{(3)}$ model X^A . Thus, we find three additional contributions, coming from $\mathbf{1}_0$ for the $\mathcal{Z}^2 = -1$, g = 0 case. Those considerations also show, that those non-poly deformations should be absent for $\mathfrak{so}_8^{(2)}$ fibers over curves with $\mathcal{Z}^2 = -4$ and g = 0 as constructed in section 5. As expected from the 6D anomalies, this fiber can not be Higgsed to $\mathfrak{g}_2^{(1)}$.

7.4 $\mathfrak{su}_3^{(2)}$ vs $\mathfrak{su}_2^{(1)}$ genus-one fibers

Finally we discuss the relation between the twisted fibrations X^A with fibers $\mathfrak{su}_3^{(2)}$ and their untwisted cousins, X^D with fibers $\mathfrak{su}_2^{(1)}$. The later geometry is obtained by the generalized Tate-vector

$$n_i = \{0, 0, 0, 0, 0, 0, 0, 0, 1\} . (7.42)$$

This theory admits an $\mathfrak{su}_2^{(1)}$ fiber, both in the Jacobian and the genus-one fibration. The Jacobian $J(X^D/B_2)$ to leading orders in z is given as

$$f = Q^{2} + \mathcal{O}(z),$$

$$g = Q^{3} + Q\mathcal{O}(z),$$

$$\Delta = z^{2}PQ^{2} + Q\mathcal{O}(z^{3}).$$

$$(7.43)$$

With P and Q polynomials in the d_i

$$Q = -d_7^2 + 4d_6d_8, (7.44)$$

$$\begin{split} P &= d_5^2 d_6^4 - d_4 d_5 d_6^3 d_7 + d_3 d_5 d_6^2 d_7^2 - d_2 d_5 d_6 d_7^3 + d_1 d_5 d_7^4 + d_4^2 d_6^3 d_8 - 2 d_3 d_5 d_6^3 d_8 - d_3 d_4 d_6^2 d_7 d_8 \\ &+ 3 d_2 d_5 d_6^2 d_7 d_8 + d_2 d_4 d_6 d_7^2 d_8 - 4 d_1 d_5 d_6 d_7^2 d_8 - d_1 d_4 d_7^3 d_8 + d_3^2 d_6^2 d_8^2 - 2 d_2 d_4 d_6^2 d_8^2 + 2 d_1 d_5 d_6^2 d_8^2 \\ &- d_2 d_3 d_6 d_7 d_8^2 + 3 d_1 d_4 d_6 d_7 d_8^2 + d_1 d_3 d_7^2 d_8^2 + d_2^2 d_6 d_8^3 - 2 d_1 d_3 d_6 d_8^3 - d_1 d_2 d_7 d_8^3 + d_1^2 d_8^4 \,. \end{split} \tag{7.45}$$

The fully resolved genus-one fibration X^D on the other hand is given as

$$p = d_1 f_0 X^4 + d_2 f_0 X^3 Y + d_3 f_0 X^2 Y^2 + d_4 f_0 X Y^3 + d_5 f_0 Y^4 + d_6 X^2 Z + d_7 X Y Z + d_8 Y^2 Z + d_9 f_1 Z^2,$$
(7.46)

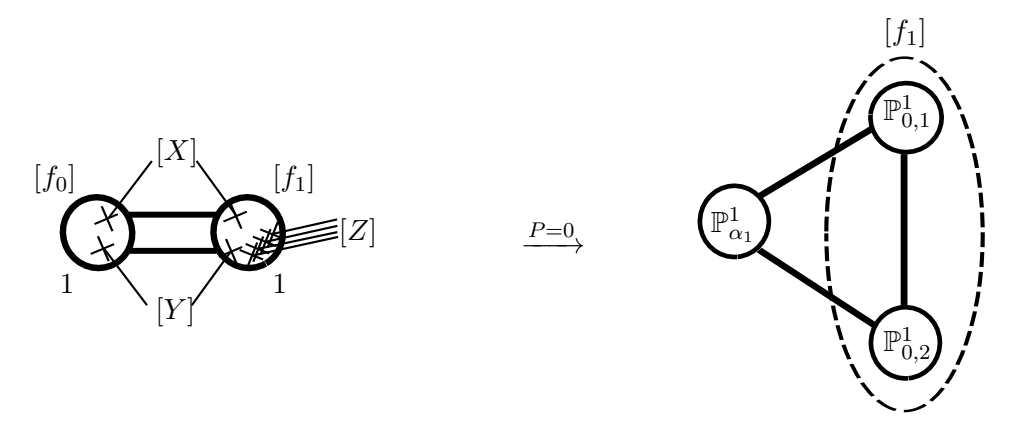


Figure 15. Depiction of the \mathfrak{su}_2 fiber in the quartic. Intersections with the fibral curves in the divisors f_0 and f_1 with respect to the two 2-section classes X and Y are depicted, as well as with the 4-section Z.

with the fibral Stanley-Reisner ideal

$$SRI: \{YX, Zf_0\}.$$
 (7.47)

The two fibral curves are given as

$$\mathbb{P}^{1}_{\alpha_{0}}: f_{1} \cap d_{1}f_{0}X^{4} + d_{2}f_{0}X^{3}Y + d_{3}f_{0}X^{2}Y^{2} + d_{4}f_{0}XY^{3} + d_{5}f_{0}Y^{4} + d_{6}X^{2}Z + d_{7}XYZ + d_{8}Y^{2}Z,$$

$$(7.48)$$

$$\mathbb{P}^{1}_{\alpha_{1}}: f_{0} \cap d_{6}X^{2} + d_{7}XY + d_{8}Y^{2} + d_{9}f_{1}.$$

This results in an intersection picture as given in figure 15: Hence again, we have to orthogonalize our reference two-section X with respect to the \mathfrak{su}_2 divisor that we want to shrink, that is f_0 which yields the discrete Shioda map

$$\sigma(X) = [X] + \frac{1}{2}[f_0]. \tag{7.49}$$

Note that the \mathfrak{su}_2 model is precisely the same as the most general quartic fibration which makes our discussion fully analogous to the one in [45] (see page 32).

To discuss the matter loci, it is again sufficient to simply deduce them from the Jacobian $J(X^D/B_2)$ and then investigate them further in the respective genus-one geometry. First there is the discriminant locus Q=0 for which we find the vanishing orders (1,2,3) in the Weierstrass model and hence a type III enhancement where no additional matter resides. Over the codimension two locus P=0 instead, we find a type I_3 fiber and hence fundamental matter. Over this locus, the fibral curve $\mathbb{P}^1_{\alpha_0}$ splits into $\mathbb{P}^1_{0,1} + \mathbb{P}^1_{0,2}$ which gives rise to $\mathbf{2}_{\frac{1}{2}}$ -plets. Note that the $\frac{1}{2}$ charge highlights a non-trivial mixing of $\mathfrak{u}_{1,E}$ with the \mathbb{Z}_2 center of the \mathfrak{su}_2 , similar to the \mathfrak{e}_7 case in section 4, resulting in a $G=\frac{\mathrm{SU}(2)\times\mathbb{Z}_4}{\mathbb{Z}_2}$ gauge group in the F-theory lift.

In order to compute the multiplicities, we use appendix B to deduce the classes of the polynomial P which is

$$[P] \sim [2d_1 + 4d_8]$$
 with $[d_8] \sim c_1 + S_9 - \mathcal{Z}$. (7.50)

This results in the multiplicity

$$n_{\mathbf{2}_{\frac{1}{2}}} = \mathcal{Z} \cdot (8c_1 - 2\mathcal{Z}) = 16(1 - g) + 6\mathcal{Z}^2,$$
 (7.51)

consistent with the 6D gauge anomalies.

Finally we are in the position to comment on the relation of the $\mathfrak{su}_2^{(1)}$ theory to that of $\mathfrak{su}_3^{(2)}$. As noted above, the $\mathfrak{su}_2^{(1)}$ geometry X^D does not posses multiple fibers and admits a consistent 6D F-theory uplift, highlighted by a matter spectrum that solves the 6D anomalies. The $\mathfrak{su}_3^{(2)}$ geometry X^A on the other hand admits two more massive $2_{\frac{1}{2}}$ -plets. We expect again, that there exists a geometric transition between the two threefolds, that preserves gauge algebra rank and number of flat direction, i.e. the exact Hodge numbers. The exact type of conifold transition between the twisted and the untwisted theory is more obscure than in the other cases as there is not much room for a rank preserving Higgsing in the $\mathfrak{su}_2 \times \mathfrak{u}_{1,E}$ theory, apart from using adjoints. Similarly to the other examples discussed in this section, we expect such fields to exist and return to this question in future works.

Toric example. We exemplify the general considerations with a toric example. The details of the toric rays, from which the threefolds X^A and X^D are constructed are summarized appendix A. The threefold X^D with $\mathfrak{su}_2^{(1)}$ fiber is engineered over a $\mathcal{Z}^2 = +1$ curve with g = 0 in a \mathbb{P}^2 base. The massless $\mathfrak{su}_2 \in \mathfrak{su}_2^{(1)}$ charged spectrum is then given by the multiplicities

$$n_{\mathbf{3}_0} = 0, \qquad n_{\mathbf{2}_{\frac{1}{2}}} = 22,$$
 (7.52)

consistent with the 6D anomalies. The corresponding $\mathfrak{su}_3^{(2)}$ model X^A on the other hand, admits 24 massive doublets states but leads to a threefold with exactly the same Hodge numbers, given as

$$(h^{1,1}, h^{2,1})) = (3, 107). (7.53)$$

Besides the fiber structure, another difference shows up in the number of non-polynomial complex structure deformations:

$$h_{np}^{2,1}(X^C) = 12, \quad h_{np}^{2,1}(X^D) = 0.$$
 (7.54)

As before, we use the twisted reduction of the $6D \mathfrak{su}_3$ theory, to give a prediction of such non-poly deformations. Those contributions come from singlets, and adjoint hypermultiplet representations as discussed in section 5.1 that sum up to

$$\delta h_{np}^{2,1} = n_{\mathbf{1}_0} + n_{\mathbf{3}_0} = 9(1-g) + 3\mathcal{Z}^2 + g.$$
 (7.55)

Thus, for our toric example we expect to have 12 singlet state contributions in X^A . Similarly we find that the $\mathfrak{su}_3^{(2)}$ fiber over a -3 curve has a trivial spectrum. Therefore, there is no transition to an $\mathfrak{su}_2^{(1)}$ consistent with the fact that there are no non-polynomial complex structure deformations.

8 Summary and outlook

In this work we have initiated a detailed exploration of the geometry of genus-one fibrations with twisted algebras and their F/M-theory physics. We have focused explicitly on the cases of $\mathfrak{e}_6^{(2)}, \mathfrak{so}_8^{(3)}$ and $\mathfrak{su}_3^{(2)}$ over an arbitrary smooth and compact curve in the 2D base. Our analysis only imposes flatness of the fibration and one non-trivial codimension one fiber over an otherwise arbitrary base.³⁰ For these cases the geometry exhibits multiple fibers over smooth points in the base and hence a non-trivial Weil-Châtalet group is a prerequisite for these twisted algebras to exist. We compute the multiplicities of the lightest BPS states charged under the \mathfrak{f}_4 , \mathfrak{g}_2 and \mathfrak{su}_2 finite sub-algebras purely from geometry and find agreement with prior results on twisted field theory reductions of 6D gauge algebras \mathfrak{e}_6 , \mathfrak{so}_8 and \mathfrak{su}_3 respectively. To gain additional insight into these M-theory backgrounds, we consider 5D geometric transitions from $\mathfrak{e}_7^{(1)}$, $\mathfrak{f}_4^{(1)}$ and $\mathfrak{g}_2^{(1)}$ respectively, to the twisted algebras.

While we do not fully determine the 6D background that leads to these twisted M-theory compactifications upon circle reduction, we do identify a range of features and symmetries that it must possess. In particular we give the explicit Jacobian fibration associated to each genus-one fibration. In each case, the fiber structure we find in the Jacobian differs from that found in the genus-one geometries and from what would be expected from a typical, field-theoretic twisted reduction. Instead of $\mathfrak{e}_6,\mathfrak{so}_8$ and \mathfrak{su}_3 we find the generic geometric cover of the twisted algebras, that is $\mathfrak{e}_7,\mathfrak{f}_4$ and \mathfrak{g}_2 respectively. As a result we find different dimensionality in the Kähler moduli spaces associated to the genus-one fibrations and their Jacobians. We further discuss several applications of the geometry of twisted algebras in SUGRAs, LSTs and SCFTs. In particular we discuss twisted T-dualities and match the generalized symmetries, following the proposal in [74], to provide another cross-check of our construction.

The connection between untwisted and twisted algebras with the same finite sub-algebra are also investigated. We find evidence of (chains of) geometric transitions among them. Surprisingly, the connected geometries admit the very same Hodge numbers, but differ not only in the fibral curve structure but also in the number of non-polynomial complex structure deformations of the CY hypersurface equation. We propose a physics interpretation for those non-polynomial deformations and further use the twisted field theory reduction as a way to understand them.

The results outlined here open up several exciting directions that deserve further exploration in the future. In particular, limits of the geometries in consideration here connect with several topics within the Swampland program [82] (see [83–85] for recent reviews) such as the weak gravity [86] and emerging string conjecture [87]. First, we find that a twisted compactification in a SUGRA theory does not only require a gauge algebra that can be twisted but also a discrete zero-form gauge symmetry to embed the twist into as the later ones are always accompanied in the respective F-theory lift of genus-one fibrations. At first glance, this observation may not come as a surprise, as one expects an unbroken discrete symmetry to be gauged in a gravity theory. However, one would have expected

 $^{^{30}}$ Note that restricting to only one non-trivial fiber implicitly restricts the 2D bases to have only curves of self-intersection $C^2 \ge -2$ otherwise. On the other hand our spectrum computations apply for any twisted algebra, that appears over any isolated curve in an arbitrary base.

that a discrete automorphism of the respective gauge algebra would have been enough to twist by. Our geometric analysis therefore suggest that an *additional* compatible discrete gauge symmetry needs to be present as well to perform a perform a twisted reduction in a SUGRA theory.

Secondly, these twisted dimensional reductions make 6D discretely charged states generally massive, and gives them a fractional 5D U(1)KK charge, which hence makes them relevant in the context of the (sub-lattice) weak gravity conjecture (see e.g. [88] and reference therein). Finally, twisted compactifications display an interesting feature in that the decompactification limit not only results in an extra dimension but also leads to a gauge algebra enhancement.

This work has also raised a number of interesting open questions. First there is the gauge symmetry of the Jacobian fibration, which is associated with the untwisted circle reduced theory. There the gauge algebra seems to always be enhanced compared to the purely field theoretic expectation (e.g. an \mathfrak{e}_7 symmetry instead of \mathfrak{e}_6 for the geometries of section 4, for example). This enhancement is also directly related to puzzles regarding the twisted reduction from 6D to 5D as outlined in section 3. One potential explanation might involve the non-polynomial complex structure deformations present in the twisted genus one fibrations studied in this work. It is possible that in the presence of such degrees of freedom the mapping to the Jacobian geometry might be modified in a way that fixes some complex structure moduli, potentially breaking the naive symmetry group to that expected from ordinary gauge theory reductions.

As a further intriguing observation, in our geometric analysis the multi-section monodromy divisors played a key role in describing the twisting of the fibers and also appears to be linked to co-dimension 2 structure in the Jacobian fibration. This co-dimension 2 structure is crucial in the cancellation of the 6D discrete gauge anomalies [50] (which were beyond the scope of the present work to explore). This observations hints at a non-trivial interplay between the 6D discrete gauge anomalies and the existence of twisted dimensional reductions that may also solve the puzzle outlined before. Moreover, the explicit form of the twisted fibrations and their Jacobians here would also in principle allow for the computation of twisted/twined elliptic genera. It would be interesting to do this and compare with the results of [19] in non-compact scenarios as well as for those for twisted T-dualities [16, 18, 74] and 5D SCFTs [7].

Finally it should be noted that fibrations exhibiting twisted algebras are not yet fully mathematically explored. While we have discussed only three different types of twisted fibers, a full Kodaira/Tate type of classification of singular genus-one fiberd threefolds would be desirable. This could in particular include series such as $\mathfrak{su}_n^{(2)}$ or $\mathfrak{so}_k^{(2)}$. As those are only degree two twisted algebras, one might succeed in constructing these in relatively simple 2-section models such as the quartic. This is linked of course, to the question of whether all possible n-section geometries can be classified. Thus far, some models for n < 6 [49] have been constructed and analyzed explicitly, with an expectation that n should not be much larger than 6 [19]. While such high multi-section degrees might not be directly required to explore the unexplored twisted algebra series', they are still relevant in cases where \mathfrak{su}_n gauge algebras are twisted to *nothing* as e.g. explored in [20–22, 47]. We hope to return to some of these questions in future work.

Acknowledgments

We thank Markus Dierigl, Zhihao Duan, Jonathan Mboyo Esole, Antonella Grassi, David Morrison, Kimyeong Lee, Nikhil Raghuram, Xin Wang and in particular Thorsten Schimannek for illuminating discussions. Furthermore we thank Jie Gu, Ling Lin, Guglielmo Lockhart, Marcus Sperling and Michele Del Zotto for related discussions. L.A. and J.G. are supported by NSF grant PHY-2014086. P.O. has received funding from the NSF CAREER grant PHY-1848089 and startup funding from Northeastern University by Fabian Ruehle.

A Toric data for threefold geometries

In this appendix we present concrete threefold examples and give their concrete spectra together with their Hodge numbers. The associated vertices of the toric variety are listed below.

A.1 $\mathfrak{su}_3^{(2)}$ example geometries

Base with $(g, \mathcal{Z}^2, \mathcal{S}_9 \cdot \mathcal{Z})$	5D Gauge Algebra	$h^{1,1}$	$h^{2,1}$	Reps
	$\mathfrak{g}_2 imes \mathfrak{u}_{1,F} imes \mathfrak{u}_{1,kk}$	5	89	$ \begin{array}{c} 5 \times 7_1 \\ 8 \times 7_0 \end{array} $
\mathbb{P}^2 with $(0,1,1)$	$\mathfrak{g}_2 imes \mathfrak{u}_{1,E}$	4	98	$ 5 \times 7_1 \\ 8 \times 7_0 $
	$\mathfrak{su}_2 imes \mathfrak{u}_{1,E} \in \mathfrak{su}_3^{(2)}$	3	107	$24 \times 2_{\frac{1}{2}}$
	$\mathfrak{su}_2 imes \mathfrak{u}_{1,E}$	3	107	$22 \times 2_{\frac{1}{2}}$
	$\mathfrak{su}_2 imes \mathfrak{u}_{1,F} imes \mathfrak{u}_{1,kk}$	4	93	$22 \times 2_{\frac{1}{2}}$
	$\mathfrak{g}_2 imes \mathfrak{u}_{1,F} imes \mathfrak{u}_{1,kk}$	6	96	$2 imes 7_1 \ 2 imes 7_0$
$\mathbb{P}^2_{1,1,2} \text{ with } (0,-2,-2)$	$\mathfrak{g}_2 imes \mathfrak{u}_{1,E}$	5	109	$2 \times 7_1 \\ 2 \times 7_0$
	$\mathfrak{su}_2 imes \mathfrak{u}_{1,E} \in \mathfrak{su}_3^{(2)}$	4	112	$6 \times 2_{\frac{1}{2}}$
	$\mathfrak{su}_2 imes \mathfrak{u}_{1,E}$	4	112	$4 \times 2_{\frac{1}{2}}$
	$\mathfrak{su}_2 imes \mathfrak{u}_{1,F} imes \mathfrak{u}_{1,E}$	5	97	$10 \times 2_{\frac{1}{2}}$

Table 14. A chain of 5D theories, obtained from genus-one fibrations over a \mathbb{P}^2 and a an \mathbb{F}_2 base with gauge algebras over a $\mathbb{Z}^2 = 0$ curve of genus g = 0 and their light BPS states.

]	\mathbb{P}^2 Base 1
Generic Fibers X (-1,1,0,0) Y (-1,-1,0,0) Z (1,0,0,0) U (0,1,0,0)	$\begin{array}{c c} \mathfrak{g}_2^{(1)} \text{ Fiber} \\ \hline f_1 & (1,0,1,0) \\ f_0 & (0,0,1,0) \\ g_1 & (1,0,2,0) \\ f_2 & (0,1,1,0) \\ \hline \end{array}$	$\mathfrak{su}_3^{(2)}$ Fiber	$\begin{array}{c c} \mathfrak{su}_2^{(1)} \text{ Fiber} \\ \hline f_1 & (1,0,1,0) \\ f_0 & (0,0,1,0) \\ \end{array}$	$\begin{bmatrix} x_0 \\ x_1 \end{bmatrix}$ $\begin{bmatrix} x \\ y \\ z \end{bmatrix}$	$ \begin{array}{c} (-3,0,-1,-1) \\ (0,0,0,1) \end{array} $ $ \begin{array}{c} 2\\112 \text{ Base 2} \\ (0,0,1,1) \\ (0,0,1,-1) \\ (-2,0,-1,0) \end{array} $

Table 15. The collection of toric rays that can be combined to the five threefolds summarized in table 14: first pick the base and elliptic fibers is picked from the leftmost column. Second a non-trivial fiber top is added from either of the other columns.

A.2 $\mathfrak{e}_6^{(2)}$ example geometries

5D Gauge Algebra	$h^{1,1}$	$h^{2,1}$	Reps
$\mathfrak{e}_7 imes \mathfrak{u}_{1,F} imes \mathfrak{u}_{1,KK}$	11	59	$4 \times 56_{1/2}$
$\mathfrak{e}_7 imes \mathfrak{u}_{1,E}$	10	82	$4 \times 56_{1/2}$
f. × 11. 5	7	95	$2 \times 26_1$
$\mathfrak{f}_4 imes\mathfrak{u}_{1,E}$			$3 \times {\bf 26}_0$
(2)	7	95	$2 \times 26_1$
$\mathfrak{f}_4 imes \mathfrak{u}_{1,E} \in \mathfrak{e}_6^{(2)}$			$3 \times 26_0$
			$2 \times 1 \times 3$

Table 16. A chain of 5D theories, obtained from genus-one fibrations over a \mathbb{F}_0 base with gauge algebras over a $\mathbb{Z}^2 = 0$ curve of genus g = 0 and their light BPS states.

Generic Fiber	\mathfrak{e}_7 Fiber		
$ \begin{vmatrix} X & (-1,1,0,0) \\ Y & (-1,-1,0,0) \\ Z & (1,0,0,0) \\ \hline e_1 & (0,1,0,0) \end{vmatrix} $	$ \begin{array}{ c c c c c } \hline f_2 & (-3,0,1,0) \\ f_4 & (-2,0,1,0) \\ g_1 & (-5,-2,2,0) \\ g_2 & (-5,-1,2,0) \end{array} $	$\mathfrak{e}_{6}^{(2)}$ Fiber $f_{2} (-3, 0, 1, 0) g_{1} (-5, -2, 2, 0) $	f_4 Fiber $f_2 (-3, 0, 1, 0) f_3 (-2, -1, 1, 0)$
$ \begin{array}{c c} \mathbb{F}_0 \text{ Base} \\ \hline x_1 & (1, 0, -1, 0) \\ y_0 & (0, 0, 0, 1) \\ y_1 & (-2, -2, 0, -1) \end{array} $	$ \begin{vmatrix} g_2 & (-4, -1, 2, 0) \\ g_3 & (-4, -1, 2, 0) \\ h_1 & (-7, -2, 3, 0) \\ h_2 & (-6, -2, 3, 0) \\ k_1 & (-9, -3, 4, 0) \end{vmatrix} $	$ \begin{vmatrix} g_2 & (-5, -1, 2, 0) \\ h_1 & (-7, -2, 3, 0) \\ k_1 & (-9, -3, 4, 0) \end{vmatrix} $	$ \begin{vmatrix} g_1 & (-5, -2, 2, 0) \\ g_2 & (-5, -1, 2, 0) \\ h_1 & (-7, -2, 3, 0) \end{vmatrix} $

Table 17. The collection of toric rays that can be combined to the five threefolds summarized in table 16: first pick the base and elliptic fibers is picked from the leftmost column. Second a non-trivial fiber top is added from either of the other columns.

A.3 $\mathfrak{so}_8^{(3)}$ example geometries

5D Gauge Algebra	$h^{1,1}$	$h^{2,1}$	Reps
60 × 114 F × 114 11	9	60	$2 \times 27_1$
$\mathfrak{e}_6 imes \mathfrak{u}_{1,F} imes \mathfrak{u}_{1,kk}$			$3 \times 27_0$
f. × 11. = × 11. =	8	62	$2 \times 26_1$
$\mathfrak{f}_4 imes \mathfrak{u}_{1,F} imes \mathfrak{u}_{1,F}$			$2 \times 27_0$
f. × 11. 5	7	67	$2 \times 26_1$
$\mathfrak{f}_4 imes\mathfrak{u}_{1,E}$			$2 \times 27_0$
(-)	5	71	$3 \times 7_1$
$\mathfrak{g}_2 imes\mathfrak{u}_{1,E}\in\mathfrak{so}_8^{(3)}$			$3 \times 7_2$
			$3 \times 7_0$
	5	71	$2 \times 7_1$
$\mathfrak{g}_2 imes\mathfrak{u}_{1,E}$			$2 \times 7_2$
			$3 \times 7_0$

Table 18. A chain of 5D theories, obtained from genus-one fibrations over a dP_1 base with gauge algebras over a $\mathcal{Z}^2 = -1$ curve of genus g = 0 and their light BPS states.

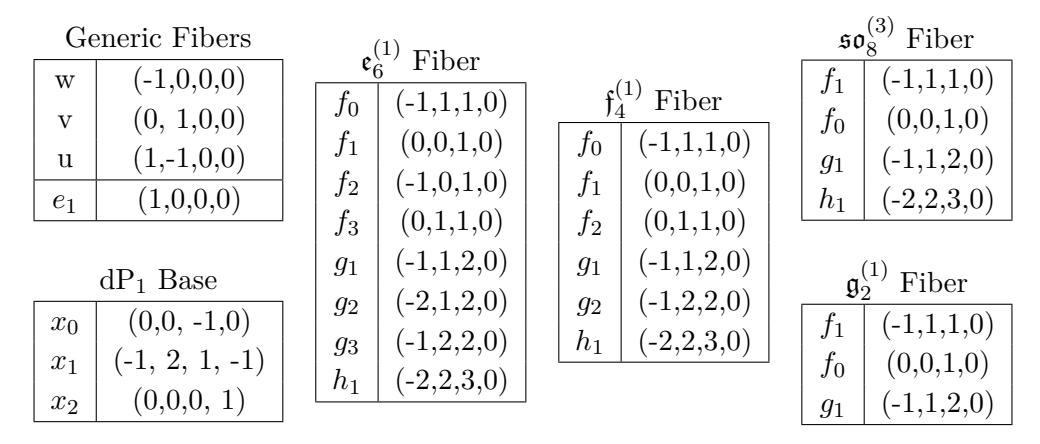


Table 19. The collection of toric rays that can be combined to the five threefolds summarized in table 18: first pick the base and elliptic fibers is picked from the leftmost column. Second a non-trivial fiber top is added from either of the other columns.

B Line bundle data for genus-one fibrations

The various \mathbb{F}_2 and \mathbb{P}_2 ambient fiber types imply that the coordinates are certain projective bundles whose data we will list here. This data is important to fix the base divisor classes of the generalized Tate-coefficients that is used throughout this work. First the Quartic $\mathbb{P}^2_{1,1,2}$ coordinates transform as given in table 20.

		Section	Divisor Class
		s_1	$3c_1-\mathcal{S}_7-\mathcal{S}_9$
Section	Bundle	s_2	$2c_1-\mathcal{S}_9$
X	$H - E_1 + S_9 - c_1$	s_3	$c_1 + \mathcal{S}_7 - \mathcal{S}_9$
Y	$H - E_1 + S_9 - c_1$ $H - E_1 - S_7 + S_9$	s_4	$2S_7 - S_9$
\overline{Z}	$2H - E_1 + S_9 - c_1$	s_5	$-c_1 + 3\mathcal{S}_7 - \mathcal{S}_9$
e_1	E_1	s_6	$2c_1-\mathcal{S}_7$
CI	$ D_1 $	s_7	c_1
		s_8	\mathcal{S}_7
		s_9	$c_1 - \mathcal{S}_7 + \mathcal{S}_9$

Table 20. Summary of the line bundle classes of a generic quartic fibration given in (2.12). Throughout most of this work, we fix $S_7 \sim c_1 + S_9$ such that s_9 is just a constant.

The second model relevant for this work is the cubic fibration with a three-section, which admits the bundle data as summarized in table 21.

		Section	Divisor Class
		s_1	$3c_1-\mathcal{S}_7-\mathcal{S}_9$
		s_2	$2c_1-\mathcal{S}_9$
Section	Bundle	s_3	$c_1 + \mathcal{S}_7 - \mathcal{S}_9$
$\frac{u}{u}$	$H + S_9 - c_1$	s_4	$2\mathcal{S}_7 - \mathcal{S}_9$
	$H + \mathcal{S}_9 - \mathcal{E}_1$ $H - \mathcal{S}_7 + \mathcal{S}_9$	s_5	$2c_1 - S_7$
v	$H = \mathcal{S}_7 + \mathcal{S}_9$	s_6	c_1
w	П	s_7	\mathcal{S}_7
		s_8	$c_1 + \mathcal{S}_9 + \mathcal{S}_7$
		s_9	\mathcal{S}_9
		s_{10}	$2\mathcal{S}_9 - \mathcal{S}_7$

Table 21. Summary of the line bundle classes of a generic cubic fibration given in (5.46).

Open Access. This article is distributed under the terms of the Creative Commons Attribution License (CC-BY 4.0), which permits any use, distribution and reproduction in any medium, provided the original author(s) and source are credited.

References

- [1] V. Kumar, D.R. Morrison and W. Taylor, Global aspects of the space of 6D N = 1 supergravities, JHEP 11 (2010) 118 [arXiv:1008.1062] [INSPIRE].
- [2] D.R. Morrison and W. Taylor, Classifying bases for 6D F-theory models, Central Eur. J. Phys. 10 (2012) 1072 [arXiv:1201.1943] [INSPIRE].
- [3] J.J. Heckman, D.R. Morrison, T. Rudelius and C. Vafa, *Atomic Classification of 6D SCFTs*, Fortsch. Phys. **63** (2015) 468 [arXiv:1502.05405] [INSPIRE].
- [4] J.J. Heckman and T. Rudelius, Top Down Approach to 6D SCFTs, J. Phys. A 52 (2019) 093001 [arXiv:1805.06467] [INSPIRE].
- [5] F. Apruzzi et al., Fibers add Flavor, Part I: Classification of 5d SCFTs, Flavor Symmetries and BPS States, JHEP 11 (2019) 068 [arXiv:1907.05404] [INSPIRE].
- [6] F. Apruzzi et al., Fibers add Flavor, Part II: 5d SCFTs, Gauge Theories, and Dualities, JHEP 03 (2020) 052 [arXiv:1909.09128] [INSPIRE].
- [7] L. Bhardwaj et al., Twisted Circle Compactifications of 6d SCFTs, JHEP 12 (2020) 151 [arXiv:1909.11666] [INSPIRE].
- [8] L. Bhardwaj and P. Jefferson, Classifying 5d SCFTs via 6d SCFTs: Rank one, JHEP 07 (2019) 178 [Addendum ibid. 01 (2020) 153] [arXiv:1809.01650] [INSPIRE].
- [9] L. Bhardwaj and P. Jefferson, Classifying 5d SCFTs via 6d SCFTs: Arbitrary rank, JHEP 10 (2019) 282 [arXiv:1811.10616] [INSPIRE].
- [10] L. Bhardwaj, On the classification of 5d SCFTs, JHEP **09** (2020) 007 [arXiv:1909.09635] [INSPIRE].
- [11] L. Bhardwaj and G. Zafrir, Classification of 5d $\mathcal{N}=1$ gauge theories, JHEP 12 (2020) 099 [arXiv:2003.04333] [INSPIRE].
- [12] F. Bonetti and T.W. Grimm, Six-dimensional (1,0) effective action of F-theory via M-theory on Calabi-Yau threefolds, JHEP 05 (2012) 019 [arXiv:1112.1082] [INSPIRE].
- [13] T.W. Grimm and A. Kapfer, Anomaly Cancelation in Field Theory and F-theory on a Circle, JHEP 05 (2016) 102 [arXiv:1502.05398] [INSPIRE].
- [14] P. Jefferson, S. Katz, H.-C. Kim and C. Vafa, On Geometric Classification of 5d SCFTs, JHEP 04 (2018) 103 [arXiv:1801.04036] [INSPIRE].
- [15] H.-C. Kim, S.-S. Kim and K. Lee, Higgsing and twisting of 6d D_N gauge theories, JHEP 10 (2020) 014 [arXiv:1908.04704] [INSPIRE].
- [16] A.P. Braun et al., Fibre-base duality of 5d KK theories, JHEP **05** (2021) 200 [arXiv:2103.06066] [INSPIRE].
- [17] H.-C. Kim, M. Kim and S.-S. Kim, Topological vertex for 6d SCFTs with \mathbb{Z}_2 -twist, JHEP 03 (2021) 132 [arXiv:2101.01030] [INSPIRE].
- [18] L. Bhardwaj, Discovering T-Dualities of Little String Theories, arXiv: 2209.10548 [INSPIRE].

- [19] K. Lee, K. Sun and X. Wang, Twisted Elliptic Genera, arXiv:2212.07341 [INSPIRE].
- [20] F. Baume, M. Cvetič, C. Lawrie and L. Lin, When rational sections become cyclic Gauge enhancement in F-theory via Mordell-Weil torsion, JHEP 03 (2018) 069 [arXiv:1709.07453] [INSPIRE].
- [21] P.-K. Oehlmann and T. Schimannek, GV-Spectroscopy for F-theory on genus-one fibrations, JHEP 09 (2020) 066 [arXiv:1912.09493] [INSPIRE].
- [22] L.B. Anderson, J. Gray and P.-K. Oehlmann, F-Theory on Quotients of Elliptic Calabi-Yau Threefolds, JHEP 12 (2019) 131 [arXiv:1906.11955] [INSPIRE].
- [23] T.W. Grimm and T. Weigand, On Abelian Gauge Symmetries and Proton Decay in Global F-theory GUTs, Phys. Rev. D 82 (2010) 086009 [arXiv:1006.0226] [INSPIRE].
- [24] D.R. Morrison and D.S. Park, F-Theory and the Mordell-Weil Group of Elliptically-Fibered Calabi-Yau Threefolds, JHEP 10 (2012) 128 [arXiv:1208.2695] [INSPIRE].
- [25] M. Cvetič, T.W. Grimm and D. Klevers, Anomaly Cancellation And Abelian Gauge Symmetries In F-theory, JHEP 02 (2013) 101 [arXiv:1210.6034] [INSPIRE].
- [26] L. Bhardwaj et al., F-theory and the Classification of Little Strings, Phys. Rev. D 93 (2016) 086002 [Erratum ibid. 100 (2019) 029901] [arXiv:1511.05565] [INSPIRE].
- [27] N. Hajouji, *Trace Zero Points on Elliptic Fibrations*, Ph.D. thesis, University of California (UC), Santa Barbara, CA 93106-9530 U.S.A. (2020). [INSPIRE].
- [28] <bbl:err:author>, Elliptic Three-folds I: Ogg-Shafarevich Theory, alg-geom/9210009.
- [29] M. Gross, Elliptic three-folds II: Multiple fibres, Trans. Am. Math. Soc. 349 (1997) 3409.
- [30] L.B. Anderson, A. Grassi, J. Gray and P.-K. Oehlmann, F-theory on Quotient Threefolds with (2,0) Discrete Superconformal Matter, JHEP 06 (2018) 098 [arXiv:1801.08658] [INSPIRE].
- [31] M. Cvetič et al., F-theory vacua with \mathbb{Z}_3 gauge symmetry, Nucl. Phys. B 898 (2015) 736 [arXiv:1502.06953] [INSPIRE].
- [32] C. Mayrhofer, D.R. Morrison, O. Till and T. Weigand, Mordell-Weil Torsion and the Global Structure of Gauge Groups in F-theory, JHEP 10 (2014) 016 [arXiv:1405.3656] [INSPIRE].
- [33] L.B. Anderson, I. García-Etxebarria, T.W. Grimm and J. Keitel, *Physics of F-theory compactifications without section*, *JHEP* 12 (2014) 156 [arXiv:1406.5180] [INSPIRE].
- [34] W. Buchmuller, M. Dierigl, P.-K. Oehlmann and F. Ruehle, *The Toric* SO(10) F-Theory Landscape, JHEP 12 (2017) 035 [arXiv:1709.06609] [INSPIRE].
- [35] D.R. Morrison and C. Vafa, Compactifications of F theory on Calabi-Yau threefolds. II, Nucl. Phys. B 476 (1996) 437 [hep-th/9603161] [INSPIRE].
- [36] D.R. Morrison and N. Seiberg, Extremal transitions and five-dimensional supersymmetric field theories, Nucl. Phys. B 483 (1997) 229 [hep-th/9609070] [INSPIRE].
- [37] J. Knapp, E. Scheidegger and T. Schimannek, On genus one fibered Calabi-Yau threefolds with 5-sections, arXiv:2107.05647 [INSPIRE].
- [38] D.R. Morrison and W. Taylor, Sections, multisections, and U(1) fields in F-theory, arXiv:1404.1527 [INSPIRE].
- [39] P. Arras, A. Grassi and T. Weigand, Terminal Singularities, Milnor Numbers, and Matter in F-theory, J. Geom. Phys. 123 (2018) 71 [arXiv:1612.05646] [INSPIRE].

- [40] A. Grassi and T. Weigand, On topological invariants of algebraic threefolds with (Q-factorial) singularities, arXiv:1804.02424 [INSPIRE].
- [41] T. Schimannek, Modular curves, the Tate-Shafarevich group and Gopakumar-Vafa invariants with discrete charges, JHEP 02 (2022) 007 [arXiv:2108.09311] [INSPIRE].
- [42] S. Katz, A. Klemm, T. Schimannek and E. Sharpe, Topological Strings on Non-Commutative Resolutions, arXiv:2212.08655 [INSPIRE].
- [43] S. Katz and T. Schimannek, New non-commutative resolutions of determinantal Calabi-Yau threefolds from hybrid GLSM, arXiv:2307.00047 [INSPIRE].
- [44] Z. Duan, K. Lee, J. Nahmgoong and X. Wang, Twisted 6d (2,0) SCFTs on a circle, JHEP 07 (2021) 179 [arXiv:2103.06044] [INSPIRE].
- [45] D. Klevers et al., F-Theory on all Toric Hypersurface Fibrations and its Higgs Branches, JHEP 01 (2015) 142 [arXiv:1408.4808] [INSPIRE].
- [46] V. Braun and D.R. Morrison, F-theory on Genus-One Fibrations, JHEP 08 (2014) 132 [arXiv:1401.7844] [INSPIRE].
- [47] P.-K. Oehlmann, J. Reuter and T. Schimannek, Mordell-Weil Torsion in the Mirror of Multi-Sections, JHEP 12 (2016) 031 [arXiv:1604.00011] [INSPIRE].
- [48] C. Mayrhofer, E. Palti, O. Till and T. Weigand, On Discrete Symmetries and Torsion Homology in F-Theory, JHEP 06 (2015) 029 [arXiv:1410.7814] [INSPIRE].
- [49] T. Schimannek, Modularity from Monodromy, JHEP 05 (2019) 024 [arXiv:1902.08215] [INSPIRE].
- [50] M. Dierigl, P.-K. Oehlmann and T. Schimannek, The discrete Green-Schwarz mechanism in 6D F-theory and elliptic genera of non-critical strings, JHEP 03 (2023) 090 [arXiv:2212.04503] [INSPIRE].
- [51] M. Cvetič and L. Lin, TASI Lectures on Abelian and Discrete Symmetries in F-theory, PoS TASI2017 (2018) 020 [arXiv:1809.00012] [INSPIRE].
- [52] T. Weigand, F-theory, PoS TASI2017 (2018) 016 [arXiv:1806.01854] [INSPIRE].
- [53] Y. Tachikawa, On S-duality of 5d super Yang-Mills on S¹, JHEP 11 (2011) 123 [arXiv:1110.0531] [INSPIRE].
- [54] S. Chaudhuri, G. Hockney and J.D. Lykken, Maximally supersymmetric string theories in D < 10, Phys. Rev. Lett. **75** (1995) 2264 [hep-th/9505054] [INSPIRE].
- [55] P. Horava and E. Witten, Eleven-dimensional supergravity on a manifold with boundary, Nucl. Phys. B 475 (1996) 94 [hep-th/9603142] [INSPIRE].
- [56] O. Aharony, Z. Komargodski and A. Patir, The moduli space and M(atrix) theory of 9d N = 1 backgrounds of M/string theory, JHEP 05 (2007) 073 [hep-th/0702195] [INSPIRE].
- [57] T.W. Grimm, A. Kapfer and D. Klevers, *The Arithmetic of Elliptic Fibrations in Gauge Theories on a Circle, JHEP* **06** (2016) 112 [arXiv:1510.04281] [INSPIRE].
- [58] V. Bouchard and H. Skarke, Affine Kac-Moody algebras, CHL strings and the classification of tops, Adv. Theor. Math. Phys. 7 (2003) 205 [hep-th/0303218] [INSPIRE].
- [59] P. Candelas and A. Font, Duality between the webs of heterotic and type II vacua, Nucl. Phys. B 511 (1998) 295 [hep-th/9603170] [INSPIRE].

- [60] M. Dierigl, P.-K. Oehlmann and F. Ruehle, Global Tensor-Matter Transitions in F-Theory, Fortsch. Phys. 66 (2018) 1800037 [arXiv:1804.07386] [INSPIRE].
- [61] F.B. Kohl, M. Larfors and P.-K. Oehlmann, F-theory on 6D symmetric toroidal orbifolds, JHEP 05 (2022) 064 [arXiv:2111.07998] [INSPIRE].
- [62] A. Grassi, Spectrum bounds in geometry, arXiv:2304.07819 [INSPIRE].
- [63] M. Del Zotto, J.J. Heckman, D.R. Morrison and D.S. Park, 6D SCFTs and Gravity, JHEP 06 (2015) 158 [arXiv:1412.6526] [INSPIRE].
- [64] E. Witten, Phase transitions in M theory and F theory, Nucl. Phys. B 471 (1996) 195 [hep-th/9603150] [INSPIRE].
- [65] S.H. Katz, A. Klemm and C. Vafa, Geometric engineering of quantum field theories, Nucl. Phys. B 497 (1997) 173 [hep-th/9609239] [INSPIRE].
- [66] P.S. Aspinwall, S.H. Katz and D.R. Morrison, *Lie groups, Calabi-Yau threefolds, and F theory*, *Adv. Theor. Math. Phys.* 4 (2000) 95 [hep-th/0002012] [INSPIRE].
- [67] H.-C. Kim, M. Kim, S.-S. Kim and K.-H. Lee, Bootstrapping BPS spectra of 5d/6d field theories, JHEP 04 (2021) 161 [arXiv:2101.00023] [INSPIRE].
- [68] L. Bhardwaj, More 5d KK theories, JHEP 03 (2021) 054 [arXiv:2005.01722] [INSPIRE].
- [69] M. Cvetič and L. Lin, The Global Gauge Group Structure of F-theory Compactification with U(1)s, JHEP 01 (2018) 157 [arXiv:1706.08521] [INSPIRE].
- [70] I. García-Etxebarria, T.W. Grimm and J. Keitel, Yukawas and discrete symmetries in F-theory compactifications without section, JHEP 11 (2014) 125 [arXiv:1408.6448] [INSPIRE].
- [71] M. Esole, R. Jagadeesan and M.J. Kang, *The Geometry of G*₂, Spin(7), and Spin(8)-models, arXiv:1709.04913 [INSPIRE].
- [72] C. Cordova, T.T. Dumitrescu and K. Intriligator, 2-Group Global Symmetries and Anomalies in Six-Dimensional Quantum Field Theories, JHEP 04 (2021) 252 [arXiv:2009.00138] [INSPIRE].
- [73] L.B. Anderson, X. Gao, J. Gray and S.-J. Lee, Multiple Fibrations in Calabi-Yau Geometry and String Dualities, JHEP 10 (2016) 105 [arXiv:1608.07555] [INSPIRE].
- [74] M. Del Zotto and K. Ohmori, 2-Group Symmetries of 6D Little String Theories and T-Duality, Annales Henri Poincare 22 (2021) 2451 [arXiv:2009.03489] [INSPIRE].
- [75] M. Del Zotto, M. Liu and P.-K. Oehlmann, Back to heterotic strings on ALE spaces. Part I. Instantons, 2-groups and T-duality, JHEP 01 (2023) 176 [arXiv:2209.10551] [INSPIRE].
- [76] M. Del Zotto, M. Liu and P.-K. Oehlmann, Back to Heterotic Strings on ALE Spaces: Part II

 Geometry of T-dual Little Strings, arXiv:2212.05311 [INSPIRE].
- [77] M. Del Zotto, M. Liu and P.-K. Oehlmann, 6D Heterotic Little String Theories and F-theory Geometry: An Introduction, arXiv:2303.13502 [INSPIRE].
- [78] Y.-C. Huang and W. Taylor, Fibration structure in toric hypersurface Calabi-Yau threefolds, JHEP 03 (2020) 172 [arXiv:1907.09482] [INSPIRE].
- [79] V.V. Batyrev and L.A. Borisov, On Calabi-Yau complete intersections in toric varieties, alg-geom/9412017 [INSPIRE].
- [80] S.B. Johnson and W. Taylor, Enhanced gauge symmetry in 6D F-theory models and tuned elliptic Calabi-Yau threefolds, Fortsch. Phys. 64 (2016) 581 [arXiv:1605.08052] [INSPIRE].

- [81] M. Esole, P. Jefferson and M.J. Kang, The Geometry of F_4 -Models, arXiv:1704.08251 [INSPIRE].
- [82] H. Ooguri and C. Vafa, On the Geometry of the String Landscape and the Swampland, Nucl. Phys. B 766 (2007) 21 [hep-th/0605264] [INSPIRE].
- [83] E. Palti, The Swampland: Introduction and Review, Fortsch. Phys. 67 (2019) 1900037 [arXiv:1903.06239] [INSPIRE].
- [84] M. van Beest, J. Calderón-Infante, D. Mirfendereski and I. Valenzuela, Lectures on the Swampland Program in String Compactifications, Phys. Rept. 989 (2022) 1 [arXiv:2102.01111] [INSPIRE].
- [85] N.B. Agmon, A. Bedroya, M.J. Kang and C. Vafa, Lectures on the string landscape and the Swampland, arXiv:2212.06187 [INSPIRE].
- [86] N. Arkani-Hamed, L. Motl, A. Nicolis and C. Vafa, *The String landscape, black holes and gravity as the weakest force, JHEP* **06** (2007) 060 [hep-th/0601001] [INSPIRE].
- [87] S.-J. Lee, W. Lerche and T. Weigand, Emergent strings from infinite distance limits, JHEP 02 (2022) 190 [arXiv:1910.01135] [INSPIRE].
- [88] D. Harlow, B. Heidenreich, M. Reece and T. Rudelius, Weak gravity conjecture, Rev. Mod. Phys. 95 (2023) 035003 [arXiv:2201.08380] [INSPIRE].